Nonaqueous chemistry of colloidal group 4 oxo clusters and metal oxide nanocrystals

Dietger Van den Eynden, Rohan Pokratath, and Jonathan De Roo*

Department of Chemistry, University of Basel, Mattenstrasse 24, BPR 1096, Basel 4058, Switzerland

E-mail: Jonathan.DeRoo@unibas.ch

Abstract

We review the nonaqueous precursor chemistry of the group 4 metals with the purpose of gaining insight in the formation of their oxo clusters and oxide nanocrystals. We first describe the properties and structures of titanium, zirconium, and hafnium oxides. Second, we introduce the different precursors that are used in the synthesis of oxo clusters and oxide nanocrystals. We thus review the structures of group 4 metal halides and alkoxides, and their reactivity towards alcohols, carboxylic acids, etc. Third, we discuss fully condensed, atomically precise metal oxo clusters, which could serve as nanocrystal models. By comparing the reaction conditions and reagents, we provide insight in the relation between cluster structure and the nature of the carboxylate capping ligands. We also briefly discuss the use of oxo clusters. Finally, we review the nonaqueous synthesis of group 4 oxide nanocrystals, including both surfactant-free and surfactant-assisted synthesis. We focus on their precursor chemistry and surface chemistry. By putting these results together, we connect the dots and obtain more insight in the fascinating chemistry of the group 4, but at the same time, we also identify gaps in our knowledge and thus areas for future research.

Contents

1 Introduction

The group 4 oxides have a large band gap, a high dielectric constant, and a high refractive index. TiO_2 nanocrystals (NCs) are used in solar cells[1] and batteries,[2] and are photocatalytically active.[3] Tantalum or niobium doped titania (TiO_2:Ta) NCs find use as electrochromic modulators for smart windows.[4,5] ZrO_2 is a catalyst support,[6,7] and is used in superconducting nanocomposites.[8] Finally, HfO_2 NCs have recently received significant attention for use in next generation memory devices,[9,10] cancer treatment,[11,12] and scintillators.[13] Additionally, group 4 oxides doped with lanthanides are interesting luminescent materials,[14–17] and doped hafnia recently generated excitement due to the stabilization of its ferroelectric crystal phase.[18]

Equally exciting are the oxo clusters of titanium, zirconium and hafnium. In contrast to oxide nanocrystals, oxo clusters are atomically precise and much smaller. To put things into perspective; the archetypical oxo clusters contain only six metal atoms while, e.g., a 5 nm spherical ZrO_2 nanocrystal has about 1800 zirconium atoms. Oxo clusters are widely used as secondary building units in metal organic frameworks (MOFs),[19–21] as building block in 3D printing,[22] as catalysts,[23,24] or as crosslinker/filler in polymer composites.[25,26] Especially the zirconium MOFs excel in thermal stability and are used in the detection and removal of antibiotics and organic explosives,[27] as Lewis acid catalyst,[28] or as support for CO_2 reduction catalysis.[29]

So far, the field of group 4 oxo clusters and the nanocrystal field have not been bridged. However, they have many features in common; for example the precursors used to synthesize them. To further connect the fields, we can take inspiration from the late transition metal oxo clusters where for example iron oxo clusters were shown to be suitable precursors for iron oxide nanocrystals.[30] The conversion of clusters to nanocrystals was also achieved in case of cadmium chalcogenide clusters.[31–34] Within the group 4 oxo clusters, there has been only a single report where researchers used zirconium oxo clusters as precursors in nanocrystal synthesis.[35] However, the crystallite size was only one nanometer and characterization of

the colloidal stability and overall particle size is absent. Alternative strategies should be explored.

Here, we take a first step in bridging the oxo cluster and the nanocrystal field. We review the nonaqueous precursor chemistry that leads to oxo clusters and oxide nanocrystals of the group 4 metal: titanium, zirconium, and hafnium. By removing the complexity of the reaction mixture that is typical for water, reactions in organic solvent can be rationalized and categorized according to their fundamental oxide formation mechanism. Nonaqueous sol–gel chemistry has also the particular advantage of slower reaction rates, leading to more controlled reactions and generally a more crystalline and less aggregated product.[36] While crystalline particles of the group 4 oxides have been obtained in supercritical water,[37,38] and the crystalline phase can be tuned in certain hydrothermal reactions,[39] aggregation of the final NCs is a significant problem in such strategies. In some particular cases, NCs can be de-aggregated using fatty acids, but the hydrothermal reaction time should be extremely short or otherwise irreversible agglomeration occurs.[40] For the above reasons, we limit the current review to nonaqueous chemistry.

2 Structural properties of the metals and their oxides

The group 4 metals share many chemical properties. The +IV oxidation state is predominant for all three metals, but titanium can also be reduced to Ti(+III). This is a recurring theme in the group 4. All three are very similar but whereas zirconium and hafnium almost react identically, titanium is the odd one out, see Table 1. A striking example is the ionic radius, which is 0.74 Å for Ti^{4+} but 0.83 Å and 0.84 Å for Hf^{4+} and Zr^{4+} respectively.[41] The similar size for hafnium and zirconium is ascribed to the lanthanide contraction, and enables the formation of solid solutions; $Hf_xZr_{1-x}O_2$.[42] Zirconium and hafnium are also often called the *twin metals*. Finally, titanium usually has a coordination number of six, while zirconium and hafnium can reach a coordination number of eight, see further.

Table 1: Properties of the group 4 elements.

	Ti	Zr	Hf
Atomic number	22	40	72
Atomic radius (pm)[43]	140	155	155
Ionic radius (pm)[41]	74	84	83
Electronegativity (Pauling)[44]	1.54	1.33	1.3
Electronegativity (corrected)[45]	2.23	2.05	2.01
Maximum coordination number	6	8	8

The standard formation Gibbs free energy of all three oxides is highly negative and becomes more negative down the group, see Table 2. The oxides have also very high melting points, high dielectric constants and high refractive indices. While the band gap of titania is close to the blue, the band gap of zirconia and hafnia are deep in the UV. Given the increasing atomic mass, it is no surprise that the density of the oxides increases down the group.

Table 2: Properties of the group 4 metal oxides.[46–50]

	TiO_2	ZrO_2	HfO_2
Density (g/cm^3)	3.83 (anatase)	5.56 (monoclinic)	9.97 (monoclinic)
	4.17 (brookite)	5.8 (tetragonal)	10.36 (tetragonal)
	4.24 (rutile)	5.99 (cubic)	10.69 (cubic)
Melting point (°C)	1870	2715	2758
Dielectric constant	80 (rutile)	25 (monoclinic)	25 (monoclinic)
Refractive Index at 632.8 nm	2.8	2.2	1.91
Band Gap (eV)	3 (rutile)	5.8	5.8
	3.2 (anatase)		
$\Delta G^0_{f,298}$ (kJ/mol)	-891.2	-1042	-1088

Titania exists in three well–known polymorphs: tetragonal rutile ($P4_2/mnm$), tetragonal anatase ($I4_1/amd$), and orthorhombic brookite (Pbca). In addition, multiple metastable (e.g., the bronze phase) and high-pressure phases have also been reported.[51–58] In all structures, titanium is coordinated by six oxygen atoms with two axial and four equatorial bonds forming a distorted TiO_6 octahedron. These octahedrons build up the crystal lattice by either sharing edges or corners in a specific manner depending on the crystal structure. Figure 1 clearly shows that rutile has more corner sharing compared to anatase where edges shar-

ing is more prevalent. In rutile, the coordination of titanium is close to the D_{4h} symmetry, while in anatase, the octahedron is more distorted. However, in both cases, we distinguish a longer axial bond and a shorter equatorial bond, with the bonds in rutile being longer than in anatase, see Figure 1.[46] The other polymorphs have different Ti-O bond distances, as well as different octahedron assemblies.

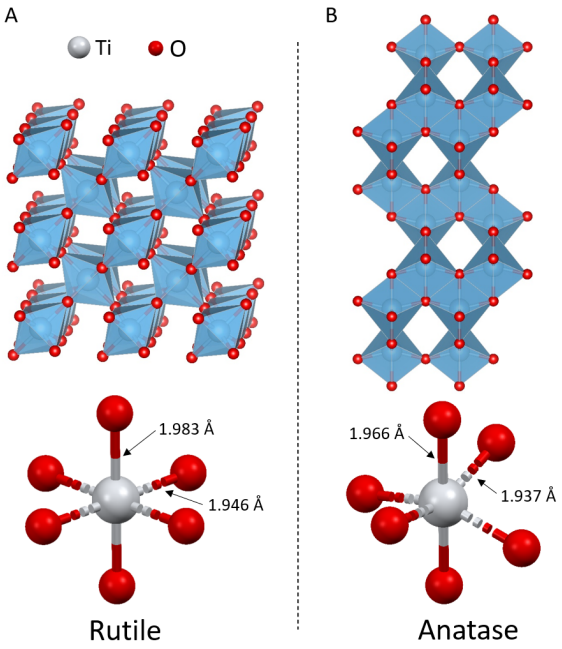

Figure 1: Illustration of corner and edge sharing octahedron assembly and Ti-O bond distances in (A) rutile and (B) anatase titanium oxide.

Zhang *et al.* investigated the phase stability of titania during crystal growth and found that phase transformation is size dependent (due to a higher contribution from the surface energy in small particles). The most stable phases are; anatase up to 11 nm, brookite in the range 11–35 nm and rutile above 35 nm.[59] These results are consistent with thermodynamic calculations.[60] However, other parameters such as temperature and pH can also influence the final phase.[59] For example, in highly acidic conditions, rutile is more stable than anatase, while anatase is more stable in highly basic conditions.

Zirconium and hafnium oxide possess similar properties and are thus called twin oxides. The three most important polymorphs of the twin oxides are: cubic (Fm-3m), tetragonal

($P4_2/nmc$), and monoclinic ($P2_1/c$). The cubic phase is thermodynamically favored at high temperatures and is structurally equivalent to the calcium fluorite structure, see Figure 2. The zirconium/hafnium atoms are eight–coordinate. At lower temperatures (2370-2600 °C, depending on the oxide), a slight distortion happens towards the tetragonal phase, but the metal atoms remain eight–coordinate. At room temperature, the monoclinic phase is most stable and can be considered a highly distorted calcium fluorite structure, see Figure 2. In this monoclinic phase, the metal is seven–coordinate. The tetragonal–to–monoclinic phase transformation is accompanied by a large volume decrease, causing undesired cracking of the material upon cooling. To avoid the phase transformations during cooling, the cubic phase is often stabilized with dopants such as yttrium. Yttrium stabilized zirconia (YSZ) is one of the prime examples of stabilized zirconia and retains the cubic crystal structure at room temperature. The oxygen vacancies created by yttrium incorporation are leveraged in solid oxide fuels cells and in other catalytic processes.[61]

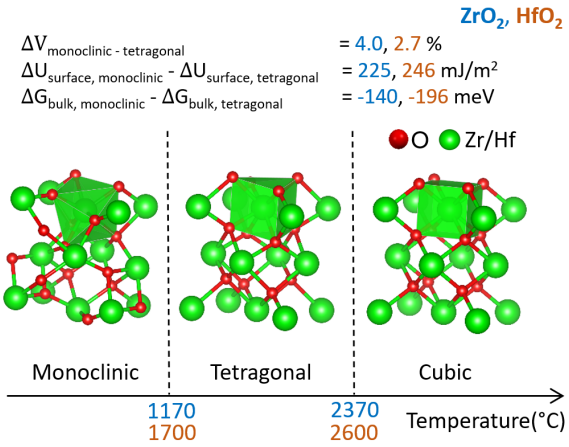

Figure 2: Phase transformation parameters for zirconia and hafnia.[62]

Similar to the case of titania, also zirconia and hafnia show size-dependent phase stability.[63–65] Given the significant difference in surface free energy for tetragonal and monoclinic zirconia, the tetragonal phase becomes stable at room temperature below a crystal size of 30 nm. Several colloidal syntheses for monodisperse zirconia are indeed in agreement with this predicted critical size.[66–68] Surface calculations of HfO_2 nanocrystals reported a critical

size of 2–10 nm.[69–71] A more precise value (4 nm) was determined experimentally by a size tunable method to synthesize hafnia nanocrystals.[72]

Stabilizing tetragonal hafnia is relevant for its use as a gate dielectric since first principle studies predict that the dielectric constant for tetragonal hafnia is about four times the value of monoclinic hafnia.[73] Even more polymorphs of hafnia are known, see Figure 3. There are non-polar (centrosymmetric) phases like the cubic phase, but there exist also polar (non-centrosymmetric) phases.[74] These polar phases are responsible for the recently discovered ferroelectric behaviour of hafnia, and they are often stabilized as solid solutions with zirconia or by the inclusion of dopants.[18,75–77]

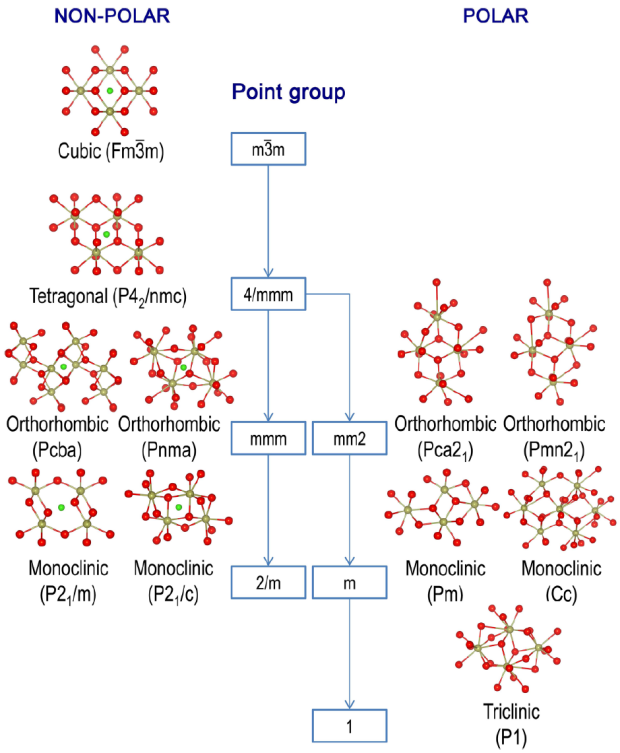

Figure 3: Symmetry-reduction flowchart of low energy phases of hafnia, starting from the m3m cubic point symmetry. These phases, labeled by space group symbols, are categorized into two branches, the nonpolar branch ending at the 2/m point symmetry on the left and the polar branch leading to the 1-point symmetry on the right. Dark yellow and red spheres represent hafnium and oxygen atoms, respectively, while green spheres locate the center of symmetry of those which are centrosymmetric. Reprinted figure with permission from Tran Doan Huan et al., Pathways towards ferroelectricity in hafnia ,Phys. Rev. B 90, 064111 (2014). Copyright 2021 by the American Physical Society.[74]

3 Precursors and their reactivity

Since we aim at obtaining more insight in the formation of oxo clusters and oxide nanocrystals, the first step is to understand the chemistry of the precursors. In this section, we discuss metal halides and metal alkoxides, the two most frequently used precursors in non-aqueous syntheses. We will highlight their reactivity with compounds that are relevant for the synthesis of oxo clusters and oxide nanocrystals. However, a full account of the group 4 chemistry is outside the scope of this review.

3.1 Metal halides

Group 4 halides (MX_4) exist with X = F, Cl, Br and I. They are highly Lewis acidic and hydrolyse quickly, even with moisture in the air. Therefore, they should be handled under inert atmosphere at all time. Otherwise HX is released and oxo bridges are formed:

$$\mathrm{M{-}X + H_2O \longrightarrow M{-}OH + HX} \quad (1)$$

$$\mathrm{2\,M{-}OH \longrightarrow M{-}O{-}M + H_2O} \quad (2)$$

The reactivity towards air depends on the halide. For example, ZrI_4 is even much more sensitive to air than the respective chloride and bromide.[78] This could be due to the reduced orbital overlap between I and Zr because of the large size of iodine. In pure water, the hydrolysis and condensation of metal chlorides do not go to completion. The release of HCl decreases the pH of the solution and stops further hydrolysis. For zirconium and hafnium, the primary hydrolysis product is the tetramer $[Zr_4(OH)_8(OH_2)_{16}]^{8+}$.[79–81] Complete hydrolysis is achieved upon adding base. Below, we discuss the titanium halides separately from the zirconium and hafnium halides because their structure and reactivity are significantly different.

3.1.1 Titanium halides

While the other halides of titanium are monomeric liquids, titanium fluoride is a polymeric solid.[82] By forming a polymer, the coordination number of titanium is increased from four to six, see Figure 4. TiF_4 and other titanium halides form monomeric Lewis acid–base pairs with a variety of Lewis bases.[83–85] For reasonably small Lewis bases, the cis configuration is retrieved, which is explained by an improved orbital overlap in the π bonding between halide p orbitals and titanium d orbitals.[86] Only for sterically hindered Lewis bases, the trans configuration is observed.

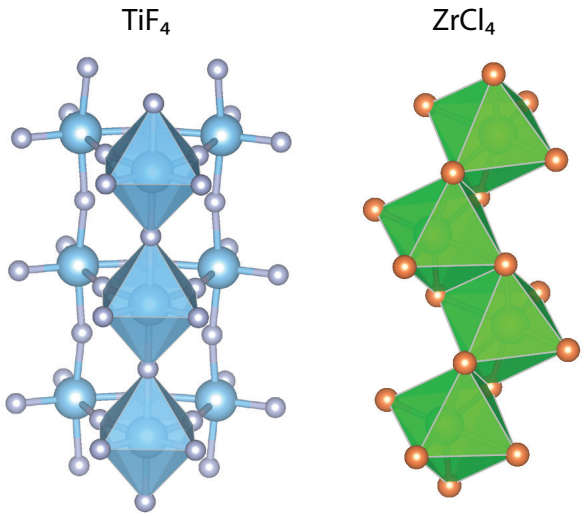

Figure 4: Crystal structures of TiF_4 and $ZrCl_4$.[82]

The reaction between $TiCl_4$ and alcohol produces a mixed chloroalkoxide, even in an excess of alcohol and under reflux.[87]

$$TiCl_4 + \text{excess ROH} \longrightarrow TiCl_2(OR)_2 \cdot ROH + 2\,HCl \tag{3}$$

The reaction does not go to completion, in contrast to the same reaction with $SiCl_4$.

$$SiCl_4 + 4\,ROH \longrightarrow Si(OR)_4 + 4\,HCl \tag{4}$$

An extra equivalent of alcohol forms a Lewis acid–base pair with the resulting titanium chloroalkoxide. The complex is a dimer, bringing the total coordination number to six, see figure 5A.[88] Internal hydrogen bonding from the alcohol to the chloride ligand further stabilizes the dimer complex. The reaction between $TiCl_4$ and a single equivalent of alcohol does not lead to exchange but produces simply the Lewis acid–base adduct, which is a dimer with bridging chloride ligands: $[TiCl_3(HOiPr)(\mu{-}Cl)]_2$.[89] With two equivalents of alcohol, the trichloride dimer was identified, featuring again bridging chloride ligands; $[TiCl_2(OiPr)(HOiPr)(\mu{-}Cl)]_2$. The reaction of titanium chloride with salicylaldehyde also results in the substitution of two chloride ligands and the final complex has a coordination number of six due to the additional coordination of the aldehyde.[90] Initially the structure was believed to have the chlorides in the *trans* geometry. However, the crystal structure of the equivalent complex with 3-tert-butyl-2-hydroxy-5-methylbenzaldehyde indicates that they are in the *cis* geometry, see Figure 5B.[91]

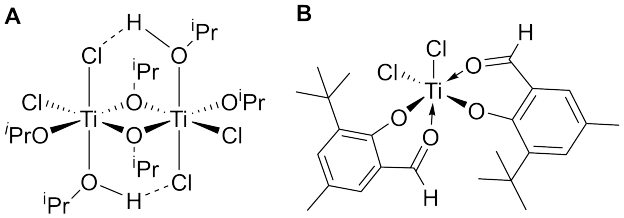

Figure 5: (A) The determined structure of $Zr(OiPr)Cl_2$.[88] (B) The proposed structure of the substitution product of $TiCl_4$ with salicylaldehyde.[91]

The alcoholysis reaction proceeds equally well for methanol, ethanol, isopropanol and isobutanol. By using the sodium salt of the alcohol, or anhydrous ammonia, the tetrasubstituted complex can be obtained.[87,89]

$$TiCl_4 + 4\,NaOR \longrightarrow Ti(OR)_4 + 4\,NaCl \tag{5}$$

$$TiCl_4 + 4\,ROH + 4\ NH_3 \longrightarrow Ti(OR)_4 + 4\,NH_4Cl \tag{6}$$

For the more acidic phenol, the substitution reaction with titanium chloride can proceed to

completion upon refluxing in excess phenol, whereas only the twice substituted product is obtained at room temperature.[92] Interestingly, it was not possible to substitute more than two salicylaldehydes (Figure 5B), even upon refluxing with excess salicylaldehyde.

$TiCl_4$ reacts with acetic acid (HOAc) and acetic anhydride to $TiCl_2(OAc)_2$.[93] The same product is obtained when $TiCl_4$ is treated with only acetic anhydride ($O(Ac)_2$). Acetyl chloride is the by-product.

$$TiCl_4 + 2\,O(Ac)_2 \longrightarrow TiCl_2(OAc)_2 + 2\,Ac{-}Cl \tag{7}$$

Attempts to further substitute the chloride by refluxing, lead to oxo bridges between titanium centers, showcasing the instability of the $TiCl(OAc)_3$ complex:

$$TiCl(OAc)_3 + TiCl_2(OAc)_2 \longrightarrow (OAc)_2ClTi{-}O{-}TiCl(OAc)_2 + Ac{-}Cl \tag{8}$$

In anhydrous trifluoroacetic acid (TFA-H) at 70 °C, the compound $TiO(TFA)_2$ is obtained.[94]

3.1.2 Zirconium and hafnium halides

While titanium chloride is a monomeric liquid, zirconium and hafnium chloride are polymeric solids with a coordination number (CN) of six, see Figure 4.[95] Given also the comparison between the different titanium halides, it seems that the tendency for expanding the coordination number is related to the relative size of metal and halide. For smaller halides and for larger metals, the polymeric structure is favored. Similar to titanium, the monomeric form of zirconium and hafnium chloride can be isolated by coordination with Lewis bases (ethers, typically THF, and esters), thus increasing the coordination number (CN = 6).[84,96] The THF complexes have been succesfully used in nanocrystal synthesis as precursors with improved solubility.[97]

Zirconium chloride is less reactive with respect to alcohols, compared to titanium chloride,

and only a single substitution takes place.[98–100]

$$ZrCl_4 + \text{excess ROH} \longrightarrow ZrCl_3(OR) + HCl \tag{9}$$

Similar to the case of titanium, anhydrous ammonia can drive the reaction towards the tetraalkoxide. However the sodium alkoxide route is not applicable to zirconium because of zirconium's tendency to form stable heterobimetallic alkoxides with alkali metals.[89] When reacting $ZrCl_4$ with 3-tert-butyl-2-hydroxy-5-methylbenzaldehyde, two chloride ligands are exchanged, bringing the total coordination number to six, similar to the case of titaniun (Figure 5B).[91] When $ZrCl_4$ is refluxed for three hours with phenol, the triphenolate complex is isolated while the fully substituted phenolate complex is only obtained after 14 hours of reflux.[92] This shows again a lower reactivity of zirconium compared to titanium. $ZrBr_4$ reacts immediately to the tetraphenolate species and appears thus more reactive than the chloride.[101]

$ZrCl_4$ slowly reacts with benzoic acid or fatty acids (stearic, palmitic and myristic acid) to the tetracarboxylate under reflux conditions in benzene.[102,103]

$$ZrCl_4 + 4\,RCOOH \longrightarrow Zr(OOCR)_4 + 4\,HCl \tag{10}$$

Upon reaction of $ZrCl_4$ with salicylic acid (Ph(OH)(COOH), the trisalicylate was obtained with one deprotonated phenoxy group; $Zr[(OOCPhOH)_2(OOCPhO)$.[104] Since the phenols also coordinate the zirconium, the coordination number is again six. In anhydrous trifluoroacetic acid (TFA-H) at 40 °C, the compound $Zr(TFA)_4$ is obtained and at 70 °C, $Hf(TFA)_4$.[94]

$$ZrCl_4 + 4\,TFA{-}H \longrightarrow Zr(TFA)_4 + 4\,HCl \tag{11}$$

$$HfCl_4 + 4\,TFA{-}H \longrightarrow Hf(TFA)_4 + 4\,HCl \tag{12}$$

$ZrCl_4$ also reacts with betadiketonates such as acetylacetone, benzoylacetone and diben-

zoylmethane in benzene.[105] However, only three chlorides are substituted.

$$ZrCl_4 + 3\,Hacac \longrightarrow Zr(acac)_3Cl + 3\,HCl \tag{13}$$

Even heating in the presence of a large excess of betadiketonate does not result in the last substitution. The resulting complex behaves like a salt with a cationic complex of zirconium with 3 betadiketonates (CN = 6) and a chloride anion. Indeed, the anion can be replaced for other anions such as $AuCl_4$.[105] In the presence of water and sodium acetylacetonate, the fourth substitution is forced and the zirconium tetraacetylacetonate is obtained as a decahydrate. The coordination number in the latter compound is eight, just like in bulk cubic zirconium dioxide. Finally, cyclopentadienyl has also been succesfully used to exchange two chloride atoms from $ZrCl_4$.[106]

3.2 Metal alkoxides

3.2.1 General properties

Another group of often used group 4 metal precursors in nanocrystal synthesis are metal alkoxides ($M(OR)_4$). These compounds are less Lewis acidic than the metal chlorides but are still coordinatively unsaturated. They are very sensitive to atmospheric moisture and prone to hydrolysis and condensation. The latter can happen either by reaction of two hydroxide units, or of one hydroxide and one alkoxide:

$$M{-}OR + H_2O \longrightarrow M{-}OH + HOR \tag{14}$$

$$2\,M{-}OH \longrightarrow M{-}O{-}M + H_2O \tag{15}$$

$$M{-}OH + M{-}OR \longrightarrow M{-}O{-}M + HOR \tag{16}$$

However, even air-free storage of $Zr(O^tBu)_4$ and $Zr(OPr)_4$ over a long time resulted in respectively $Zr_3O(O^tBu)_{10}$ and $Zr_4O(OPr)_{14}(HOPr)_2$.[107,108] Coordination oligomerization is a

general structural feature of metal alkoxides, if allowed by sterics.[89] Metal alkoxides with bulky ligands such as tert butoxide, will form monomers (4–fold coordination). In general, oligomerization is favored in electron deficient, large metals. Titanium methoxide and ethoxide are tetramers in solid state whereas zirconium and hafnium isopropoxide are dimers and have an additional, neutral isopropanol ligand (CN = 6). Oligomerization is indeed directly competing with additional Lewis bases and the most stable compound is determined by the nature of alkoxide and base. Very often, the dimer $M_2(OR)_8L_2$ is formed with octahedral coordination, two bridging alkoxo ligands and the additional Lewis base on opposing axial positions. Intramolecular hydrogen bonding further stabilizes the complex, evidenced by the distortion of Zr-OR bonds, see Figure 6.[109,110] The geometry is typical for zirconium and hafnium isopropoxide, complexed with isopropanol or other Lewis bases. Also titanium isopropoxide forms such a complex with butylamine, benzylamine and cyclohexylamine. Complexes with secondary amines are more difficult to obtain,[110] and coordination polymers are retrieved with diamines.[111] In the liquid state, the configuration can be different, for example, titanium ethoxide becomes a trimer (5-fold coordination). Titanium alkoxides with bulkier ligands, such as isopropoxide, are monomeric species.[112] The zirconium alkoxides remain dimers, also in solution.[113]

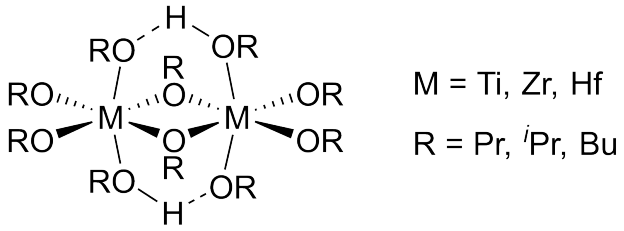

Figure 6: The dimeric structure of many group 4 metal alkoxides, coordinated with Lewis base (primary alcohols or amines). Here we show the hydrogen bonding for the case where the Lewis base is alcohol.

Metal alkoxides react with a variety of protic reagents such as alcohols, alkanolamines, carboxylic acids, diketones, oximes, Schiff bases, hydroxylamines, etc. Substitution of one or more alkoxide ligands typically leads to a lower reactivity towards water and the resulting

compounds were therefore of great significance for sol–gel processing of metal oxides.[114–116] In the following we will only discuss the most relevant reactions for oxo cluster and oxide nanocrystal formation. A more elaborate account is found elsewhere.[89]

3.2.2 Ligand exchange with alcohol

Metal alkoxides feature facile ligand exchange with other alcohols.[89]

$$\mathrm{M{-}OR + R'OH \rightleftharpoons M{-}OR' + ROH} \tag{17}$$

This equilibrium and thus the extent of exchange can be steered in several ways. If R'OH has a higher boiling point, the fully exchanged product is retrieved by boiling off ROH. Other factors are: sterics, solubility, the O-H bond strength, and the metal-alkoxide bond strength. The relative exchange strength has the following order: MeOH > EtOH > *i*PrOH > *t*BuOH.[89,116] Apart from the simple sterics argument, also the possibility for dimerization adds to the exchange enthalpy. For example, whereas zirconium tert butoxide is a monomer, zirconium isopropoxide is a dimer. The influence of sterics on the exchange rate is clearly illustrated by NMR. While only one type of ethoxy signal is observed for a mixture of titanium ethoxide and ethanol (fast exchange), two types of methyl signal are observed for a mixure of titanium *tert*-butoxide and *tert*-butanol (slow exchange).[89]

Electron withdrawing groups decrease both the O-H bond strength (lower pKa) and the metal-alkoxide bond strength. While the first factor favors substitution, the second factor has the opposite effect. From substitution experiments with titanium ethoxide (or isopropoxide) and fluorinated alcohols (R^fOH), it follows that the metal-alkoxide bond strength is the most important factor.[117]

$$\mathrm{Ti(OR) + excess\, R^fOH \longrightarrow Ti(OR^f)_x(OR)_{4-x} + x\, ROH} \tag{18}$$

Upon treating $Ti(O\mathit{i}Pr)_4$ with an excess of $HOCH(CF_3)_2$ only two alkoxides are exchanged

(x = 2). Full exchange is observed for phenol (R= C_6H_5) and substituted phenols (R= 2,4−$F_2C_6H_3$, 4−FC_6H_4). However, x = 3 for phenol with too many electron withdrawing group (R = C_6F_5 and 2,6−$F_2C_6H_3$).[117] Also for $Zr(OiPr)_4$, full exchange is achieved with phenol.[104] Importantly, alcohol exchange stops when coordination saturation is reached. For example, when exposed to an excess of salycilaldehyde, $Ti(OR)_4$ (R = Et, *i*Pr or *t*Bu) reacts exothermically to exchange only two of the OR groups. Upon disubstitution, the stable 6-fold coordination is obtained for the complex.[90]

Another strategy for exchanging alkoxides is transesterification.

$$M{-}OR + CH_3COOR' \rightleftharpoons M{-}OR' + CH_3COOR \tag{19}$$

This approach is often preferred when there is a larger difference in boiling points of the esters compared to the parent alcohols.

3.2.3 Reaction with carboxylic acid (anhydride)

Metal carboxylates are thermodynamically favored over alkoxides due to the chelating binding mode. It allows the metals to reach their desired coordination number (6 for Ti and 8 for Zr and Hf). The reaction of titanium ethoxide or isopropoxide with acetic acid anhydride was studied as early as 1957 by Kapoor and Mehrotra.[118] Upon addition of one equivalent of acetic acid anhydride, one equivalent of ester is formed together with the mixed titanium complex of alkoxide and acetate (Figure 7A. A second equivalent reacts in the same way and both reactions are fast and exothermic. The third exchange is slower and the triacetate complex reacts with the diacetate complex to form an oxo bridged dimer. Finally, the last alkoxo group is exchanged by refluxing the dimer with an excess of acetic acid anhydride. It should not come as a surprise that the di–acetate is the last stable monomeric compound since it features already its maximum coordination number of six.

It is interesting to compare this reactivity with the direct ligand exchange of alkoxide for

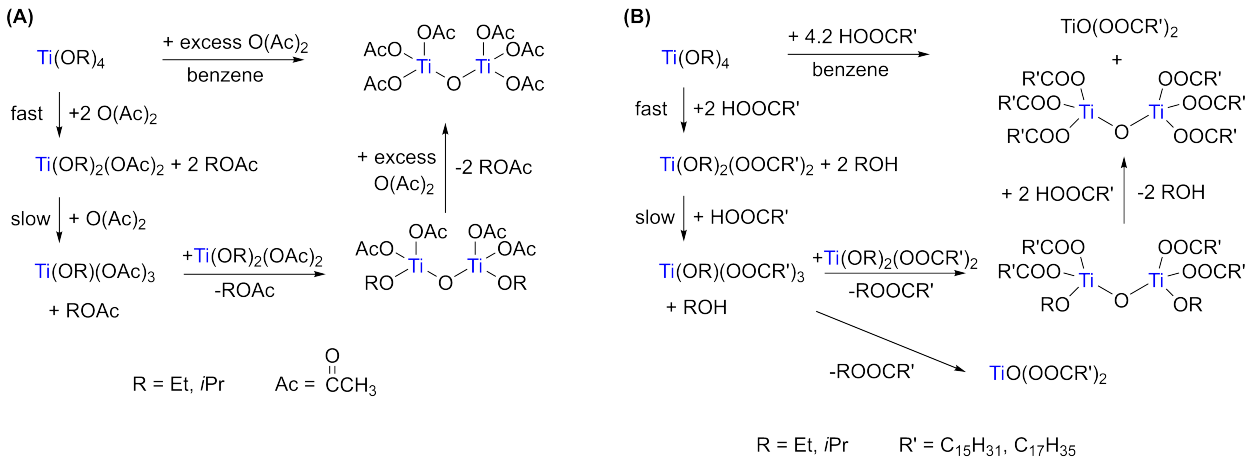

Figure 7: (A) Reaction of acetic acid anhydride with titanium ethoxide or isopropoxide. (B) Reaction of fatty acids with titanium ethoxide or isopropoxide.

acetic acid. Titanium ethoxide and isopropoxide undergo facile exchange for two equivalents of fatty acids (R' = $n-C_{15}H_{31}$, and $n-C_{17}H_{35}$), reaching a coordination number of six (Figure 7B.[119] This reaction liberates two equivalents of alcohol. The third exchange is again slower, and similar to the reaction with acetic acid anhydride, the oxo bridged dimer is formed. However, also a second compound was observed, consistent with the formula $TiO(OOCR')_2$. Also the reaction of excess acetic acid and butanoic acid with titanium ethoxide and isopropoxide form a mixture of those two compounds. The relative ratio of the two final products depends strongly on the carboxylic acid chain length, see Table 3.

Table 3: Product composition of the reaction of fatty acids with titanium isopropoxide. The number of carbons in the fatty acids is indicated in brackets.

	$TiO(OOCR')_2$	$O[Ti(OOCR')_3]_2$
Acetic acid (1C)	1	1
Butanoic acid (4C)	4	1
Palmitic acid (16C)	8	1
Stearic acid (18C)	8	1

With increasing chain length, the $TiO(OOCR')_2$ product is more favored. Such a dependence gives us insight in the reaction mechanism. Whereas the reaction of the tricarboxylate complex with the dicarboxylate is subject to sterical hinderance from the alkyl chains, the formation of $TiO(OOCR')_2$ seem less hindered. Therefore, we infer that the latter is formed

by reaction of the tricarboxylate $Ti(OR)(OOCR')_3$ with released alcohol, to form ester and a titanium hydroxide: $Ti(OH)(OR)(OOCR')_2$. Two or more such units can condense via

$$n\ Ti(OH)(OR)(OOCR')_2 \longrightarrow [TiO(OOCR')_2]_n + n\ ROH \tag{20}$$

An alternative mechanism would be an intra-coordination sphere reaction where the actual molecular compound $TiO(OOCR')_2$ is formed with a Ti–oxygen double bond. In the latter, titanium would be only five-coordinated and therefore this compound is less likely to be an intermediate. A third mechanism proposes that the titanium tricarboxylate is never formed. Instead, the third carboxylic acid directly forms an ester with the titanium dicarboxylate.[120]

$$Ti(OR)_2(OOCR')_2 + HOOCR' \longrightarrow Ti(OH)(OR)(OOCR')_2 + ROOCR' \tag{21}$$

Several decades later, Sanchez et al. reported that titanium *n*-butoxide does react with one equivalent acetic acid to the monoacetate,[116] but two equivalents of acetic acid already lead to the hexameric cluster $Ti_6O_4(OnBu)_8(OOCCH_3)_8$.[112] Similar clusters were found in the reaction of titanium ethoxide with 2 equivalents methacrylic acid: $Ti_6O_4(OEt)_8(OOCR)_8$.[121] Detailed IR spectroscopy by Schubert et al. detected the presence of uncoordinated carboxylic acid already after 1.3 equivalents of acid added.[121] Ester can be formed from free acid and free ethanol or catalyzed by titanium as described above, thus liberating water for the oxo bridges. Comparing these observations to the results of Kapoor and Mehrotra, we note that the latter only reported the titanium dicarboxyate for palmitic acid and stearic acid. They did not perform a stepwise reaction with acetic acid. In addition, Kapoor and Mehrotra heated their solutions to high temperatures (100 and 150 °C) while Schubert and Sanchez worked at room temperature. Since this pioneering work, a whole variety of different oxoalkoxo clusters have been synthesized and the structure depends on the specific alkoxide, the specific carboxylic acid and the number of equivalents added.[25] We will discuss these clusters in more detail in the next section.

The reactions of zirconium isopropoxide isopropanol complex with fatty acids (R' = $n{-}C_5H_{11}$, $n{-}C_{11}H_{23}$, $n{-}C_{15}H_{31}$, and $n{-}C_{17}H_{35}$) are quite similar, but the tricarboxylate product is more stable than the titanium analogue and could be isolated at low temperature.[102] When decomposed the tricarboxylate gave the $ZrO(OOCR')_2$ product. The tetracarboxylate is formed slowly and reacts with the tricarboxylate:

$$Zr(OOCR')_4 + Zr(O\mathit{i}Pr)(OOCR')_3 \longrightarrow Zr_2O(OOCR')_6 + R'COO\mathit{i}Pr \qquad (22)$$

With IR and NMR spectroscopy it was confirmed that zirconium propoxide reacts with two equivalents of methacrylic acid to $Zr(OR)_2(OOCR')_2$.[121] However, it was also noticed that such solutions were not stable for long. Water liberated by esterification causes hydrolysis and the formation of oxo bridges. In contrast to fatty acids, benzoic acid readily forms the tetrabenzoate from zirconium isopropoxide.[104] $Zr(O\mathit{i}Pr)_4$ forms the tris salicylate in the reaction with salicylic acid. One phenoxy group binds to zirconium, even in excess of salicylic acid.[104] This is the same compound ($Zr[(OOCPhOH)_2(OOCPhO)$) as obtained with zirconium chloride.

3.2.4 Reaction with hydrogen halide

The reaction of metal alkoxides with hydrogen halides yields essentially the same product as the reaction of metal halides with alcohols. In the case of titanium, the dihalide is formed while in the case of zirconium a mixture of trihalide and dihalide is formed.[89] The liberated alcohol binds to the metal complex as a Lewis base.

$$Ti(OR)_4 + 2HX \longrightarrow TiX_2(OR)_2 \cdot ROH + ROH \qquad (23)$$

$$2\,Zr(OR)_4 + 5HX \longrightarrow ZrX_3(OR) \cdot 2\,ROH + ZrX_2(OR)_2 \cdot ROH + 2\,ROH \qquad (24)$$

A strategy to obtain any desired chloroalkoxide involves the reaction of the metal alkoxides with acylhalides (chloride and bromide), where the stoichiometry of the final complex is determined by the number of acylhalide equivalents.[122]

$$\mathrm{M(OR)_4 + x\,CH_3COCl \longrightarrow MCl_x(OR)_{4-x} + CH_3COOR} \tag{25}$$

The resulting ester can also coordinate as a Lewis base. These reactions work well for metal ethoxides and isopropoxides but are very slow for tertbutoxides. Upon additon of an excess of acylchloride, the mechanism changes and zirconium chlorotriacetate was obtained.

$$\mathrm{Zr(O}t\mathrm{Bu)_4 + excess\,CH_3COCl \longrightarrow ZrCl(OOCCH_3)_3 + 3\,}t\mathrm{BuCl + CH_3COO}t\mathrm{Bu} \tag{26}$$

3.2.5 Other exchanges and thermal decomposition

Equimolar reaction of $\mathrm{M(O}i\mathrm{Pr)_4}$ (M = Ti, Zr, Hf) with phosphinic acid ($\mathrm{R_2P(O)(OH)}$) results in a single exchange and the final compound is a dimer with bridging ligands.[123] Tetrakis-β-diketonates of titanium cannot be prepared by reacting titanium isopropoxide with excess β-diketones. Only the bisalkoxide bis-β-diketonate was obtained. Interestingly, when $\mathrm{Ti(OR)_2(acac)_2}$ is reacted with HCl, $\mathrm{TiCl_2(acac)_2}$ is formed. These results stand in stark contrast to the behaviour of zirconium and hafnium alkoxides, which react in stoichiometric amounts with β-diketonates. One equivalent of acetylacetone leads to the dimer $\mathrm{[Zr(O}i\mathrm{Pr)_3(acac)]_2}$ or $\mathrm{[Hf(O}i\mathrm{Pr)_3(acac)]_2}$. Higher substitutions lead to monomeric complexes. The tris-β-diketonates complex is unstable and undergoes a disproportionation to the tetrakis complex and the original alkoxide, for example:[107,108]

$$\mathrm{4\,Zr(O}i\mathrm{Pr)(acac)_4 + \longrightarrow 3\,Zr(acac)_4 + Zr(O}i\mathrm{Pr)_4} \tag{27}$$

The similarity between Zr and Hf and the contrast with Ti is obviously related to their relative size. It is clear from the above that the smaller titanium has the tendency to form

complexes with coordination numbers of six, while the larger zirconium and hafnium easily accomodate coordination numbers up to eight.

Finally, the metal alkoxides thermally decompose at various temperatures,[89] depending on the nature of the alkoxide. For example, when heated at the 340 °C for three hours, zirconium ethoxide only slowed a slight decomposition while the isopropoxide decomposed to oxide, releasing propene and isopropanol. The *tert*-butoxide and *tert*- amyloxide are even less thermally stable and also release alkene and alcohol upon heating to 250 °C.

3.3 Metal chloroalkoxides

3.3.1 Mixing metal halides and metal alkoxides

When metal halides and metal alkoxides are mixed at room temperature, ligands are rapidly redistributed among the metal centers.[122,124]

$$MX_4 + M(OR)_4 \longrightarrow 2MX_2(OR)_2 \tag{28}$$

The equimolar reaction between titanium chloride and titanium ethoxide indeed delivers predominantly $TiCl_2(OEt)_2$, but also contains small amounts of $TiCl_3(OEt)$ and $TiCl(OEt)_3$. Titanium chloro alkoxides have a tendency towards complete disproportionation when heated under vacuum.[122]

$$2TiCl_3(OMe) \longrightarrow TiCl_2(OMe)_2 + TiCl_4 \tag{29}$$

In solution, the disproportionation reaction has an equilibrium constant of approximately 10^{-4},[124,125] indicating a non–random distribution. One can calculate the speciation in solution for various alkoxide to Ti ratios, see table 4.[125] In an equimolar mixture of $Ti(OR)_4$ and $TiCl_4$, the ratio OR/Ti = 2 and the dominant species is $TiCl_2(OR)_2$. Small amounts of $TiCl_3(OR)$ and $TiCl(OR)_3$ are also present. Unfortunately, solution NMR cannot distinguish the various species at room temperature because of fast exchange.

Table 4: Calculated speciation (in percent) in a mixture of $Ti(OR)_4$ and $TiCl_4$. The percentage of $Ti(OR)_4$ is below 10^{-3} in all cases.[125]

OR/Ti	$TiCl_4$	$TiCl_3(OR)$	$TiCl_2(OR)_2$	$TiCl(OR)_3$
1	1	98	1	10^{-6}
1.7	10^{-3}	30	70	10^{-2}
2	10^{-6}	1	98	1
2.3	10^{-10}	10^{-2}	70	30

3.3.2 Reaction of titanium chloride with ethers

In general, ethers forms a Lewis–Base Adduct with titanium chloride (*e.g.,* $TiCl_4 \cdot 2\,OEt_2$).[85] However, the thermal stability of these complexes is limited. The decomposition (etherolysis) temperature of the ether complex decreases in the series: dioxane (180 °C) > tetrahydrofuran (125 °C) > anisole (45 °C). It is not possible to isolate the diisopropyl ether complex of $TiCl_4$ since it decomposes immediately at room temperature. Instead, $TiCl_3(O\mathit{i}Pr)$ and isopropyl chloride are obtained according to Equation 30.

$$TiCl_4 + 2\,O\mathit{i}Pr_2 \longrightarrow TiCl_3(O\mathit{i}Pr) + \mathit{i}Pr{-}Cl \tag{30}$$

The result is again a mixed chloroalkoxide.

3.3.3 Thermal decomposition of mixed chloroalkoxides

In 1997, Vioux *et. al.* reported the formation of titania gels from either (i) titanium chloride with titanium isopropoxide, or from (ii) titanium chloride and diisopropyl ether.[125] Both reactions lead to Ti–O–Ti bridges through pre–coordination and subsequent condensation between Ti–Cl and Ti–O*i*Pr moieties. Since this alkylhalide elimination mechanism turned out to be quite general we write the chemical equations using the generic symbols M for metal, X for halide and R for alkyl groups, see Equation 31.

$$M{-}X + RO{-}M \longrightarrow M{-}O{-}M + R{-}X \tag{31}$$

In case of titanium chloride and titanium isopropoxide mixtures, the mixed chloroalkoxides are formed by ligand distribution (Equation 28). In case of titanium chloride and diisopropyl ether, the chloroalkoxide is formed by alkoxylation (= etherolysis, Equation 30).

Vioux *et. al.* studied the kinetics of the condensation and alkoxylation reactions via solution NMR. In contrast to the extreme reactivity of titanium alkoxides towards hydrolysis and condensation, the non–hydrolytic condensation proceeds slowly. In mixtures of $Ti(O\mathit{i}Pr)_4$ and $TiCl_4$, isopropyl chloride was found as sole co–product, confirming the mechanism in Equation 31. The reaction progress (amount of iPrCl) has a sigmoidal shape and the induction time increases with an increasing ratio of OiPr/Ti (R), see Figure 8. Given the speciation in Table 4, it appears that $TiCl_3(OR)$ is most reactive. In its absence (at R = 2.3), the reaction does not even take place within the observed time window. While it is possible that $TiCl_3(OR)$ catalyzes the condensation reaction (just like $FeCl_3$ and $AlCl_3$ catalyze the condensation between Si–Cl and Si–OR), the sigmoidal kinetics point towards an autocatalytic mechanism. Neither isopropyl chloride nor titania gel had a significant effect on the reaction rate and therefore, it is most likely that the intermediate $TiOCl_2$ is the active catalyst. This agrees with the higher reactivity of $TiOCl_2$ compared to $Ti(O\mathit{i}Pr)Cl_3$ in the polymerization of olefins.[126]

The equimolar reaction between $TiCl_4$ and $Ti(O\mathit{i}Pr)_4$ can be compared to the reaction between $TiCl_4$ and 2 equivalents isopropyl ether since both reactions yield theoretically an OR/Ti ratio of 2. At room temperature, the first alkoxylation reaction (Equation 30) proceeds in 20 min, yielding basically $TiCl_3(OR)$, which is likely coordinated by isopropyl ether. The second alkoxylation reaction is much slower (Figure 9), and condensation does not occur within the first 24 hours. At 100 °C, the second alkoxylation reaction reaches full yield and condensation starts after three hours. This induction period is much shorter than for the equimolar reaction between $TiCl_4$ and $Ti(O\mathit{i}Pr)_4$, and this is probably due to the speciation of the mixture with higher concentrations of $TiCl_3(OR)$.

This alkylhalide elimination strategy has been exploited to make mixed gels of zirco-

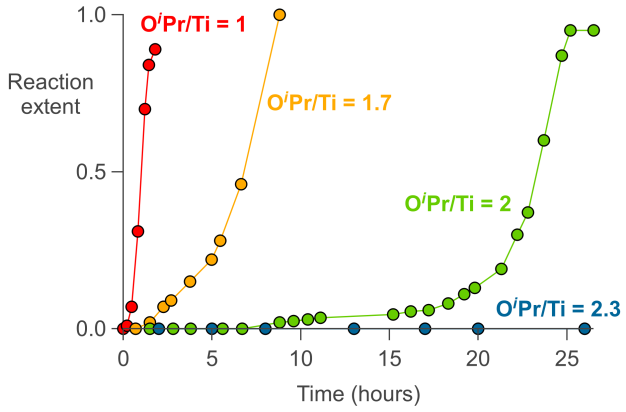

Figure 8: Extent of condensation at 100 °C in mixtures of Ti(OiPr)$_4$ and TiCl$_4$, with varying OiPr/Ti ratios (R). R = 1, 1.7, 2, and 2.3. Replotted with the data from reference.[125] Note that there appears to be a mistake in the original paper. The main text of the paper states an induction period of 300 hours for a ratio of 2.3 but the original figure shows an induction time of 20 hours for the ratio 2.3, and a much longer induction delay for a ratio of 2. We assume that the extensive description in the text is correct and that the figure contains the error.

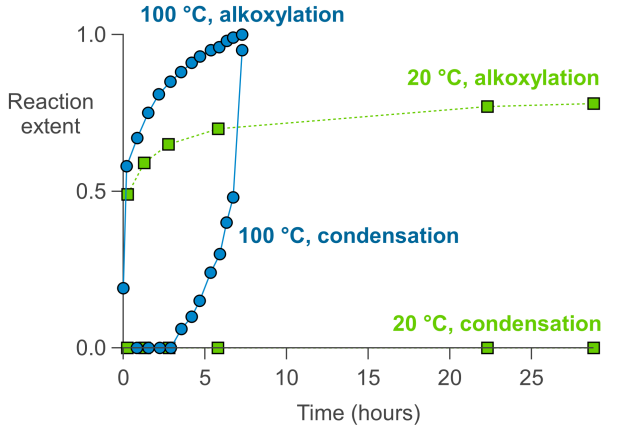

Figure 9: Extent of alkoxylation and condensation at 20 °C and 100 °C, for the reaction between TiCl$_4$ and 2 equivalents of iPr$_2$O. Replotted with the data from reference.[125]

nium and titanium oxides, which were subsequently crystallized in $ZrTiO_4$ at 700 °C.[127,128] Homogeneous gels were obtained at 110 °C from either

- $Ti(OiPr)_4$ and $ZrCl_4$
- $TiCl_4$ and $Zr(OEt)_4$
- $TiCl_4$, $ZrCl_4$ and R_2O (R = *i*Pr, Et, *n*Pr)

Given that in these processes, ligand redistribution is rapid, both homo and heterocondensation could in principle take place. However, EDX and ICP elemental analysis confirmed the equimolar ratio in both the gel and the crystallized product. Alkyl chloride was detected by GC and NMR. Interestingly, a 50:50 ratio of *i*PrCl and *n*PrCl was found in the reaction with *n*-propyl ether. When the alkyl chloride was distilled off, a 20:80 ratio was found. The authors conclude that an S_N1 reaction mechanism is unlikely since it would lead to rearrangement of the carbocation and thus *i*PrCl as the main product. The observed isomerization to *i*PrCl is explained by the presence of strong Lewis acids which are known to catalyzed the isomerization of alkyl halides. The extent of catalytic isomerization is reduced by distilling off the alkyl halide. Therefore, the authors propose that, for primary alkoxides, the reaction follows an S_N2 mechanism. Based on the final degree of condensation in the gels, the effectiveness of the oxygen donor was ranked as $iPr_2O > Zr(OEt)_4 > Et_2O > Ti(OiPr)_4 > nPr_2O$.

4 Metal oxo clusters

We define here oxo clusters as an arrangement of metal atoms connected by oxo bridges. A prototypical example is $Zr_6O_4(OH)_4(OOCR)_{12}$, where six zirconium atoms are arranged as an octahedron, see Figure 10. Every zirconium atom has a coordination number of eight, reminiscent of tetragonal/cubic zirconia. The largest Zr-Zr distance in the cluster is 0.5 nm. Since their surface is also capped by ligands, one can regard such clusters as the smallest

possible nanocrystals, with the additional benefit that they are atomically defined (polydispersity = 0 %). They can be crystallized and their structure determined via single crystal XRD. Although many mixed oxoalkoxy clusters exist, such (carboxylate capped) clusters have been extensively reviewed before.[25,80,129,130] In addition, there are also oxoalkoxy cluster with phosphonate and phosphinate ligands.[130,131] However, oxoalkoxy compounds are not stable to atmospheric water. Here we focus on fully condensed (= no alkoxy ligands) oxo clusters with either carboxylate or phosphonate ligands, since those are the most representative models for oxide nanocrystals. Finally, we only describe clusters synthesized by nonaqueous methods. A comprehensive overview of clusters obtained from water (e.g., capped with sulfate ligands) is found elsewhere.[80]

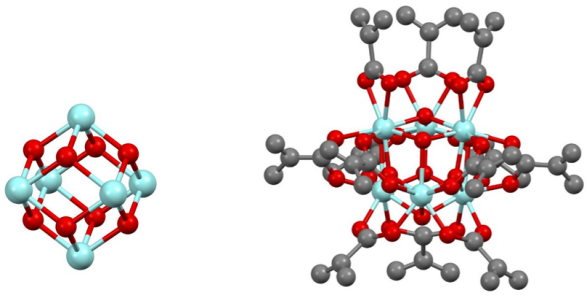

Figure 10: Structure of $Zr_6O_4(OH)_4(OOCR)_{12}$ formed from zirconium propoxide and methacrylic acid. On the left is only the core presented while on the right all covalently attached ligands are shown. Hydrogens are not shown for clarity.

4.1 Titanium oxo clusters

As we have seen in the section on precursors, the reaction of titanium alkoxides with carboxylic acids is not a straightforward ligand exchange. One equivalent of acid simply exchanges for an alkoxide ligand but more equivalents lead to oxo bridges and ester. The ester can be formed from released alcohol with excess acid or by direct reaction of titanium alkoxide with titanium carboxylate. In the first possible mechanism water is formed which can hydrolyze the alkoxide, with subsequent condensation steps forming oxo bridges. In the

second mechanism an oxo bridge is directly formed. Either way, ester formation seems to be Lewis acid catalyzed by the titanium alkoxide. The ester could also be formed when free alcohol reacts with free acid however, when mixing alcohol with acid (without metal precursor) no ester formation is observed. Hence, this pathway can be excluded.

At room temperature, titanium alkoxides react with an excess acetic acid to a poorly crystalline titanium oxoacetate with the minial formula $TiO(OOCMe)_2$.[119,120] The nature of the alkoxide does not change the final product but more sterically hindered alkoxides react slower (at room temperature).[120] In contrast, a solvothermal synthesis leads to well-defined, crystalline $Ti_8O_8(OOCR)_{16}$ clusters, where R = CH_3, Ph, or $C(CH_3)_3$.[132] For example, titanium isopropoxide reacts with 10 equivalents benzoic acid in acetonitrile to $Ti_8O_8(OOCPh)_{18}$.

$$Ti(O\mathit{i}Pr)_4 + 10\,PhCOOH \xrightarrow[ACN]{100^\circ C,15h} Ti_8O_8(OOCPh)_{18} \tag{32}$$

The cluster is isolated as yellow crytals (99 % yield) with solvent and water co-crystallized: $Ti_8O_8(OOCPh)_{18} \cdot (CH_3CN)_2 \cdot H_2O$ The structure of the clusters is depicted in Figure 11. Eight corner-sharing TiO_6 octahedra form a ring with 16 bridging carboxylate ligands. Eight carboxylate ligands are equatorial and eight are axial with respect to the ring. Equatorial and axial ligand can be differentiated by ^{13}C MAS solid state NMR since they appear as two signals at 176.9 and 175.8 ppm, distinct from pure benzoic acid (172 ppm). A similar cluster structure was obtained with pivalic acid ($HOOCC(CH_3)_3$), but the inital white crystals needed to be recrystallized in THF. The *tert*-butyl groups provide a higher solubility to the cluster, enabling liquid NMR measurement, where again two sets of resonances are found in the ^{13}C NMR spectrum. The cluster with acetate ligands is microcrystalline (precluding single crystal XRD analysis) but the clusters can be interconverted in one another by ligand exchange (by mass action) showing that the cluster core is identical in all cases. The $Ti_8O_8(OOCR)_{18}$ clusters are stable towards nucleophiles (like water), can be handled without precaution, and can be stored for weeks without structural change. This stands in

contrast to an earlier report of $Ti_8O_8(OOCR)_{16}$ clusters, where R = $C(CH_3)_3$, $CH_2C(CH_3)_3$, or $C(CH_3)_2Et$.[133] Although the crystal structure of the pivalic acid capped clusters show the same structure are discussed before, all three clusters were unstable to air. This might be related to the synthesis, which involved the reaction of only 2 equivalents of carboxylic acids with titanium isopropoxide at room temperature in toluene, followed by crystallization using the slow evaporation method. The yields were also low (24-55 %).

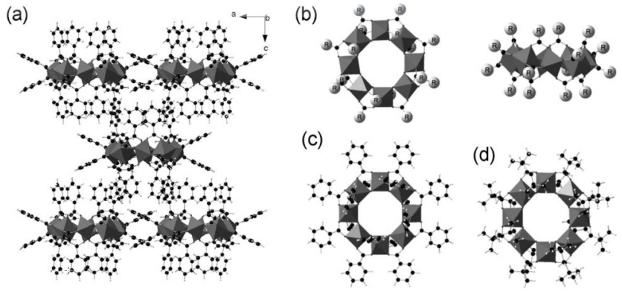

Figure 11: (a) Crystallographic packing of the $Ti_8O_8(OOCPh)_{18}$ clusters. (b) general structure of the ring shaped $Ti_8O_8(OOCR)_{18}$ clusters. (c) $Ti_8O_8(OOCPh)_{18}$ cluster structure and (d) $Ti_8O_8(OOCC(CH_3)_3)_{18}$.[132] Copyright © 2010 WILEY-VCH Verlag GmbH & Co. KGaA, Weinheim.

Interestingly, already in 1995 a similar ring shaped cluster was reported with pentafluorobenzoic acid.[134] This highly acidic molecule reacts with titanium chloride towards the cluster and produced the acylchloride as by-product upon refluxing in toluene.

$$8TiCl_4 + 24\,C_6F_5COOH \xrightarrow[\text{toluene}]{\text{reflux,4h}} Ti_8O_8(OOCC_6F_5)_{18} + 8\,C_6F_5COCl + 24HCl \qquad (33)$$

4.2 Zirconium oxo clusters

4.2.1 Synthesis and structure

As discussed before, the addition of 2 equivalents of carboxylic acids to zirconium alkoxide first leads to a zirconium dicarboxylate complex, but over time esterification occurs. The formed water causes hydrolysis and condensation. In contrast to the case of titanium, crystalline oxocarboxo zirconium clusters are readily obtained at room temperature, possibly

due to the lower reactivity of zirconium. Indeed, fast reactions typically lead to amorphous products. In the following, we describe reactions of zirconium alkoxides with carboxylic acids where water is formed *in–situ* by esterification. Attempts to add small amounts of water to control cluster formation were typically less reproducible.[135]

Crystalline $Zr_6O_4(OH)_4(OOCR)_{12}$ (**Zr6**) and $Zr_4O_2(OOCR)_{12}$ (**Zr4**) clusters were first synthesized from zirconium propoxide and 5 or 21 equivalents of methacrylic acid respectively.[136] The structure of $Zr_6O_4(OH)_4(OOCR)_{12}$ is shown in Figure 10. The zirconium atoms are arranged in an octahedron and on every triangular face of the octahedron either a μ_3–O or a μ_3–OH connects the three zirconium atoms. The cluster core is capped by 12 carboxylates of which three are chelating and nine are bridging two zirconium atoms (edge-bridging the octahedron). Interestingly, all three chelating ligands are on the same face of the octahedron and the cluster has C_{3v} symmetry (Figure 10). The cluster also co-crystallizes with extra methacrylic acid, which is hydrogen bonded to the cluster core. In the highly compact **Zr6** cluster, every zirconium atom has a coordination number of eight. The **Zr4** cluster has a more open structure and one zirconium atom is even only 7-coordinate. **Zr4**-methacrylate has two isomers in the solid state; a symmetric and an asymmetric one.[136,137] In the Raman spectrum, the Zr-O-Zr modes appear at 190 and 250 cm^{-1} for **Zr6**-methacrylate and at 230 cm^{-1} for **Zr4**-methacrylate.[113,138]

While the **Zr4** cluster has only been obtained under specific circumstances with methacrylic acid, the **Zr6** cluster core appears as a more universal structural motif. Also 5-norbornene-2-carboxylic acid yields the **Zr6** cluster.[139] Slight variations were obtained with methacrylic, isobutyric and benzoic acid where one bridging ligand (opposite the chelating face) becomes monodentate and a propanol (or water) molecule fills the empty coordination site, e.g, $Zr_6O_4(OH)_4(OOCR)_{12}(PrOH) \cdot 3\,RCOOH$.[140,141] Again tree carboxylic acids co-crystallize with the cluster. The opening and closing of the bridging ligand seems to be a reversible process since all coordinated alcohol could be removed by vacuum.[141] Interestingly, it is possible to obtain a pure, high symmetrical **Zr6** cluster with pivalic acid or 2,2-dimethylbutanoic

acid, when two equivalents of acid is reacted with $Zr(OiPr)_4$ or $Zr(OC(Me)_2Et)_4$, in a mixture of hexane and isopropanol.[142] Initially, the reaction mixture is turbid but it becomes clear after 12 hours. Crystals of the **Zr6** cluster were isolated by slow evaporation. The observed yield (61-67 %) agrees with the overall reaction stoichiometry:

$$6\,Zr(OR')_4 + 20RCOOH \xrightarrow{RT} Zr_6O_4(OH)_4(OOCR)_{12} + 8RCOOR' + 16R'OH \qquad (34)$$

The structure has no chelating ligands, only edge-bridging carboxylates, as evidenced by single crystal XRD and IR spectroscopy. A sharp but weak OH stretch was clearly observed at 3672 cm^{-1} in IR, indicating the absence of hydrogen bonding. The four protons do migrate between all eight μ_3–O bridges, causing disorder in the crystal. The compounds are insoluble in aliphatic solvents and sparingly soluble in aromatic solvents. Interestingly, early DFT calculations showed that an isolated **Zr6** cluster with only edge-bridging ligands (O_h symmetry) is more stable than the (experimentally observed) cluster with three chelating ligands.[143] Most likely, hydrogen bonding lowers the free energy of the chelated cluster. Indeed, in the rare case where no carboxylic acid was co-crystallized, the structure with all edge-bridging ligands was observed.[142]

Other carboxylic acids such as acetic, acrylic, propionic, 3-mercaptopropionic, 5-hexynoic, and 3-butenoic yield the dimer of this **Zr6** cluster: $[Zr_6O_4(OH)_4(OOCR)_{12}]_2 \cdot xRCOOH$ (**Zr12**).[140,144–146] One can formally construct the dimer when two bridging ligands of **Zr6** (opposite the chelating face) are no longer edge-bridging but instead link two cluster cores (Figure 12). Also the clusters synthesized with mixtures of acetic/methacrylic acid or propionic/methacrylic acid crystallized according to the **Z12** structure. Interestingly, the bridging ligands were either acetate or propionate, never methacrylate.[144] The preference of methacrylate decreases in the series: chelating > edge-bridging >> cluster-bridging. Although this has never been explicitly stated by others, we infer that steric hindrance at the carbon adjacent to the carbonyl is the determining factor in forming the structures **Zr6** or **Zr12**. This

is supported by an overview of the different ligands and their corresponding cluster structure (Figure 13). It is clear that the **Zr6** cluster is formed as soon as the α carbon is secondary (or tertiary). Steric hindrance at the β position does not preclude the formation of the dimer. Both the **Zr6** and **Zr12** cluster are quite stable in air and neutral water, but decompose in acidic or basic conditions, forming lower nuclearity or polymeric species respectively.[23] For long term storage however, we have found that the clusters are best stored under inert atmosphere.

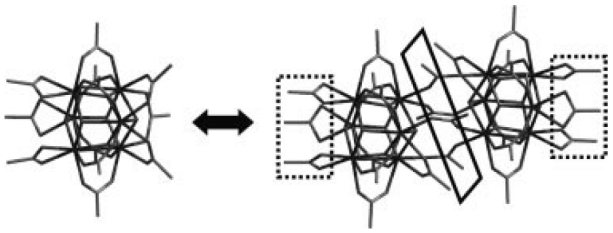

Figure 12: Relation between a **Zr6** and a **Zr12** cluster. In both clusters, there are chelating and bridging ligands. In the **Zr12** cluster, some ligands bridge the two cluster monomers.[144]

Larger (monomeric) clusters are also known. For example, zirconium propoxide reacts with salicylic acid to $Zr_{10}O_6(OH)_4(OOCPhOH)_8(OOCRPhO)_8$.[147] At the core of the cluster there is the Zr6 octahedron $Zr_6O_4(OH)_4(OOCPhOH)_4(OOCRPhO)_8{}^{8-}$, with all carboxylates edge-bridging. Two $Zr_2O(OOCPhOH)_2{}^{4+}$ units are condensed to this core. Each phenolate on the core binds to the attached zirconium atoms, see Figure 14A. The largest clusters obtained via nonaqueous methods are $Zr_{18}O_{21}(OH)_2(OOCPh)_{28}$ (from $ZrCl_4$, benzoic acid and thiourea in acetonitrile),[148] and $Zr_{26}O_{18}(OH)_{30}(HCOO)_{38}$ (from $ZrOCl_2 \cdot 8\,H_2O$ and formic acid in DMF).[149] The latter contains a central Zr6 octahedron, connected by the four equatorial zirconium atoms to four more Zr6 octahedra, see Figure 14B. The structure is intrinsically porous.

$ZrOCl_2 \cdot 8\,H_2O$ has been used as a cost effective precursor for clusters. The **Zr12**-acetate clusters were obtained from $ZrOCl_2$ in DMF (110 °C, 1 day).[150] Note that $ZrOCl_2 \cdot 8\,H_2O$ is actually the tetrameric cluster: $Zr_4(OH)_8(H_2O)_{16}{}^{8+}$, charge balanced by chlorides. The clus-

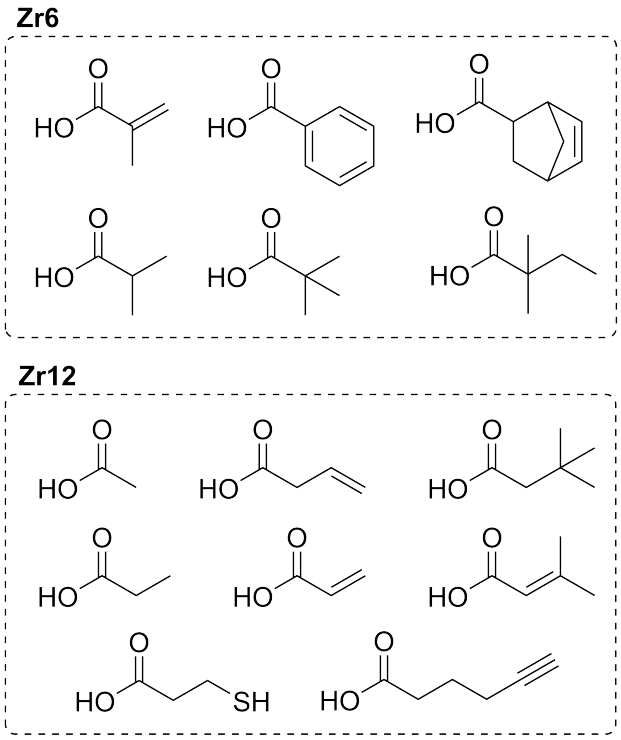

Figure 13: Overview of the different carboxylic acids used for cluster formation, grouped according to the specific cluster structure.

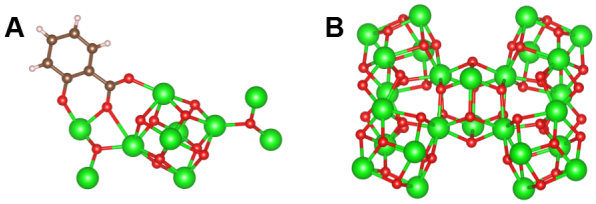

Figure 14: (A) Coordination of double deprotonated salicylic acid in the $Zr_{10}O_6(OH)_4(OOCPhOH)_8(OOCRPhO)_8$ cluster. (B) Structure of the $Zr_{26}O_{18}(OH)_{30}(HCOO)_{38}$ cluster with the formate ligands omitted.

ter has 8 μ_2-OH bridges and is quite different from the **Zr4**-methycrylate cluster. $ZrOCl_2 \cdot 8\,H_2O$ is also a good starting point for the formation of a diverse set of zirconium oxo clusters in aqueous media. The reader is referred to a dedicated review by Parac-Vogt *et al.* for a description of cluster products via the aqueous route.[80]

4.2.2 Mechanistic insights

For the above, it is clear that cluster formation (from zirconium alkoxide and carboxylic acids) proceeds in three steps: (i) ligand exchange (alkoxide for carboxylate), (ii) esterification, and (iii) condensation. The overall chemical equation for the reaction is written in Equation 34. While the ligand exchange step has been studied to some extent, mechanistic studies on the esterification or condensation steps are rare. As an exception, Gross *et al.* performed an EXAFS study to gain a better understanding of the reaction between zirconium butoxide and methacrylic acid.[113] Zirconium butoxide in butanol is a dimeric complex with a coordination number for Zr of six and a single Zr-Zr backscattering interaction (Figure 15). Upon addition of methacrylic acid, the coordination number increases over time to eight and the Zr-Zr interactions increases to two. The Zr-Zr distance is 3.4 Å, which is shorter than the 3.51 Å distance in the final **Zr6** cluster. These results are consistent with a Zr_3 triangular intermediate, a structural motif that is known for several oxoalkoxo structures. Unfortunately, the final **Zr6**-methacrylate cluster precipitated from solution and its time–dependent concentration could not be tracked by EXAFS. Gross *et al.* also analyzed the rate of ester formation in various solvents which shows the relative trend: THF << benzene < DCM. The coordinating solvent THF is believed to block coordination sites on zirconium and thus slow down the reaction. While the above results give us some insight, a fully comprehensive picture of the mechanism is still missing.

To gain some empirical insight in cluster formation, we have assembled Table 5 with an overview of the synthetic conditions for the different zirconium oxo clusters. It appears that zirconium propoxide (70 w% solution in propanol) can be easily exchanged for zirconium

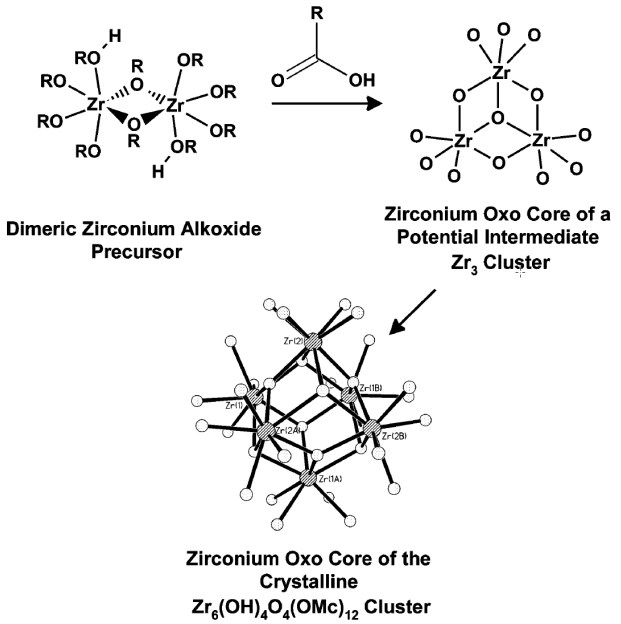

Figure 15: Inferred mechanism of **Zr6** formation from an EXAFS study.[113] Reproduced from Reference[113] with permission from the Royal Society of Chemistry.

butoxide (80w% solution in butanol) and identical results are obtained.[113,141,144] However, in mixed cluster syntheses (see below), there are cases where this change does have an impact. When mixing different metal alkoxides they will have different reaction rates and therefore different reaction products can be obtained. Most cluster syntheses are performed without solvent but in case of **Zr6**-acetate clusters, dichloromethane improves the crystallinity of the final product (and co-crystallizes). The **Zr6** cluster is only formed when there are at least two alkyl substituents at the α position of the carboxylic acid, otherwise the **Zr12** dimer is formed, see also Figure 13. It is unclear how to steer the synthesis between **Zr4**- and **Zr6**-methacrylate. Although it was initially reported that 4-5 equivalents of methacrylic acid delivered **Zr6** and 7-20 equivalents resulted in **Zr4**, one can find counterexamples in Table 5.

4.2.3 Ligand exchange, NMR characterization and purification

The carboxylate ligands are easily exchanged for other carboxylic acids. This is already clear from the ^{1}H NMR spectrum of **Zr6**-methacrylate clusters where only a single set of

Table 5: Synthetic procedures to zirconium oxo clusters

Precursor	RCOOH	RCOOH/ Zr ratio	Zr (mol/L)	Solvent	Time	Temp	outcome	Reported yield	Ref
$Zr(OPr)_4$	methacrylic acid	21	0.5	/	7 days	RT	$Zr_4O_2(OOCR)_{12}$	quant	[136]
$Zr(OBu)_4$	methacrylic acid	6.5	1	/	1 day	RT	$Zr_4O_2(OOCR)_{12}$	86 %	[137]
$Zr(OPr)_4$	methacrylic acid anhydride	8.2	0.9	/	2 days	RT	$Zr_4O_2(OOCR)_{12}$	94 %	[137]
$Zr(OPr)_4$	methacrylic acid	5.3	1.1	/	1 day	RT	$Zr_6O_4(OH)_4(OOCR)_{12}$	quant	[136]
$Zr(OPr)_4$	methacrylic acid	9	0.8	/	11 days	RT	$Zr_4O_2(OOCR)_{12}$[a]	140 %	[140]
$Zr(OPr)_4$	benzoic acid	81	0.02	n-propanol	14 days	RT	$Zr_4O_2(OOCR)_{12}$[a]	very low	[140]
$Zr(OBu)_4$	benzoic acid	25	0.08	n-butanol	12 hours	reflux	Zr_6 cluster no single crystal XRD	63 %	[141]
$Zr(O^iPr)_4$	pivalic acid	10	0.6	/	1 day	80 °C	Zr_6 cluster no single crystal XRD	76 %	[151]
$Zr(O^iPr)_4$ or $Zr(OC(Me)_2Et)_4$	pivalic acid	2	0.6	HO^iPr / hexane	2 days	RT	$Zr_6O_4(OH)_4(OOCR)_{12}$	61 %	[142]
$Zr(O^iPr)_4$ or $Zr(OC(Me)_2Et)_4$	2,2-dimethyl butanoic acid	2	0.6	HO^iPr / hexane	2 days	RT	$Zr_6O_4(OH)_4(OOCR)_{12}$	67 %	[142]
$Zr(OBu)_4$	isobutyric acid	7	0.9	/	4 weeks	RT	$Zr_6O_4(OH)_4(OOCR)_{12}$[a]	37 %	[141]
$Zr(OBu)_4$	isobutyric acid	7	0.9	/	1 week	RT	$Zr_6O_4(OH)_4(OOCR)_{12}$[a]	91 %	[141]
$Zr(OBu)_4$	methacrylic acid 5-norbornene-2-carboxylic acid	6.58	0.12	heptane	1 week	RT	$Zr_6O_4(OH)_4(OOCR)_{12}$[a]	99.8 %	[139]
$Zr(OBu)_4$	acetic acid	10	0.5	CH_2Cl_2	3 hours	RT	$[Zr_6O_4(OH)_4(OOCR)_{12}]_2$[a]	68 %	[144]
$Zr(OPr)_4$	acetic acid	29	0.5	/	12 hours	RT	$[Zr_{12}$ cluster no single crystal XRD	117 %	[152]
$ZrOCl_2$	acetic acid	39	0.3	DMF	1 day	110 °C	$[Zr_6O_4(OH)_4(OOCR)_{12}]_2$	64 %	[150]
$Zr(OBu)_4$	acetic acid and methacrylic acid	5	1.3	/	12 hours	RT	$[Zr_6O_4(OH)_4(OOCR)_{12}]_2$[a]	98 %	[144]
$Zr(OBu)_4$	propionic acid	10	0.8	/	8 hours	RT	$[Zr_6O_4(OH)_4(OOCR)_{12}]_2$[a]	75 %	[144]
$Zr(OBu)_4$	propionic acid and methacrylic acid	7	1	/	24 hours	RT	$[Zr_6O_4(OH)_4(OOCR)_{12}]_2$[a]	85 %	[144]
$Zr(acac)_4$	propionic acid	26	0.4	/	1 hour	160 °C	$[Zr_6O_4(OH)_4(OOCR)_{12}]_2$	70 %	[153]
$Zr(OBu)_4$	3-mercapto-propionic acid	7.27	0.92	/	3 days	RT	$[Zr_6O_4(OH)_4(OOCR)_{12}]_2$[a]	63 %	[145]
$Zr(OPr)_4$	acrylic acid	6.5	1.1	/	3 days	RT	$[Zr_6O_4(OH)_4(OOCR)_{12}]_2$[a]	111 %	[140]
$Zr(OBu)_4$	vinylacetic acid	7	1	/	2 days	RT	$[Zr_6O_4(OH)_4(OOCR)_{12}]_2$[a]	63 %	[144]
$Zr(OBu)_4$	dimethyl acrylic acid	3.8	0.4	toluene	20 days	RT	$[Zr_6O_4(OH)_4(OOCR)_{12}]_2$[a]	88 %	[144]
$Zr(O^iPr)_4$	3,3-dimethyl butanoic acid	2	0.5	HO^iPr / hexane	2 days	RT	$[Zr_6O_4(OH)_7(OOCR)_9]_2$	65 %	[154]
$Zr(OPr)_4$	salicylic acid	5.24	0.12	n-propanol	14 days	RT	$Zr_{10}O_6(OH)_4(OOCR)_{16}$[a]	136 %	[140]
$Zr(OBu)_4$	5-hexynoic acid	3.9	0.8	/	3 weeks / 12 days	RT / -21 °C	$[Zr_6O_4(OH)_7(OOCR)_9]_2$[a]	14.4 %	[146]

[a] co-crystallized solvent or carboxylic acid was reported but omitted from this formula

resonances is observed because of fast exchange between the bound carboxylates and the co-crystallized carboxylic acid.[141,143] After careful removal of the free acid, three different sets of ligands were observed, see Figure 16A. The resonance with the highest ppm value in ^{13}C NMR was assigned to the chelating ligands. Those chelating ligands appeared the most labile and dynamic in solution.[144] The **Zr12**-acetate cluster shows five different resonances at room temperature and the **Zr12**-propionate cluster shows an even more complex pattern of CH_2 resonances (Figure 16B). By decreasing the temperature to -40 °C, the structure becomes less dynamic and one can more clearly observed different CH_2 environments (Figure 16B).[144]

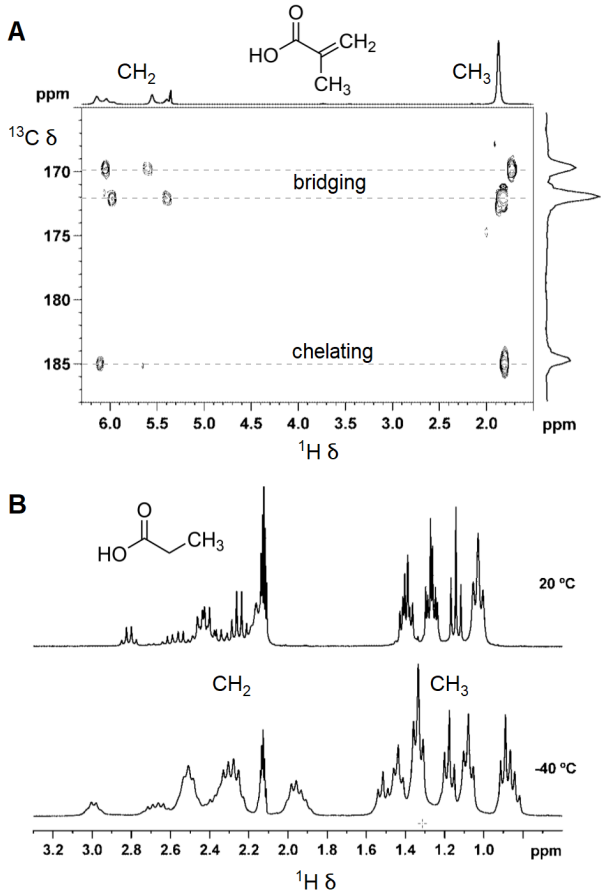

Figure 16: (A) HMBC NMR spectrum of the **Zr6**-methacrylate clusters at room temperature. (B) Spectra of **Zr12**-propionate cluster in toluene-d_8 at different temperatures. Adapted from Puchberger et al.[144] Copyright © 2006 WILEY-VCH Verlag GmbH & Co. KGaA, Weinheim.

Upon repetitive addition of excess propionic acid and subsequent evaporation, the original

methacrylate ligands on the **Zr6**-methacrylate cluster could be completely exchanged.[144] Taking the **Zr12** mixed propionate/methacrylate (3:9) cluster – with the propionates in the cluster-bridging position – and exposing it to multiple cycles of excess propionic acid, again removed all original methycrylate ligands. In the first case, the **Zr6**-propionate cluster was formed and in the second case the **Zr12**-propionate. When the **Zr12**-propionate cluster was treated excessively with acetic acid, the ligand exchange was however not complete. According to NMR integration the ratio of acetate to propionate was 3:1 in the final product. From the above results, the authors concluded that the **Zr6** and **Zr12** cluster could not be converted into one another and that the cluster-bridging ligands are not available for ligand exchange.[144] Since the NMR signatures of the **Zr6**- and **Zr12**-propionate clusters are distinct, they indeed do not simply interconvert in solution at room temperature. However, the inertness of the cluster-bridging ligands towards ligand exchange is not fully proven, in our opinion. Since the exchange relied on mass action and evaporation of the free acid, the lower boiling point of acetic acid might have hampered the ligand exchange. A more convincing proof would consist of exchanging the **Zr12**-acetate clusters with propionic aicd, instead of the other way round. Whether the **Zr12** dimer can be broken by heating has not been studied as such, but **Zr6** MOFs can be synthesized from a **Zr12** precursor, indicating that the dimer can be converted to the monomer under particular conditions.[150]

The **Zr4** cluster is more dynamic than the **Zr6** or **Zr12** clusters. At room temperature only a single set of resonances is observed in NMR (even after removal of free acid).[143] At -80 °C, four different sets of resonances are observed and the chelating ligands were again the most dynamic. The ligand exchange reaction of the **Zr4**-methacrylate cluster for pivalic acid ligands was successful and retained the cluster core. Finally, ligand scrambling was observed when pure **Zr4**-methacrylate and **Zr4**-pivalate are mixed.

The **Zr4** and **Zr6** clusters react differently with acetylacetone (a typical chelating ligand).

The **Zr4** cluster degrades according to Equation 35.[155]

$$Zr_4O_2(OOCR)_{12} + 8\,acac{-}H \longrightarrow 4\,Zr(acac)_2(OOCR)_2 + 4\,RCOOH + 2\;H_2O \qquad (35)$$

In contrast, even an 50-fold excess of acetylacetone results in only a double exchange on the **Zr12** cluster, forming $[Zr_6O_4(OH)_4(OOCR)_{11}(acac)]_2$.[156] Per **Zr6** cluster core, one chelating carboxylate was replaced with one chelating acetylacetonate. This really showcases the higher stability of the **Zr6** cluster. Even more, $Zr(acac)_4$ reacts with an excess of propionic acid at 160 °C to the mixed **Zr12**-acetate/propionate cluster.[153]

Hydrogen bonding plays a crucial role in these oxo clusters. We already discussed that co-crystallized acid interacts with the cluster core via hydrogen bonding.[144] The OH of a free carboxylic acid hydrogen bonds to an oxygen of a bound ligand, and the carbonyl of the free acid binds simultaneously with the μ_3–OH. Schubert *et al.* also proposed that during a rearrangement from the chelating to the bridging mode, the transition state is stabilized by hydrogen bonding to a μ_3–OH.[143] More recently, Tsai *et al.* investigated ligand exchange reactions on a **Zr6** cluster using DFT calculations, see Figure 17.[157] The approach of a carboxylic acid to the cluster and subsequent hydrogen bonding was found to be exothermic and without barrier. Furthermore, proton transfer from the new to the old ligand considerably lowered the activation barrier for exchange. Therefore, more acidic ligands exchange faster.

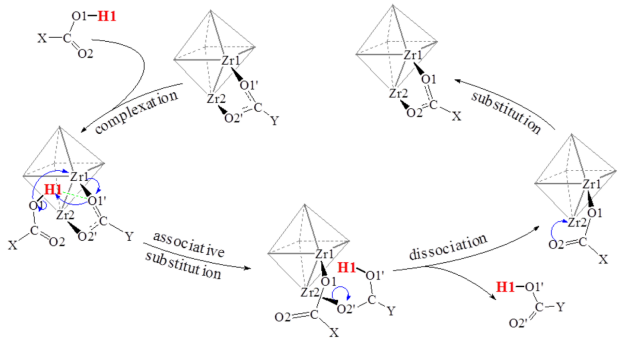

Figure 17: The mechanism of carboxylate exchange are derived from DFT calculations by Tsai *et al.*[157] Reprinted with permission from reference.[157] Copyright 2019 American Chemical Society.

Despite the ease of ligand exchange, obtaining the pure, exchanged cluster is not trivial. Crystallization is limited since it is poorly applicable to disordered, mixed ligands shells or flexible ligands. Purification by evaporation is also limited to the lower carboxylic acids (with sufficiently low boiling points). Recently, a purification method for **Ti8** and **Zr6** oxo clusters with mixed ligand shells was developed based on resins with amine groups.[151] Unfortunately, about 20 % free acid persisted in the final product.

4.3 Hafnium oxo clusters

Hafnium forms clusters that are isostructural to the zirconium clusters, see Table 6. **Hf12** clusters were thus synthesized from acetic acid and hafnium butoxide,[144] while **Hf4** and **Hf6** clusters were obtained with methacrylic acid.[158] The **Hf6** cluster has the structural formula: $Hf_6O_4(OH)_4(OOCR)_{12}(BuOH)$, with one carboxylate ligand binding monodentately and the free coordination spot being filled by butanol.

4.4 Mixed metal oxo clusters

Clusters consisting of multiple metals have also been synthesised, see Table 6. A 1:3 mixture of $Ti(OBu)_4$ and $Zr(OBu)_4$ with four equivalents of methacrylic acid leads to a mixture of three clusters: $Ti_2Zr_4O_4(OBu)_2(OOCR)_{14}$, $Ti_4Zr_6O_4(OBu)_6(OOCR)_{10}$ and $Ti_2Zr_6O_6(OOCR)_{20}$. Replacing $Zr(OBu)_4$ with $Zr(OPr)_4$ exclusively yields the $Ti_4Zr_6O_4(OBu)_6(OOCR)_{10}$ cluster.[155] This shows that the choice between $Zr(OBu)_4$ and $Zr(OPr)_4$ can impact the final product. Using a 1:1:1 mixture of $Ti(OBu)_4$, $Zr(OBu)_4$ and $Hf(OBu)_4$, the $Ti_2Zr_5HfO_6(OOCR)_{20}$ cluster is obtained.[158] All the above mixed clusters have an open structure, comprising TiO_6 octahedra and ZrO_7 or ZrO_8 polyhedra (or the hafnium equivalents), see Figure 18. Similar open structures are obtained from the metal alkoxides and methacrylic acid for the mixed titanium-yttrium clusters, e.g., $Y_2Ti_4O_4(OOCR)_{14}(MeO(CH_2)_2OH)$.[160] In an alternative approach titanium isopropoxide is reacted with several lanthanide acetates and methacrylic acid, resulting in $LnTi_4O_3(O\mathit{i}Pr)_2(OOCR)_{11}$ (Ln = La, Ce), $Ln_2Ti_6O_6(OOCR)_{18}(HO\mathrm{i}Pr)$

Table 6: Synthetic procedures to hafnium oxo clusters and mixed metal clusters

Precursor	RCOOH	RCOOH/ M ratio	M (mol/L)	Solvent	Time	Temp	outcome	Reported yield	Ref
$Hf(OBu)_4$	methacrylic acid	4	1.2	/	1 hour / 15 days	RT / 4 °C	$Hf_4O_2(OOCR)_{12}$	73 %	[158]
$Hf(OBu)_4$	methacrylic acid	7.55	0.34	benzene	1 hour / 20 days	RT / 4 °C	$Hf_6O_4(OH)_4(OOCR)_{12}$ [a]	51 %	[158]
$Hf(OBu)_4$	acetic acid	10	0.52	CH_2Cl_2	1 day	RT	$[Hf_6O_4(OH)_4(OOCR)_{12}]_2$ [a]	98 %	[144]
$Ti(OBu)_4$ $Zr(OBu)_4$ $Hf(OBu)_4$	methacrylic acid	4	1.3	/	1 hour / 20 days	RT 4 °C	$Ti_2Zr_5HfO_6(OOCR)_{20}$	30%	[158]
$ZrCl_4$ $Ti(O^iPr)_4$	acetic acid	16	0.15	ACN	1 day	100 °C	$Ti_8Zr_2O_{12}(OOCR)_{16}$	/	[159]
$ZrCl_4$ $Ti(O^iPr)_4$	propionic acid	12	0.15	ACN	1 day	100 °C	$Ti_8Zr_2O_{12}(OOCR)_{16}$	/	[159]
$ZrCl_4$ $Ti(O^iPr)_4$	benzoic acid	7.27	0.15	DMF	1 day	140 °C	$Ti_8Zr_2O_{12}(OOCR)_{16}$	/	[159]
$ZrCl_4$ $Ti(O^iPr)_4$	p-toluic acid	6.68	0.15	DMF	1 day	140 °C	$Ti_8Zr_2O_{12}(OOCR)_{16}$	/	[159]
$ZrCl_4$ $Ti(O^iPr)_4$	p−^{t}Bu−benzoicacid	5.1	0.15	ACN	1 day	100 °C	$Ti_8Zr_2O_{12}(OOCR)_{16}$	/	[159]
$Ti(O^iPr)_4$ $Y(O(CH_2)_2OMe)_3$	methacrylic acid	7	0.7	/	1 week	RT	$Y_2Ti_4O_4(OOCR)_{14}$ [a]	87 %	[160]
$Ti(O^iPr)_4$ $Ln(acetate)_3$	methacrylic acid	4.5	1.44 - 1.53	/	1-2 weeks	RT	$Ln_2Ti_6O_6(OOCR)_{18}$ [a] (Ln = La, Ce, Nd or Sm) $Ln_2Ti_4O_4(OOCR)_{14}$ [a] (Ln = Sm, Eu, Gd or Ho)	37 - 84 %	[161]
$Ti(O^iPr)_4$ $Ln(acetate)_3$	acetic acid or p-toluic acid or anthracene-9-carboxylic acid	4.55	0.04	ACN / diethyl ehter	2 days	85 °C	$Ln_2Ti_8O_{10}(OH)_2(OOCR)_{16}$ [a] (Ln = Eu or Tb)	20 - 40 %	[20]
$Ti(O^iPr)_4$ $Ln(acetate)_3$	acetic acid	2.9	0.61	ACN	2 days	60 °C	$Ln_2Ti_8O_{10}(OH)_2(OOCR)_{16}$ [a] (Ln = Eu, Tb or Yb)	45 - 49 %	[162]

[a] co-crystallized solvent or carboxylic acid was reported but omitted from this formula

(Ln = La, Ce, Nd, Sm) or $Ln_2Ti_4O_4(OOCR)_{14}(HOOCR)_2$ (Ln = Sm, Eu, Gd, Ho).[161] One clearly observes a preference for a particular structure depending on the size of the lanthanide ion.

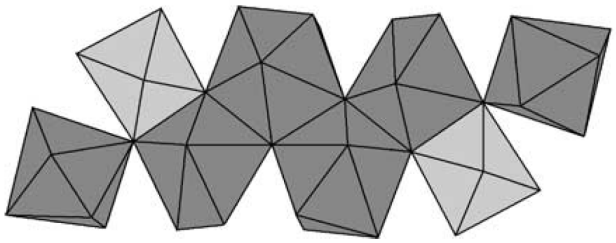

Figure 18: The connected polyhedra of cluster $Ti_2Zr_5HfO_6(OOCR)_{20}$. The light gray octahedra represent the TiO_6 unit. The corners of the polyhedra are oxygen atoms.[158] Reproduced from Ref.[158] with permission from the Royal Society of Chemistry.

More condensed mixed metal clusters were recently synthesized through a solvothermal reaction.[159] The resulting $Ti_8Zr_2O_{12}(OOCR)_{16}$ (R = Me, Et, Ph, Ph-Me, Ph-*t*Bu) clusters can be conceived as an expansion of the **Zr6** cluster core (Figure 19), where the four equatorial zirconium atoms are replaced by a cube of 8 titanium atoms. In the $Ti_8Zr_2O_{12}(OOCR)_{16}$ cluster, four μ_2–O make up the equatorial plane, each bridging two titanium atoms. The $Ti_8O_4^{24+}$ center is connected to a zirconium atom on the top and bottom by eight μ_3–O, resulting in the $Ti_8Zr_2O_{12}^{16+}$ core of the cluster.

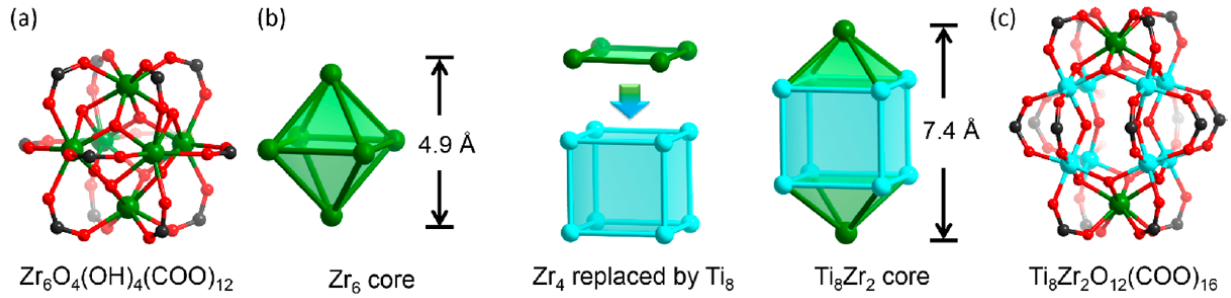

Figure 19: (a) $Zr_6O_4(OH)_4(COO)_{12}$ cluster; (b) the relationship between $Zr_6O_4(OH)_4(COO)_{12}$ and $Ti_8Zr_2O_{12}(COO)_{16}$ clusters; (c) $Ti_8Zr_2O_{12}(COO)_{16}$ cluster.[21] Reprinted with permission from reference.[21] Copyright 2018 American Chemical Society.

Taking almost the same Ti_8 center and attaching two lanthanides atoms instead of zirconium atoms, results in the cluster: $Ln_2Ti_8(\mu_2{-}O)_2(\mu_3{-}O)_8(\mu_2{-}OH)_2^{16+}$ (Ln = Eu,

Tb).[162,163] The only difference in the center is that there are not four μ_2-O bridges, but two and two additional μ_2-OH bridges. This is obviously a charge balancing act as a consequence of replacing one Zr_4^+ with one Ln_3^+. The clusters are capped with acetic acid, p-toluic acid, or anthracene-9-carboxylic acid. The **Eu2Ti8**-acetate cluster has the highest photoluminescence quantum yield (PLQY = 15.6 %) since the PL is quenched by the aromatic ligands. The **Ln2Ti8**-acetate clusters are water soluble and form stable 3-4 nm aggregates.[162] As expected, the PLQY is lower in water (10 %).

4.5 Applications of oxo clusters

4.5.1 Metal organic frameworks (MOFs)

In DMF/methanol mixtures, titanium isopropoxide reacts at 150 °C with terephtalic acid to a MOF (MIL-125) with the $Ti_8O_8(OH)_4(OOCR)_{12}$ cluster as secondary building unit.[164] MIL-125 shows interesting photochromic behaviour: absorbed alcohol reduces Ti(IV) to Ti(III) upon exposure to light, leading to a dark purple color. The Ti(III) is reoxidized in the presence of oxygen. The same MIL-125 MOF can be produced from a pre-synthesized $Ti_8O_8(OOCR)_{16}$ cluster with terephtalic acid in DMF/methanol.[165] The cluster does not retain its exact structure during the MOF synthesis since it is complexed by 16 carboxylates in the original cluster while complexed by 12 carboxylates and 4 hydroxides in the MOF. However, a particular advantage of using the pre-synthesized clusters is that the formation of TiO_2 (a side product of the direct synthesis) is avoided and the yields are higher.[25] Recently, even **Ti44** oxo–alkoxo–carboxo clusters were found to be effective precursors for synthesizing Ti-MOFs with the $Ti_8O_8(OOCR)_{16}$ node.[166] Since the cluster nuclearity has changed, we infer that the titanium oxo cluster can dissolve and reform during MOF synthesis. A further limitation of using preformed oxo clusters could be their solubility. For example, efforts to produce a MOF from $Ti_6O_6(O\mathit{i}Pr)_6(OOCR)_6$ (with OOCR being 4-aminobenzoate) through reversible imine bonds with benzene-1,4-dialdehyde failed due to the low solubility of the cluster.[167]

In 2008, the **Zr6** cluster was first used as building block to create MOFs (UiO-66 and UiO-67) by directly reacting an aromatic dicarboxylic acid and $ZrCl_4$ in DMF (120 °C, 24 hours).[19] Such MOFs had an exceptionally high thermal stability (540°C) and are stable in water, DMF, benzene and acetone. Dehydroxylation of the cluster core starts at 250°C and is completed at 300°C.[19] Two of the four OH bridges leave the structure with an additional proton, yielding a Zr_6O_6 cluster core with a Lewis acidic seven-coordinated zirconium. While the cluster structure is changed considerably, this process maintains the overall integrity of the MOF and is reversible.[19] Incoorporation of trifluoroacetate during the synthesis and its subsequent thermal removal even further enhances the Lewis acidity of UiO-66, evidenced by the enhanced cyclization rate of citronellal to isopulegol.[28] Zr-MOFs are also catalytically active towards peptide bond hydrolysis, thus acting as artificial proteases.[168,169] Many more zirconium MOFs have been developed in the last two decades and these are reviewed elsewhere.[20,21] Also hafnium based MOFs are known, which are often isoreticular with the zirconium MOFs.[170–173]

In 2010, the **Zr6**-methacrylic cluster was used as a well-defined precursor for UiO-66.[174] The reaction conditions were mild (120 °C, 24 hours), but the MOF crystal size was smaller compared to the direct synthesis method from $ZrCl_4$. More interestingly, the direct synthesis of a MOF from $ZrCl_4$ and trans,trans muconic acid failed, while a nanocrystalline MOF (isostructural to UiO-66) was obtained with the **Zr6**-methacrylic cluster, even at room temperature. In another example, the **Zr12**-acetate cluster was used as precursor and depending on the linker, the dimeric nature of cluster was retained in the final MOF.[150] Also mixed metal clusters were used as precursors for MOFs.[21,159] Several MOFs were recently synthesized at room temperature by mechanochemical synthesis from the **Zr6**-methacrylate cluster or the **Zr12**-acetate cluster.[152,175] In this way, the highest quality UiO-97 was obtained, which a surface area of 2250 m^2/g, and outstanding catalytic activity in the hydrolysis of dimethyl 4-nitrophenyl phosphate (a nerve agent).[152] Multimetallic MOFs were recently produced via mechanochemical synthesis by combining **Zr12**-acetate and **Hf12**-acetate clusters with

bridging ligands.[173] The above results suggest that the zirconium and hafnium oxo clusters remain intact during MOF synthesis.

4.5.2 Polymer and all-inorganic composites

Zr6-methacrylate clusters have 12 methacrylate ligands with each a polymerizable double bond. Schubert *et al.* used these clusters as cross-linkers during the radical polymerization of methylmethacrylate or styrene.[176–178] While cluster fractions of 0.5-1 mol% (equivalent to 3.2-6.3 w%) yield glassy, transparent polymers, a white solid is obtained for 2 mol% or 100 mol% (no monomer added). In contrast to undoped polymer, the cluster-polymer composites were insoluble. They only swell in solvent, the extent of which decreases with increasing cluster concentration (= increasing cross-linking density). The composites have also a higher thermal stability because thermal depolymerization is inhibited. The **Zr4**-methacrylate cluster reacts similarly and can achieve an even higher cross-linking density, possibly due to its more open structure.[137,177,179] Polymerization with 10 w% of **Zr4**-methacrylate, results in a improved bend strength (47 MPa) and improved bend modulus (1900 MPa). The composite maintains its strength even after storage in water for seven days. In general, there are two effects in such composites: cross-linking and inert filler effect.[180] The higher cross-linking ability causes the decrease in the swellability and the increase in glass transition temperature. The filler effect delays the thermal degradation. Oxo clusters also improved the mechanical properties of shape memory materials without compromising the shape memory effect itself.[181] Next to the mechanical properties, also the (di)electrical properties are influenced by the inclusion of oxo clusters (conductivity, dielectric constant, etc).[182] The **Zr4**-methacrylate cluster has also been used in a photopolymerization process with methylmethacrylate monomer, producing hard and transparent coatings.[183] Depending on the type of carboxylic acid, the clusters can be used in other types of polymerization reactions as well. **Zr6** clusters capped with 5-norbornene-2-carboxylic acid were used as cross linkers in ring opening metathesis polymerizations.[139] **Zr12** clusters capped with 3-mercaptopropionic

acid were embedded in polymethylmethacrylate using a photothiol-ene polymerization.[145,184] The cluster reinforced polymer featured improved hardness. The above composite materials fit in a wider class of cluster-reinforced polymers featuring also titanium, tin, silicon, and tungsten oxo clusters.[135,185,186] The effect of oxo clusters on the structural and functional properties of these organic-inorganic composites was reviewed in more detail elsewhere.[187]

Going one step further, **Zr4** or **Hf4**-methacrylate clusters were co-polymerized with (hydrolyzed) methacryloxymethyl)triethoxysilane and subsequently calcined at 800 - 1000 °C.[188,189] The resulting all-inorganic composites consisted of silica and ZrO_2 or HfO_2 nanoparticles. A portion of the nanoparticles was crystalline but the majority was amorphous. By combining both **Zr4** and **Hf4**-methacrylate clusters, the ternary system ZrO_2–HfO_2–SiO_2 was accessed.[190] This strategy of using composite precursors was thoroughly reviewed elsewhere.[191]

Zirconium and hafnium oxo clusters have received increasing attention as building block for extreme UV patterning, and 3D printing.[22,151] The principle is similar as with the composites but here the photosensitivity of the methacrylate ligands is exploited to cross-link the cluster and thus change their solubility. The resolution of the laser determines the resolution of the final pattern or even 3D structure.

4.5.3 Oxo cluster catalysts

Zr6-methacrylate and **Zr12**-vinylacetate clusters were used to activate hydrogen peroxide.[23] Under these oxidative conditions, Zr-peroxo complexes are formed, which serve as catalysts for the oxidation of methyl p-tolyl sulfide to its corresponding sulfoxide and sulfone. This is a model reaction for the oxidative desulfurization of fuels. Improved performance was achieved by using **Zr4**-methacrylate clusters and incorporation in polymer composites.[138,192,193] On the other hand, $Hf_{18}O_{10}(OH)_{26}(SO_4)_{13} \cdot (H_2O)_{33}$ clusters were used as heterogeneous catalyst for the selective hydrolysis of proteins.[24]

5 Colloidal metal oxide nanocrystals

Nonaqueous strategies are very effective in producing highly crystalline oxide nanocrystals. A comprehensive, general overview of the different mechanisms in nonaqueous synthesis is provided elsewhere.[194,195] In the following overview of group 4 oxide nanocrystals, we make a distinction between surfactant-free and surfactant-assisted strategies. We will discuss synthetic strategies, surface chemistries, and the current level of mechanistic insight (also pointing out areas that require more research). Finally, we highlight several applications of group 4 metal oxide nanocrystals.

5.1 Surfactant-free synthesis

In the absence of surfactants, nonaqueous chemistry often provides amorphous gels. A prime example is the formation of titania gels from titanium chloride and titanium isopropoxide, which was discussed in section 3.3. However under particular conditions, crystalline nanoparticles can be obtained. Benzyl alcohol turned out to be one of the most versatile solvents in this respect.[196] A metal precursor is typically dissolved in benzyl alcohol and heated in a pressurized vessel (steel bomb or microwave vessel) and a nanocrystal powder is retrieved at the end of the reaction. Table 7 provides an overview of the group 4 oxide nanocrystal syntheses in benzyl alcohol and these reactions are discussed in more details in the following sections. Despite the fact that these syntheses result in aggregated powders it is often possible to functionalize the nanocrystal surface with ligands to obtain stable colloidal dispersions with minimal or no residual agglomeration. Stability in nonpolar solvent is typically provided by fatty acids,[197–201] and stability in polar solvents is achieved using 2-[2-(2-methoxyethoxy)ethoxy]acetic acid,[202–204] or 2-aminoethyl phosphoric acid.[15]

Table 7: Synthetic procedures to synthesize group 4 oxide nanocrystal in benzyl alcohol.

MO_2	Precursor	[M] (mol/L)	Temp.	time	crystal phase	size (nm)	reported yield	Ref
TiO_2	$TiCl_4$	0.11	40 °C	7 days	anatase	4.0	/	[205]
TiO_2	$TiCl_4$	0.22	40 °C	7 days	anatase	4.1	/	[205]
TiO_2	$TiCl_4$	0.45	40 °C	7 days	anatase	5.0	/	[205]
TiO_2	$TiCl_4$	0.90	40 °C	7 days	anatase	5.6	/	[205]
TiO_2	$TiCl_4$	0.45	50 °C	24 h	anatase	5.0	/	[205]
TiO_2	$TiCl_4$	0.45	75 °C	24 h	anatase	6.1	/	[205]
TiO_2	$TiCl_4$	0.45	100 °C	24 h	anatase	7.3	/	[205]
TiO_2	$TiCl_4$	0.45	150 °C	24 h	anatase	8.3	/	[205]
ZrO_2	$ZrCl_2OPr$	0.27	200 °C	3 min[a]	cubic	2.3	98 %	[206]
ZrO_2	ZrO^iPr	0.17	210 °C	3 days	cubic	3.5	/	[200]
ZrO_2	ZrO^iPr	0.29	210 °C	2 days	cubic	3 - 4	95 %	[197]
ZrO_2	ZrO^nPr	0.32	220 °C	3 days	monoclinic + tetragonal	4.5	/	[203]
ZrO_2	ZrO^nPr	0.32	270 °C	3 days	tetragonal	4.5	/	[203]
ZrO_2	ZrO^iPr	0.13	270 °C	4 h[a]	cubic	3 - 4	98 %	[199]
ZrO_2	ZrO^iPr	0.13	230 °C	6 h[a]	cubic	3.0	23 %	[199]
ZrO_2	$ZrCl_4$	0.13	230 °C	6 h[a]	monoclinic	3.8	95 %	[199]
ZrO_2	ZrOEt	0.13	230 °C	6 h[a]	cubic	3.0	25 %	[199]
ZrO_2	$Zr(ac)_4$	0.13	230 °C	6 h[a]	cubic	2.8	47 %	[199]
ZrO_2:Eu	ZrO^iPr + $Eu(ac)_3$	0.29	230 °C	3 days	cubic	3 - 4	/	[207]
ZrO_2:Eu	ZrO^nPr + $Eu(ac)_3$	0.19	230 °C	3 days	cubic	3 - 4	81 %	[15]
ZrO_2:Tb	ZrO^nPr + $Tb(ac)_3$	0.19	230 °C	3 days	cubic	3 - 4	81 %	[15]
HfO_2	HfO^tBu	0.04	300 °C	2 days	monoclinic	3.0	/	[206]
HfO_2	HfOEt	0.07	250 °C	2 days	monoclinic	6 × 3	/	[208]
HfO_2	$HfCl_4$	0.03	220 °C	3 days	monoclinic	4 - 9	/	[209]
HfO_2	$HfCl_4$	0.01	220 °C	3 days	monoclinic	5.0	quant.	[210]
HfO_2	$HfCl_4$	0.03	220 °C	3 h[a]	monoclinic	4.0	quant.	[210]
HfO_2	$HfCl_4$	0.09	220 °C	3 h[a]	monoclinic	5.0	/	[198]
HfO_2	HfO^tBu	0.12	220 °C	4 days	monoclinic	4.0	/	[204]
HfO_2:Eu	HfO^tBu + $Eu(ac)_3$	0.12	220 °C	4 days	cubic[b]	3.0	/	[211]
HfO_2:Tb	HfO^tBu + $Tb(ac)_3$	0.12	220 °C	4 days	cubic[b]	3.0	/	[211]
HfO_2:Lu	HfO^tBu + $Lu(ac)_3$	0.12	220 °C	4 days	cubic[b]	3.0	/	[211]

[a] microwave heating [b] For doping percentages higher than 8 %, otherwise monoclinic.

5.1.1 Titania nanocrystals

In the reaction of $TiCl_4$ and benzyl alcohol, TiO_2 NCs are formed with a size that can be tuned (4-8 nm) by changing the reaction conditions.[205] Higher temperature and higher precursor concentration lead to larger NC sizes, see also Table 7. Under all conditions (as low as 40 °C), the anatase crystal phase of titania is retrieved (Figure 20). The addition of dopamine or 4-tert-butylcatechol allows dispersing the nanocrystals in water or tetrahydrofuran respectively.[212]

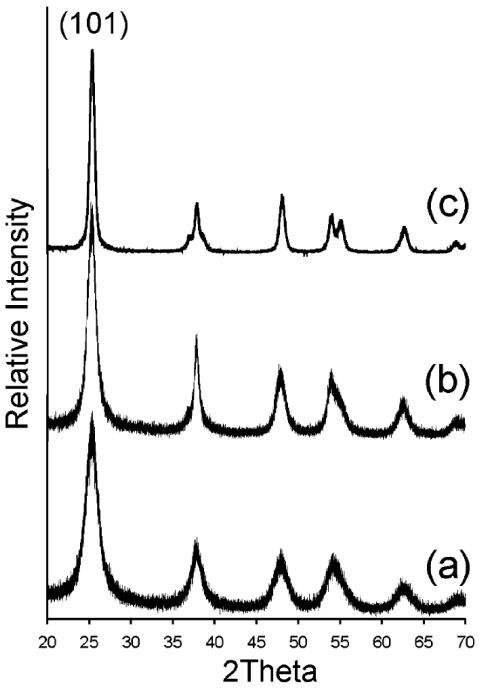

Figure 20: XRD powder patterns of nanocrystalline anatase samples prepared with a constant benzyl alcohol to $TiCl_4$ ratio of 20 at (a) 40 °C, (b) 100 °C, and (c) calcined at 450 °C.[213] Reprinted with permission from reference.[213] Copyright 2002 American Chemical Society.

Regarding the precursor chemistry, alkoxo species are formed *in– situ* by ligand exchange.

$$TiCl_4 + x\,BnOH \longrightarrow TiCl_{4-x}(OBn)_x + x\,HCl \tag{36}$$

Given the general reactivity of titanium chloride towards alcohols (see section 3), x is most

likely two. The formed chloroalkoxide species can condense to metal oxide nanocrystals, eliminating benzyl chloride (or benzyl ether, to a lesser extent).

$$\mathrm{TiCl_2(OBn)_2} \longrightarrow \mathrm{TiO_2} + 2\,\mathrm{BnCl} \tag{37}$$

The condensation reaction likely follows a mechanism involving a pre–coordination and an S_N1 nucleophile substitution (Figure 21). This is supported by the stability of the benzyl carbocation and the low reaction rate of primary alcohols.[214,215]

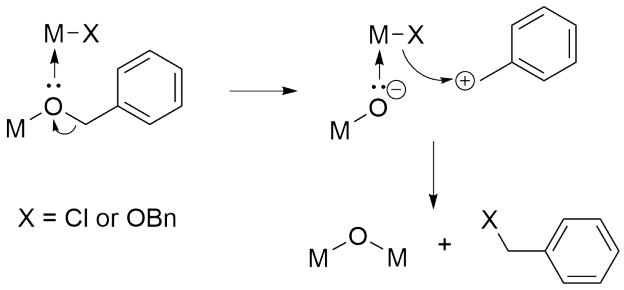

Figure 21: Condensation reaction (alkyl halide or ether elimination) according to a mechanism of pre–coordination and S_N1 nucleophilic substitution.

As an alternative to the ligand exchange pathway (Equation 36), it was proposed that benzyl alcohol could react directly with titanium chloride (Equation 38).[195]

$$\mathrm{Ti{-}Cl} + \mathrm{ROH} \longrightarrow \mathrm{Ti{-}OH} + \mathrm{RCl} \tag{38}$$

The two pathways are hard to distinguish since both essentially yield HCl and benzyl chloride as co-products after condensation. The presence of some amount of benzyl ether in the reaction mixture seems to support the ligand exchange pathway,[194] but a more detailed kinetic study is necessary to distinguish between the different mechanisms.

Regarding the crystallization mechanism, detailed (*in–situ*) x-ray scattering studies have shown that the particles are slightly anisotropic (elongated along the c-axis) and only formed after an induction time of 60 min at a reaction temperature of 85 °C.[216] The nanocrystals grow first isotropically, and subsequently switch to anisotropic growth.[216] The yield devel-

opment could be fitted by a sigmodial growth curve, with an additional sedimentation term. Sigmoidal kinetics are typically related to autocatalytic processes,[217] but the precise underlying mechanism is still unclear. Interestingly, these kinetics are highly reminiscent of the ones observed by Vioux, see section 3.3.

Also other solvents can be used in the nonaqueous synthesis of titania. The tertiary alcohol *tert*–butanol readily reacts with $TiCl_4$ to TiO_2 NCs (3 nm) at 80 °C.[218] When TiF_4 is used, the *tert*–butyl fluoride product was detected using ^{19}F NMR, which is the expected product for the S_N1 alkylhalide elimination mechanism.[219] On the other hand, the reaction of $TiCl_4$ with *tert*–amyl alcohol at 80 – 100 °C results in TiO_2 NCs and follows predominantly an E1 mechanism. The stable tertiary carbocation eliminates a proton and titanium hydroxide is formed, see Figure 22.[220] The titanium hydroxide further condenses to titania, with the elimination of water. The results in amyl alcohol bring up the question whether the E1 elimation is also active for the reaction in *tert*–butanol.

$$2\mathrm{Ti{-}OH} \longrightarrow \mathrm{Ti{-}O{-}Ti} + \mathrm{H_2O} \tag{39}$$

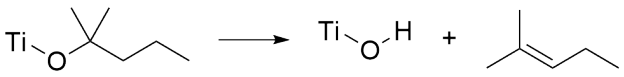

Figure 22: Precursor decomposition according to an E1 mechanism.

A similar E1 elimination pathway was found during the synthesis of TiO_2 from titanium isopropoxide in benzylamine at 200 °C.[221] Benzylamine does not exchange for isopropoxide due to the unfavorable pKa difference. It is interesting that isopropylether was not detected, thus excluding the S_N1 pathway. Instead titanium isopropoxide releases propene and forms titanium hydroxide. The latter condenses with titanium isopropoxide motieties to oxide and releases isopropanol.

$$\mathrm{TiOH} + \mathrm{RO{-}Ti} \longrightarrow \mathrm{Ti{-}O{-}Ti} + \mathrm{HOR} \tag{40}$$

Even though benzylamine also self-condenses to dibenzylamine – producing ammonia, TiO_2

was formed and not TiN, showcasing the high oxophilicity of titanium.

5.1.2 Zirconia nanocrystals

ZrO_2 NCs have been synthesized via an S_N1 nucleophile substitution mechanism. Smarsly *et al.* first synthesized $ZrCl_2(OR)_2$ from zirconium chloride via two steps (Equations 41–42) or from zirconium propoxide and acetyl chloride (Equation 25).[206]

$$ZrCl_4 + \text{excess}ROH \longrightarrow ZrCl_3OR + HCl \tag{41}$$

$$2\,ZrCl_3OR + Zr(OR)_4 \longrightarrow ZrCl_2(OR)_2 \tag{42}$$

The resulting precursor is mixed with hexanol and benzyl alcohol and ZrO_2 NCs (2-2.5 nm) are formed in a few minutes at 200 °C under microwave radiation, see Figure 23. Benzyl chloride was found as the main reaction by–product, confirming the mechanism. Only at an equal ratio of alkoxide to chloride, crystalline material (cubic zirconia) was obtained. The nanocrystals are dispersible in water, up to 45 w% ZrO_2.

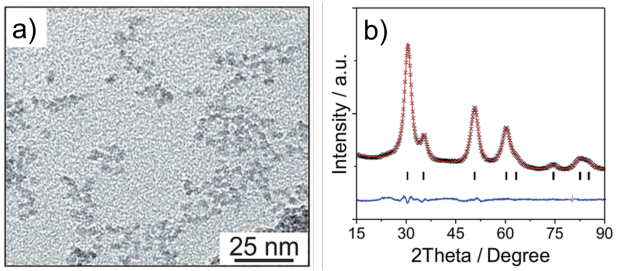

Figure 23: ZrO_2 nanocrystal synthesized from $ZrCl_2(OR)_2$ in benzylalcohol. (A) TEM image and (B) XRD diffractogram showing cubic zirconia.[206] Reproduced from Ref.[206] with permission from the Royal Society of Chemistry.

ZrO_2 NCs are also produced on a large scale by reacting zirconium isopropoxide (complexed with isopropanol) in benzyl alcohol for 2 days at 210 °C.[197,200] Benzyl ether and isopropanol were detected by ^{13}C NMR as the main reaction by–products, suggesting ligand

exchange as a first step.

$$\mathrm{Zr(O}i\mathrm{Pr)_4 + x\,BnOH \longrightarrow Zr(O}i\mathrm{Pr)_{4-x}(OBn)_x + x\,}i\mathrm{PrOH} \tag{43}$$

In a second step, the alkoxide groups condense to form the oxide.

$$\mathrm{Zr{-}OBn + BnO{-}Zr \longrightarrow Zr{-}O{-}Zr + Bn{-}O{-}Bn} \tag{44}$$

After synthesis, the particles can be easily dispersed in nonpolar solvents by the addition of carboxylic acids, e.g., octadecanoic acid (Figure 24). Using zirconium isopropoxide, the NCs are 3-4 nm in size and have the cubic crystal structure. However, using the cheaper zirconium *n*-propoxide (70 w% in propanol), the NCs are 4.5 nm and a mixture of tetragonal and monoclinic zirconia.[203] The monoclinic fraction can be minimized by performing the reaction at 270 °C but the resulting particles cannot be dispersed with carboxylic acids. A note is in order regarding the distinction between the cubic and tetragonal phase of zirconia. Due to the broadening of the refections, XRD cannot make the distinction and other techniques such as Raman spectroscopy,[203] or x-ray Pair Distribution Function analysis are required.[222] It is likely that most (if not all) of the cubic phases that are mentioned in this section are actually tetragonal.

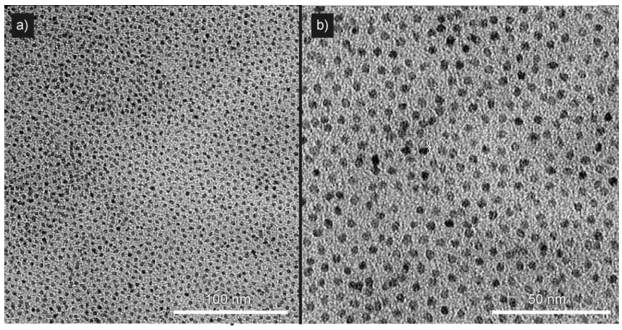

Figure 24: TEM images of ZrO_2nanocrystals after post-functionalization with octadecanoic acid at two different magnifications.[197] Copyright © 2007 WILEY-VCH Verlag GmbH & Co. KGaA, Weinheim.

The reaction of zirconium isopropoxide in benzyl alcohol can be accelerated under mi-

crowave heating and reaches full yield after 4 hours at 270 °C.[199] Here, 4 nm tetragonal (or cubic) zirconia is obtained. At 230 °C, zirconium isopropoxide, zirconium ethoxide, or zirconium acetate yield tetragonal zirconia while zirconium chloride yields monoclinic zirconia (see also Table 7). The difference in crystal structure was ascribed to the presence of HCl in the latter reaction mixture.[199] The presence of water can also steer the outcome of the synthesis and is even capable of transforming tetragonal ZrO_2 NCs into monoclinic NCs upon prolonged heat treatment at 210 °C.[223] Small amounts of water, generated by ZrO_2-catalyzed alcohol dehydration, cause monoclinic impurities in the final product. By adding sodium as a dessicant to the reaction mixture, phase pure tetragonal ZrO_2 was obtained.

5.1.3 Hafnia nanocrystals

Monoclinic HfO_2 NCs were synthesized from $Hf(OEt)_4$ in benzyl alcohol at 200 °C. The NCs are ellipsoidal with a long axis of around 6 nm and a short axis of 3 nm. The by-products are mainly dibenzyl ether, with trace amounts of ethyl benzyl ether.[208] Diethyl ether was not detected. Therefore, it was concluded that the first step in this mechanism is ligand exchange between ethoxide and benzyl alcohol.

$$\mathrm{Hf(OEt)_4 + x\,BnOH \longrightarrow Hf(OEt)_{4-x}(OBn)_x + x\,EtOH} \tag{45}$$

In a second step, the alkoxide groups condense to form the oxide.

$$\mathrm{Hf{-}OR + RO{-}Hf \longrightarrow Hf{-}O{-}Hf + R{-}O{-}R} \tag{46}$$

Primary alcohols are ideal substrates for S_N2 reactions and benzyl alcohol is both reactive in a S_N1 and S_N2 mechanism. Since the ethyl ethers were hardly observed, the condensation reaction most likely proceeds through an S_N1 mechanism, as shown before in Figure 21.

When hafnium *tert*-butoxide is heated in benzyl alcohol at 300 °C, 3 nm monoclinic hafnia is obtained after 48 hours.[224] Similar particles (4 nm) are obtained by heating the mixture

at 220 °Cfor 4 days.[204] When the same precursor is heated in benzylamine, 2.6 nm cubic hafnia is obtained.[224] Given the absence of an ether elimination mechanism in benzylamine, we speculate that the oxide is formed by an E1 mechanism. The oxygen deficient reaction mixture is most likely responsible for oxygen vacancies and thus stabilization of the cubic phase.

The synthesis of monoclinic HfO_2 NCs from $HfCl_4$ in benzyl alcohol at 220 °C also delivers large quantities of dibenzylether.[209,210] The process probably involves a ligand exchange, releasing HCl.

$$HfCl_4 + x\,BnOH \longrightarrow HfCl_{4-x}(OBn)_x + x\,HCl \tag{47}$$

The formed alkoxo ligands can undergo an ether elimination condensation. However, it cannot be fully excluded that benzyl chloride was transiently formed and subsequently reacted with benzyl alcohol to dibenzyl ether and HCl. The large excess of ether (up to 80 % of the final reaction mixture) is due to the Williamson ether synthesis, catalyzed by HCl. When the reaction is performed over three days with conventional heating in a pressure bomb, the nanocrystals are slightly larger (5 nm) compared to three hours of microwave heating (4 nm).[210] In both cases, full yield was achieved. After microwave synthesis, the nanocrystal aggregates can be dispersed in ethanol or water, since they are charge stabilized by HCl (produced during synthesis), see Figure 25. The aggregates can be broken up in chloroform by a combination of carboxylic acid ligands and a suitable base. The base is necessary to remove the initially present HCl from the surface. In nonpolar solvents, HCl cannot be displaced by carboxylic acids because HCl is a stronger acid. However, under basic conditions, the carboxylate anion outcompetes the chloride ligand (Figure 26).[198,225]

5.1.4 Lanthanide doped zirconia and hafnia nanocrystals

The benzyl alcohol route can also produce ZrO_2 and HfO_2 NCs doped with lanthanides. Europium acetate and zirconium isopropoxide isopropanol complex react at 230 °C to cubic zirconia, with varying doping levels from 1-13 %.[207] Note the higher temperature required

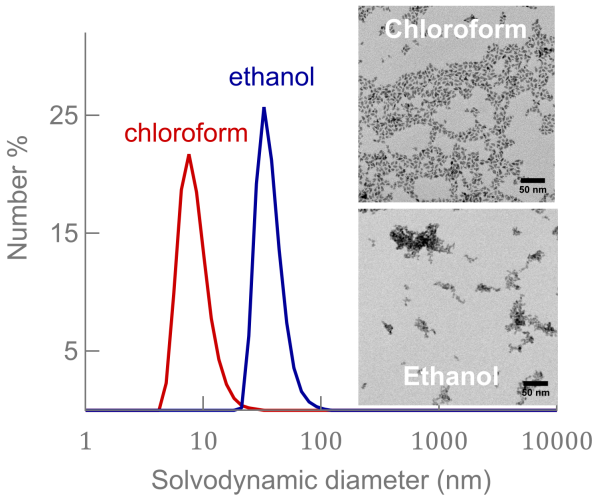

Figure 25: Size distribution by DLS of HfO_2 NCs dispersed in either ethanol (as synthesized) or chloroform (with dodecanoic acid and oleylamine, dispersion was five times purified). The insets show the corresponding TEM images.[198] Reprinted with permission from reference.[198] Copyright 2014 American Chemical Society

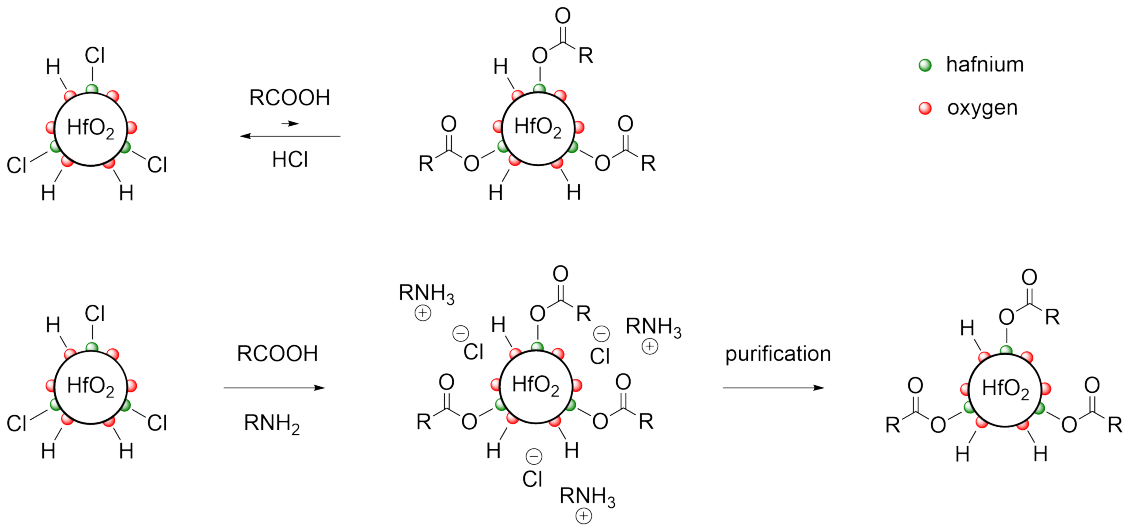

Figure 26: The exchange of HCl for carboxylic acids is unfavorable due to the pKa difference. By adding a base (amine), the proton transfer step is eliminated and carboxylate can replace chloride.

compared to the pure zirconia synthesis (210 °C). The NCs are 4 nm in size and have an optimized PLQY of 8.7 % at 11 % Eu doping. The nanocrystals can be dispersed in chloroform by eicosanoic acid. A similar procedure with zirconium *n*-propoxide and either europium or terbium acetate also produces excellent yields (80 %).[15] The particles could be dispersed in water by a surface functionalization with 2-aminoethyl phosphoric acid. The Eu-doped particles have red emission (PLQY = 33 %) and the terbium doped particles have green emission (PLQY = 5 %), see Figure 27. Lanthanide doped HfO_2 NCs were synthesized from the corresponding lanthanide acetate, hafnium tertbutoxide and benzyl alcohol at 220°C.[211] Below 5 % lanthanide doping, the monoclinic structure is obtained, while above 5 % the cubic structure is stabilized.

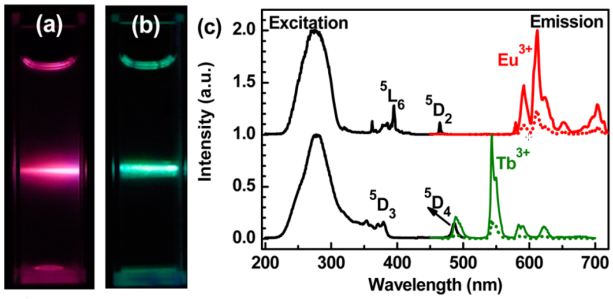

Figure 27: (a) Eu-doped ZrO_2 (10 mol % Eu) and (b) Tb-doped ZrO_2 (10 mol % Tb) nanocrystals in water. (c) PL excitation (left) and PL emission (right) spectra for both types of nanocrystals when either indirectly excited at 280 nm (solid line) or directly excited at 395 nm for Eu and at 380 nm for Tb (dotted line).[15] Reprinted with permission from reference.[15] Copyright 2012 American Chemical Society.

5.2 Surfactant-assisted synthesis

Surfactant-assisted syntheses generally lead to the highest quality of nanocrystals, especially regarding polydispersity and colloidal stability. For the group 4, a popular and powerful strategy involves the reaction of metal halides with metal alkoxides in tri-*n*-octylphosphine oxide above 300°C. Other methods are typically based on nucleophilic substitution (ester or amide formation).

5.2.1 Reaction of metal chlorides with metal alkoxides

Table 8: Synthetic procedures to synthesize group 4 oxide nanocrystal via surfactant assisted reactions between metal chloride and metal alkoxides.

MO_2	surfactant	Precursors	[M] (mol/kg)	Temp.	time	crystal phase	size (nm)	reported yield	Ref
TiO_2	1.6 eq TOPO	TiF_4 + TiO^iPr	0.2	300 °C	5 min	anatase	9.2	< 50 %	[226]
TiO_2	1.6 eq TOPO	$TiCl_4$ + TiO^iPr	0.2	300 °C	5 min	anatase	7.3	< 50 %	[226]
TiO_2	13.0 eq TOPO	$TiCl_4$ + TiO^iPr	0.2	300 °C	5 min	anatase	5.5	< 50 %	[226]
TiO_2	1.6 eq TOPO	$TiBr_4$ + TiO^iPr	0.2	300 °C	5 min	anatase	6.1	< 50 %	[226]
TiO_2	1.6 eq TOPO	TiI_4 + TiO^iPr	0.2	300 °C	5 min	anatase[a]	3.8	< 50 %	[226]
TiO_2	4.7 eq TOPO 0.5 eq Lauric acid	$TiCl_4$ + TiO^iPr	0.3	300 °C	20 min	anatase	3.5 × 12-18	/	[227]
TiO_2	4.2 eq TOPO 1 eq Lauric acid	$TiCl_4$ + TiO^iPr	0.3	300 °C	20 min	anatase	2.7 × 14-22	/	[227]
TiO_2	2.2 eq TOPO 2 eq Lauric acid	$TiCl_4$ + TiO^iPr	0.3	300 °C	20 min	anatase	2.7 × 17-28	/	[227]
ZrO_2	5.8 eq TOPO	$ZrCl_4$ + ZrO^iPr	0.45	340 °C	2 h	tetragonal	4.0	90 %	[68]
ZrO_2	5.8 eq TOPO	$ZrBr_4$ + ZrO^iPr	0.45	340 °C	2 h	tetragonal	3.0	/	[68]
ZrO_2	5.8 eq TOPO	$ZrCl_4$ + ZrO^iPr	0.45	340 °C	2 h	tetragonal	4.0	46 %	[97]
ZrO_2	5.8 eq TOPO	$ZrCl_4$ + ZrO^iPr	0.45	340 °C	2.5 h	tetragonal	3.7	49 %	[228]
ZrO_2	6.5 eq TOPO	$ZrCl_4$ + ZrO^iPr	0.4	340 °C	2 h	tetragonal	4.0	60 %	[229]
HfO_2	6.5 eq TOPO	$HfCl_4$ + HfO^iPr	0.4	360 °C	2 h	tetragonal[b]	5.5	/	[42]
HfO_2	6.5 eq TOPO	$HfCl_4$ + HfO^iPr	0.4	400 °C	2 h	monoclinic	3.4 × 7.6	/	[42]
HfO_2	6.5 eq TOPO	$HfBr_4$ + HfO^iPr	0.4	360 °C	2 h	monoclinic	3.7	/	[42]
HfO_2	6.5 eq TOPO	$HfCl_4$ + HfO^iPr	0.4	340 °C	2 h	monoclinic	2.4 × 6.9	/	[66]
HfO_2	6.5 eq TOPO	$HfCl_4$ + HfO^tBu	0.4	340 °C	2 h	monoclinic	2.3 × 13	/	[62]
HfO_2	6.5 eq TOPO	$HfCl_4$ + HfO^iPr	0.4	360 °C	2 h	monoclinic	3.5 × 9.2	/	[230]
HfO_2	1.5 eq OLAm	$HfCl_4$ + HfO^iPr	0.4	315 °C	2 h	monoclinic	2.6 × 10.5	/	[230]
HfO_2: Ce	6.5 eq TOPO	$HfCl_4$ + CeO^tBu	0.4	340 °C	2 h	tetragonal	3.1	/	[72]
HfO_2: La	6.5 eq TOPO	$HfCl_4$ + LaO^iPr	0.4	340 °C	2 h	tetragonal	3.3	/	[72]
$Zr_xHf_{1-x}O_2$	6.5 eq TOPO	$ZrCl_4$ + HfO^iPr	0.4	360°C	2 h	tetragonal	4.3	/	[42]
$Zr_xHf_{1-x}O_2$	6.5 eq TOPO	$HfCl_4$ + ZrO^iPr	0.4	360°C	2 h	tetragonal	4.6	/	[42]
$Zr_xHf_{1-x}O_2$	6.5 eq TOPO	$HfCl_4$ + ZrO^iPr	0.4	340°C	2 h	tetragonal	5.6	/	[66]
$Zr_xHf_{1-x}O_2$	6.5 eq TOPO	$ZrCl_4$ + HfO^iPr	0.4	340°C	2 h	tetragonal	5.6	/	[66]
$Zr_xHf_{1-x}O_2$	6.5 eq TOPO	$HfCl_4$ + ZrO^tBu	0.4	340°C	2 h	monoclinic	2.5 × 5.7	/	[66]
$Zr_xHf_{1-x}O_2$	6.5 eq TOPO	$ZrCl_4$ + HfO^tBu	0.4	340°C	2 h	monoclinic	2.8 × 5.1	/	[66]

[a] with a small rutile impurity [b] with a small monoclinic impurity

Titanium oxide nanocrystals. In 1999, Colvin et al reported the synthesis of anatase TiO_2 NCs, see Figure 28.[226] Titanium chloride was dissolved in heptadecane with 12.5 m% tri–*n*–octylphosphine oxide (TOPO) as surfactant (1.6 equivalents to Ti), and titanium isopropoxide was injected at 300 °C.

$$TiCl_4 + Ti(OiPr)_4 \xrightarrow[TOPO,\, heptadecane]{0.2\, mol/kg,\, 300°C} 2\, TiO_2 + 4\, iPrCl \tag{48}$$

The nanocrystals are very crystalline but somewhat aggregated and irregular in size and shape. In the absence of TOPO, the reaction is finished in seconds and the crystallite size is

above 10 nm. In the presence of TOPO, the reaction slows down (5 min until completion) and yields smaller nanocrystals (5.5 nm in pure TOPO and 7.3 nm in the mixture). This is consistent with surfactant binding to the nanocrystal surface, slowing down the particle growth rate, leading to more particles with smaller sizes.[231]

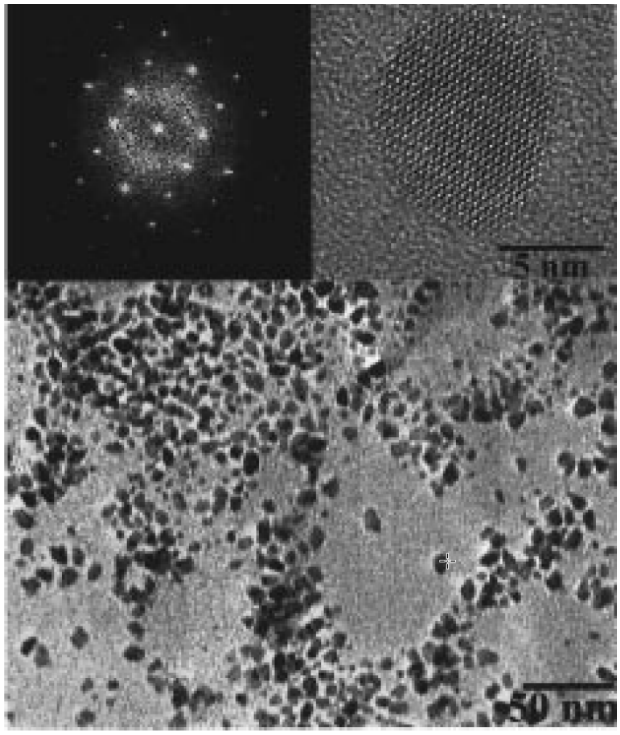

Figure 28: TEM characterization of anatase titania nanocrystals synthesized from titanium chloride and titanium isopropoxide in TOPO/heptadecane at 300°C.[226] Reprinted with permission from reference.[226] Copyright 1999 American Chemical Society.

Also other titanium halide and alkoxides can be used. While the reaction rate is insensitive to the halide, it increases with the branching of the alkoxide (Me < Et < *i*Pr < *t*Bu). This confirms again that the reaction proceeds primarily through an S_N1 or E1 mechanism. Surprisingly, the reaction rate did not have an influence on the nanocrystal size. Varying the halide from fluoride to iodide did change the size from 9.2 nm to 3.8 nm. Note that using TiI_4, a small rutile impurity was detected via XRD. The impact of the halide on size and crystal structure is not surprising since HCl was found bound to the TiO_2 NC surface, together with hydrogen bonded TOPO and also dioctylphsophinic acid (a decomposition product of TOPO).[97] As such, we hypothesize that the larger halide ligands slow the growth

rate of the nanocrystals. Under basic conditions (presence of amine), all original surface species can be exchanged for oleic acid, yielding a uniform ligand shell.[97]

The reaction products where charaterized via GC–MS and in case of $Ti(OEt)_4$, mostly ethylchloride was detected. In case of $Ti(O\mathit{i}Pr)_4$, propene and 2–chloropropane was detected. The presence of propene could be due to a competing E1 mechanism (see above) or because of the dehalogenation reaction of 2–chloropropane:

$$CH_3{-}CHCl{-}CH_3 \longrightarrow CH_2{=}CH{-}CH_3 + HCl \tag{49}$$

To explain the formation of crystalline material and not the formation of gels, the authors hypothesized that the titanium halide is the crystallization agent.[226] However, upon injection of the second precursor, ligand redistribution competes with direct halide elimination. As a result titanium chloroisopropoxides are formed. It is possible that simply the high reaction temperature or the presence of HCl (see further) provides the necessary energy to induce chemical reversibility and allow the elimination of defects. Other researchers obtained (poorly crystalline) anatase TiO_2 upon injection of titanium isopropoxide in TOPO at 300 °C, without titanium chloride.[3] This reaction most likely follows the E1 pathway.

Alivisatos *et al.* used a similar procedure but introduced lauric acid as a co–surfactant and varied the TOPO/lauric acid ratio while keeping the total amount of surfactant at 5.2 equivalents to Ti.[227] Low concentrations of lauric acid yielded bullet (3.5 × 12 nm) and diamond (3.5 × 18 nm) shaped NCs. High concentrations of lauric acid delivered nanorod with lengths up to 28 nm. The authors attributed the anisotropic growth to selective binding of lauric acid to the (001) facets. When the nanorods are left in the reaction mixture for 24 hours, they ripen to spheres.[227]

Zirconium oxide nanocrystals. Zirconium chloride and zirconium isopropoxide isopropanol complex are dissolved at 80 °C in pure, molten TOPO and heated to 340 °C for 2 hours to form 4 nm ZrO_2 NCs, see Figure 29.[68] While originally $ZrCl_4$ was used,[68] its

polymeric structure causes irreproducibility in dissolution and instead the monomeric THF complex was introduced.[97]

$$1.25\ \mathrm{ZrCl_4} + \mathrm{Zr(O}i\mathrm{Pr)_4} \cdot i\mathrm{PrOH} \xrightarrow[TOPO]{0.45\,mol/kg,\,340^\circ\mathrm{C}} 2.25\ \mathrm{ZrO_2} + 5\ i\mathrm{PrCl} \tag{50}$$

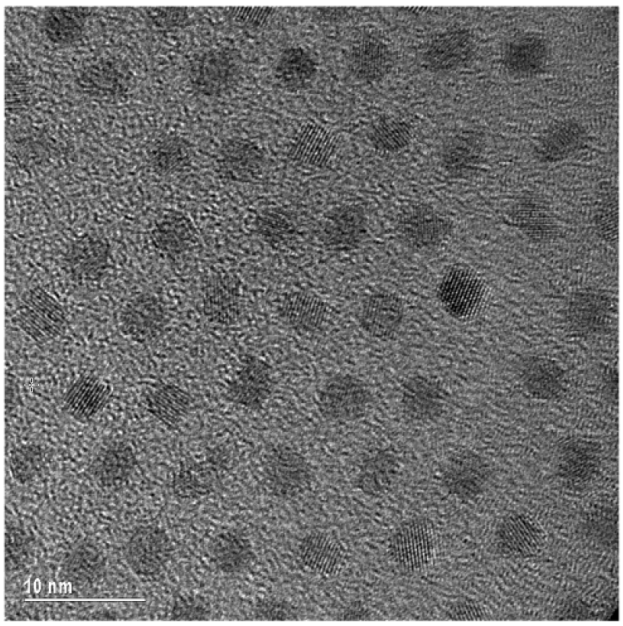

Figure 29: Zirconia nanocrystals synthesized in TOPO from zirconium chloride and zirconium isopropoxide.[68] Reprinted with permission from reference.[68] Copyright 2003 American Chemical Society.

Similar to the above described synthesis of TiO_2, smaller nanocrystals are obtained with $ZrBr_4$ (3 nm). However, there are also some differences. First, a heat–up method is used for ZrO_2, not a hot–injection. Second, the reaction temperature is higher. Third, $Ti(O{i}Pr)_4$ is a liquid, while $Zr(O{i}Pr)_4 \cdot {i}PrOH$ is a solid, precluding injection. Fourth, the ratio of $ZrCl_4$ and Zr(O*i*Pr)4.*i*PrOH is 1.25. Joo *et al.* introduced this $ZrCl_4$ excess to compensate for the extra isopropanol in the isopropoxide complex. Fifth, the reaction is performed in pure TOPO. Finally, and most importantly, the resulting nanocrystals are exceptionally monodisperse and of unprecedented crystalline quality, as confirmed by Pair Distribution Function analysis.[222] Banerjee *et al.* varied the nature of the alkoxide (Et, Pr, ^{i}Pr, Bu, ^{t}Bu) and found that the final ZrO_2 NCs have consistently the tetragonal crystal structure.[66] The

authors also report slight changes in final nanocrystal diameter (4.2-5.7 nm), depending on the alkoxide.

Unfortunately, the surface chemistry is highly complex. While it was initially assumed that TOPO was the sole ligand, small amounts of TOPO decompose to potent ligands; dioctylphosphinic acid and P,P'-(dioctyl) pyrophosphonic acid.[42,97] The latter is the self–condensation product of octylphosphonic acid. In addition, the reaction mixture contains large amounts of HCl. Consequently, the surface is covered by HCl, hydrogen bonded TOPO, dissociated dioctylphosphinic acid and deprotonated P,P'-(dioctyl) pyrophosphonate, see Figure 30.[97] Under basic conditions (amine), oleic acid can replace chloride, TOPO and dioctylphosphinic acid but not P,P'-(dioctyl) pyrophosphonate. A uniform ligand shell could only be obtained by ligand exchange for a phosphonic acid.[97] Phosphonic acids have a much higher binding affinity for oxide surfaces than carboxylic acids.[232]

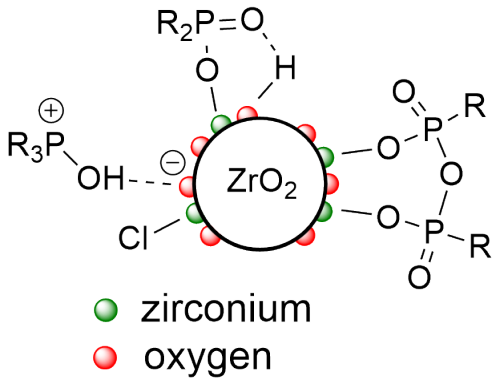

Figure 30: The surface chemistry of ZrO_2 NCs synthesized via an alkyl halide elimination in TOPO.

The precursor chemistry and the precursor conversion mechanism was recently studied in detail.[229] Upon dissolution of the reagents, the mixed chloroalkoxide is formed as the actual precursor, see Equation 51).

$$ZrCl_4 + Zr(O^iPr)_4 \cdot {}^iPrOH \longrightarrow 2\,ZrCl_2(O^iPr)_2 + {}^iPrOH \tag{51}$$

As expected based on section 3, the zirconium dichloride diisopropoxide is unreactive to

isopropanol. There is thus no need to work with an excess of $ZrCl_4$. Upon heating to 340 °C, the precursor decomposes, generating extra isopropanol and regenerating $ZrCl_4$ (evidenced by ^1H and ^{31}P NMR spectroscopy respectively). Quantitative GC measurements revealed a large amount of propene and only a minor fraction of isopropyl chloride. From this data, the mechanism in Figure 31 was proposed. In a first step, the precursors decomposes according an E1 elimination (releasing propene). Subsequently, the ligands redistribute and the hydroxide moieties condense with isopropoxide, forming zirconia and isopropanol. While this is a formal pathway, reality could be more complex and not necessarily sequential. Other condensation steps can be conceived, with the elimination of HCl or water. However, both these elimination products can react with the isopropoxide, releasing isopropanol, and the overall outcome will be the same as the one presented in Figure 31. The E1 based mechanism has a theoretical yield of 50 % while the S_N1 mechanism predicts 100 % yield.

$$ZrCl_2(O^iPr)_2 \longrightarrow ZrO_2 + 2\ i\mathrm{PrCl} \tag{52}$$

Based on the experimental yield of 60 %, the ratio of E1 and S_N1 is 80:20. Given that $ZrCl_4$ is formed as a by-product of the reaction, it could be used as a precursor for the seeded-growth of the ZrO_2 NCs. Repeated injections of zirconium isopropoxide isopropanol complex (dissolved in TOPO at 150°C), regenerates the active chloroalkoxide precursor, and the nanocrystals grow from 4 nm to 5.4 nm.[229] The procedure simultaneously increases the yield since a higher fraction of zirconium precursor ends up in the final ZrO_2 NC. This approach has the potential to grow even larger nanocrystals and thus provide a reliable, size–tunable synthesis.

Hafnium oxide nanocrystals. HfO_2 nanocrystals were synthesized from $HfCl_4$ and $Hf(Oi\mathrm{Pr})_4 \cdot i\mathrm{PrOH}$ in pure TOPO by Brus *et al.*[42] At 360 °C, quasi–spherical 5.5 nm HfO_2 NCs in the tetragonal crystal structure were obtained, although small impurities of monoclinic hafnia are present. The same mechanism and surface chemistry was found to apply as

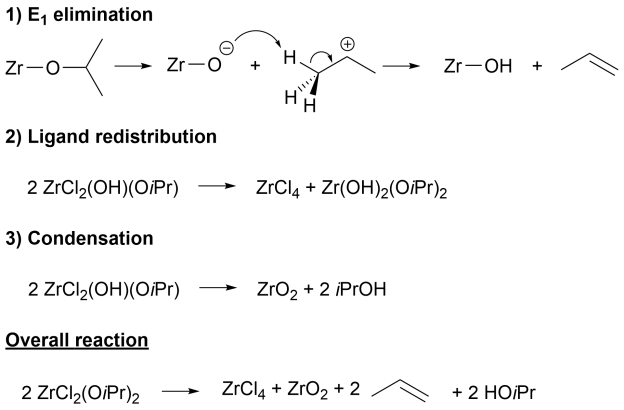

Figure 31: The proposed pathway for the formation of zirconia nanocrystals is based on E1 elimination, ligand redistribution, and condensation reactions.[229] Reprinted with permission from reference.[229] Copyright 2022 American Chemical Society

for zirconia NCs.[97,229]

$$\mathrm{HfCl_4 + Hf(O^iPr)_4 \cdot {}^iPrOH \xrightarrow[TOPO]{0.4\,mol/kg,\,360-400^\circ C} HfO_2 + HfCl_4 + 2\ C_3H_6 + 3\ {}^iPrOH} \quad (53)$$

Similar to the TiO_2 and ZrO_2 case, smaller NCs (3.7 nm) are obtained with $HfBr_4$. In addition, the crystal phase changed to the monoclinic structure. This reminds us of the rutile impurities in TiO_2 with titanium iodide. At 400 °C, hafnia nanorods (3.4 × 7.6 nm) are formed with the monoclinic crystal structure.[42]

In contrast to the original report of Brus *et al.*, other authors obtained monoclinic hafnia nanorods at temperatures varying from 315 - 360 °C.[66,230] Interestingly, the HfO_2 nanorods synthesized in TOPO exhibited paramagnetic behaviour due to oxygen defects.[230] The defected nature of the nanorods was confirmed by TEM and UV-Vis (absorption below the band gap energy). Even more defected HfO_2 nanorods with a reduced bandgap were synthesized in octadecene and oleylamine at 315 °C. The latter nanorods feature a strong ferromagnetic component, next to a paramagnetic component, and have a strong absorption in UV-VIS around 4.6 and 5.4 eV. Nanocrystals that were annealed at 750 °C displayed diamagnetic character, confirming the relation between oxygen defects and the magnetic properties. No ferromagnetic nanocrystals are obtained when oleic acid is added in addition to oleylamine.

This is likely due to a change in mechanism towards nucleophilic addition elimination (see further). The authors briefly mention that ferromagnetic nanocrystals could be obtained in octadecene or benzyl ether at lower temperature (200-300 °C) but no characterization is provided.[230] A word of caution is in place since octadecene has been shown to polymerize at these reaction temperatures and the resulting polymer impurity is difficult to separate from the formed nanocystals.[233] In addition, given the known reaction of ethers with titanium halides,[125] also benzyl ether is most likely not an inert solvent.

Banerjee *et al.* reported the monoclinic crystal structure for different types of alkoxide precursors (Et, ^{i}Pr, ^{n}Bu, ^{t}Bu, 2-Et-Hex).[66] However, they observe large size differences.[62] For the primary alkoxides (Et, ^{n}Bu), the NCs are very small (2-3 nm). With increased branching (^{i}Pr, ^{t}Bu), nanorods are obtained with increased aspect ratio. For hafnium *tert*–butoxide, nanorods 2.3 nm in diameter and 13 nm in length were obtained. The authors report a lower yield for the reaction with $Hf(OEt)_4$ compared to $Hf(O\mathit{t}Bu)_4$. Therefore, the observed size differences are likely due to the faster kinetics of hafnium *tert*–butoxide. Furthermore, it was possible to grow even longer nanorods (2.9 × 32 nm, see Figure 32) by periodically injecting the reaction mixture with small amounts of $Hf(O\mathit{t}Bu)_4$ precursor, in an effort to keep the monomer concentration below the nucleation threshold and promote growth.[62] The final ratio of *tert*–butoxide to chloride increase is 10, and this seeded growth mechanism can be rationalized in the same way as for the case of zirconia. Structurally, the nanorods consist of multiple crystalline domains, separated by twinning planes, see Figure 32. It is believed that the nanocrystals nucleate in the tetragonal structure and undergo a phase transformation upon cooling.[62]

Tetragonal HfO_2 NCs are obtained by reacting one equivalent of hafnium chloride with one equivalent of cerium tert-butoxide or lanthanum isopropoxide.[72] The nanocrystals are smaller than 4 nm and contain either 2.4 % Ce or 4.7 % La. The author attribute the stabilization of the tetragonal phase to the small nanocrystals size. However, this contradicts the earlier observation of 2-3 nm monoclinic HfO_2 obtained from hafnium ethoxide. It is

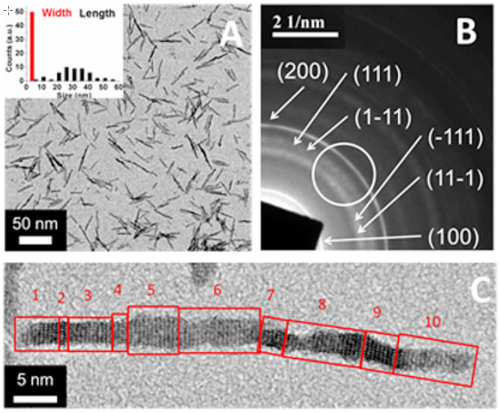

Figure 32: TEM characterization of HfO_2 nanorods synthesized from hafnium chloride and hafnium tert butoxide in TOPO. The nanorods have multiple domains of monoclinic hafnia.[62] Reprinted with permission from reference.[62] Copyright 2014 American Chemical Society.

more likely that also the incorporation of the lanthanide plays a crucial role, given similar results for the surfactant-free synthesis in benzyl alcohol.[211]

Mixed metal oxide nanocrystals. Given the almost identical ionic radius of Zr^{4+} and Hf^{4+}, hafnia and zirconia easily form solid solutions of any composition in bulk. Brus et al synthesized $Hf_xZr_{1-x}O_2$ nanocrystals with compositions varying from x = 0.11 – 0.84 by adjusting the ratio of zirconium and hafnium precursors.[42] Care was taking to balance the number of isopropoxides and halides (of course disregarding the coordinated isopropanol). ICP analysis shows that the Zr/Hf ratio is consistently higher in the final nanocrystals, compared to the reagent mixture.[42,66] This indicates a higher reactivity of Zr compared to Hf and an incomplete reaction. The incorporation of hafnium seems to depend on the choice of precursor. For example, from an equimolar mixture of $HfCl_4$ and $Zr(OiPr)_4$, $Hf_xZr_{1-x}O_2$ nanocrystals are obtained with x = 0.35, while for an equimolar mixture of $Hf(OiPr)_4$ and $ZrCl_4$, x = 0.45.[42]

$Hf_xZr_{1-x}O_2$ NCs with $x < 0.5$ are quasi–spherical and have the tetragonal structure.[42] If $HfBr_4$ or $ZrBr_4$ are used, instead of the chlorides, the particles are smaller and still tetragonal. For $x < 0.5$, the reaction temperature does not have a significant effect on the morphology or phase of the NCs. In contrast, NCs with $x > 0.5$ form in the tetragonal structure at 360 °C, but the NCs are polydisperse and have irregular shape. At 400 °C, monoclinic nanorods

are formed, 3.4 nm in diameter and 7.6 nm in length.[42] Steigerwald *et al.* later explained the tetragonal to monoclinic phase transformation by a Martensitic tranformation.[67] In a Martensitic transformation all the atoms in a crystallite move simultaneously, in contrast to diffusion mediated transformations. They argue that tetragonal NCs already form at 340 °C after 10 min, and heating further to 400 °C takes 30 min. Therefore, the monoclinic nanorods must be formed by transformation of previously formed NCs. The tetragonal to monoclinic transformation is associated with 4 % volume increase, resulting in nanorods with twinned structures.

Banerjee *et al.* reported that the composition and structure of $Hf_xZr_{1-x}O_2$ NCs can be steered by the nature of the alkoxide (Et, Pr, ^{i}Pr, ^{n}Bu, ^{t}Bu, 2-Et-Hex).[66] For equimolar Zr and Hf reagent mixtures, x varied from 0.27-0.49. For most metal alkoxide/ metal chloride combinations, x = 0.37 and the structure is tetragonal. Notable exceptions are

- $Hf(O^tBu)_4$ and $Zr(O^tBu)_4$ yield monoclinic nanorods.
- $Hf(OEt)_4$ and $Zr(OEt)_4$ yield x = 0.44
- $Zr(O^nPr)_4$ yields x = 0.49
- $Hf(O(2-Et-Hex))_4$ yields x = 0.27

The authors acquired most of their data at 340 °C because of the better crystal quality, but mention that similar trends were observed at 300 and 400 °C. Interestingly, Banerjee *et al.* observes no difference in composition between a reaction of $HfCl_4$ and $Zr(Oi Pr)_4$, and a reaction of $Hf(Oi Pr)_4$ and $ZrCl_4$, nor for the other alkoxides.[66] Finally, the authors hypothesize that the monoclinic structure is favored in faster reactions and thus represent the kinetic product while the tetragonal phase is more thermodynamically stable in nanocrystals $<$ 30 nm. This seems to contradict the theory of Martensitic transformation.

Brus *et al.* did not succeed in synthesizing $ZrTiO_4$ or $HfTiO_4$ nanocrystals. The Ti precursors are much more reactive than the Hf or Zr precursors and therefore, no cross-

condensation happened. Only anatase TiO_2 NCs are retrieved.[42] Indeed, Doong *et al.* studied the cross-condensation between titanium and zirconium in more detail and found that only small amounts of Zr were incorporated in the TiO_2 NCs.[234] Even in the case where ICP-MS and XPS suggested higher contents of Zr, the XRD did not show any reflections of $ZrTiO_4$.

Discussion. From the above collection of results, we infer that the reactivity of the metals can be ranked as Ti >> Zr > Hf. The precursor conversion follows mostly an S_N1 and E1 mechanism, with E1 being the dominant mechanism for zirconia and hafnia. Consequently, the rate of the reaction increases with branching of the alkoxide. While the alkoxide has no influence on the size for TiO_2, there are small differences for ZrO_2, and even larger sizes differences of HfO_2 nanorods. Given the slower kinetics of Zr and Hf, this is most likely due to incomplete reaction of the slower precursors. The nature of the halide has little influence on the rate but changes the NC size and sometimes even the crystal structure. There seems to be some disagreement on the structure of HfO_2 and $Hf_xZr_{1-x}O_2$ NCs, with some authors reporting a tetragonal structure below 360 °C and others a monoclinic structure. Finally, while the precursor conversion mechanism of these reactions is thus well–studied, insight in the precise mechanism of nucleation and growth is still missing, hampering the development of more complex oxide NCs.

5.2.2 Nucleophilic addition/elimination

Nucleophilic addition and elimination is another mechanism for oxide formation. The carbonyl carbon of a carboxylic acid can be attacked by nucleophiles such as alcohols/alkoxides or amines. In one particular strategy, a metal carboxylate directly reacts with a metal alkoxide, giving an ester as a coproduct.

$$\mathrm{M{-}OOCR + RO{-}M \longrightarrow M{-}O{-}M + RCOOR}$$

Mixed metal oxide gels can be obtained, e.g., from the reaction between zirconium propoxide and silicon acetate.[36] One can also start from metal carboxylates and react them with alcohols (*alcoholysis*) or amines (*aminolysis*) to form esters or amides respectively.

$$\mathrm{M{-}OOCR + ROH \longrightarrow M{-}OH + RCOOR} \tag{54}$$

$$\mathrm{M{-}OOCR + RNH_2 \longrightarrow M{-}OH + RCONHR} \tag{55}$$

The metal hydroxide species formed in this process can further condense to oxide with the elimination of water. While many oxide NCs are prepared by reacting metal acetates with benzyl alcohol, this strategy has not been pursued for the group 4 oxides.[235] This could be related to the difficulty in preparing pure metal acetates (or other carboxylates) for these metals. As a notable exception, trifluoroacetates have been prepared directly from the respective metal chloride, see section 3. Using oleylamine and hafnium trifluoroacetate, monoclinic HfO_2 NCs (5 nm) were produced in almost quantitative yield, see Figure 33.[13] The authors mention a gel-like phase at 290 °C, and a subsequent decrease in viscosity at 330 °C, presumable because of crystallization of the gel into NCs. Similarly, monoclinic ZrO_2 NCs (5.5 nm) are formed.[236] The amide of trifluoroacetic acid and oleylamine was detected via mass spectrometry. Similar attempts with zirconium acetate, oleate and trichloroacetate failed. In addition, the crystallinity is lower using saturated amines such as octadecylamine. The same strategy with $TiO(TFA)_2$ also yields anatase TiO_2 NCs (6 nm).

Titanium oleate species are formed *in situ* by the dissolution of $TiCl_4$ or TiF_4 in octadecene by oleic acid (see also section 3).[237,238] The uncharacterized precursors (possibly $TiCl_2(OOCR)_2$) were injected in an octadecanol or oleylamine solution in octadecene and heated to 290 °C to form very small seed crystals. Subsequent slow injection of more precursor solution leads to growth of the nanocrystals with control over crystal structure (anatase and brookite), shape, and the exposed facets by choice of nucleophile (alcohol or amine) and halide (chloride or fluoride), see Figure 34.[238] By adding other transition metal oleates to the

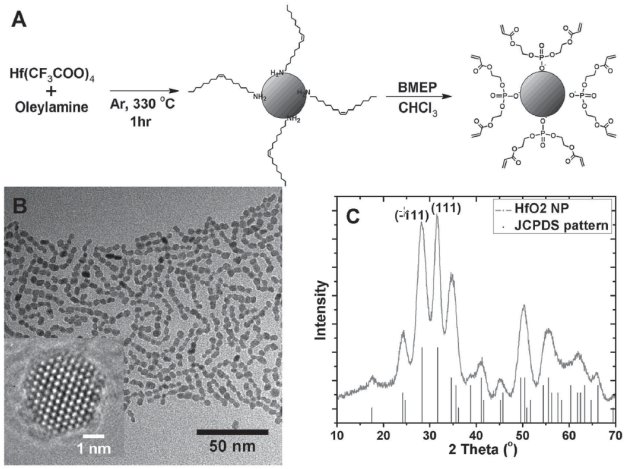

Figure 33: (A) Scheme of the aminolysis of hafnium trifluoroacetate into HfO_2 NCs. (B) TEM image and C) powder XRD pattern of the NCs showing a monoclinic crystal structure.[13] Copyright © 2015 WILEY-VCH Verlag GmbH & Co. KGaA, Weinheim.

precursor solution, doped brookite TiO_2 nanorods were synthesized from $TiCl_4$ following a pure aminolysis strategy.[239] The above syntheses produces large amounts of polymerized octadecene because the polymerization is catalyzed by titanium halides and it is recommended to use octadecane instead.[233]

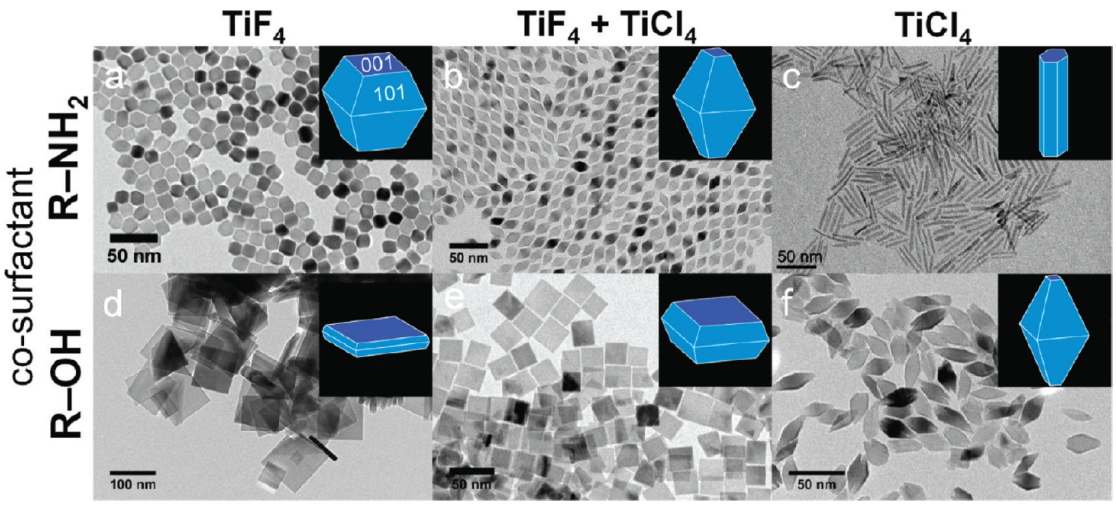

Figure 34: TEM images of TiO_2 NCs synthesized using different precursors and co–surfactants (apart from oleic acid).[238] Reprinted with permission from reference.[238] Copyright 2012 American Chemical Society.

The reaction of titanium isopropoxide ([Ti]= 0.9 M) in pure oleic acid (3.5 equivalents) yields anatase TiO_2 NCs at 270 °C.[240] It is interesting to note how similar this reaction is to

the formation of titanium oxo clusters, the main differences being the temperature and the length of the carboxylic acid. This pure esterification mechanism yields a mixture of spherical NCs and nanorods. The nanorod diameter decreases when also oleylamine is introduced in the reaction mixture, thus changing the mechanism to a mixed ester/amide formation. Another group simultaneously explored the same chemistry but used 1-octadecene as solvent and thus the titanium concentration was much lower (0.13 M). Under these conditions, no TiO_2 NCs were obtained with 5 equivalents of oleic acid. Injection of 1 – 4 equivalents of oleylamine at 260 °C is required to obtain TiO_2.[241] Under the right conditions, the TiO_2 nanorods can self-organize in superstructures.[242] Alternatively, TiO_2 NCs were obtained by a low temperature esterification (100 °C) after 48 hours; titanium isopropoxide reacts with oleic acid and ethyleneglycol, in the presence of a base, e.g., triethylamine.[243] In light of the discussion on precursor chemistry and cluster formation, we find it most likely that in the above reactions, first a ligand exchange takes place, consuming two equivalents of oleic acid.

$$Ti(OR)_4 + 2\,RCOOH \longrightarrow Ti(OR)_2(OOCR)_2 + 2\,ROH$$

Instead of a third ligand exchange, esterification takes place and it seems likely that clusters are formed as intermediates. Amide and ester formation are a strategy of attacking the carboxylate capping ligands on the clusters and allow for further condensation and growth into nanocrystals. However, efforts to use **Zr6**-methacrylate clusters as well–defined precursors for ZrO_2 NCs have not been successful so far.[35] We hypothesize a few possible reasons for this failure: (i) the methacrylate ligands will crosslink at the reaction temperature (400 °C), (ii) titanium oxo clusters are more labile than zirconium oxo clusters, (iii) no amine or alcohol was added to the reaction to induce alcoholysis or aminolysis.

Niobium doped anatase TiO_2 NCs were synthesized by Milliron *et al.* from titanium ethoxide (1 mmol), niobium chloride, oleic acid (1 mmol), octadecanol (13 mmol) in octadecene at 290 °C.[5] A pure esterification mechanism would limit the yield to 50 %. However,

the authors report 75 % yield and a control experiment shows that oxide nanocrystals are also obtained without oleic acid. The mechanism is thus a mixture of several non-hydrolytic processes. The size (10-15 nm) and morphology (cube or short rod) of the particles depend on the dopant concentration. Recently the method was expanded to W and Mo doped TiO_2 NCs.[244] Furthermore, tantalum doped TiO_2 NCs were synthesized from the metal ethoxides, oleic acid, oleylamine, octadecanol and ammonium fluoride.[4] After reaction at 280 °C for 60 min, 9-12 nm TiO_2 NCs with up to 22 % atom Ta were retrieved (Figure 35). The addition of ammonium fluoride is essential to obtain complete tantalum incorporation. The size of the NCs can be somewhat tuned by varying the oleic acid and oleylamine ratio.

An attempt was made to react a series of hafnium alkoxides with oleylamine and oleic acid to hafnium oxide, but only amorphous, aggregated particles were obtained.[245] From the above description, it seems that titania nanocrystals can be easily synthesized by the nucleophilic addition/elimination mechanism, but the strategy is less suitable for zirconium and hafnium oxide. As a dopant, it was possible to incorporate Ti, Zr, and Hf in In_2O_3 nanocrystals, but the overall concentration of the group 4 metals was low (about 1 %).[246]

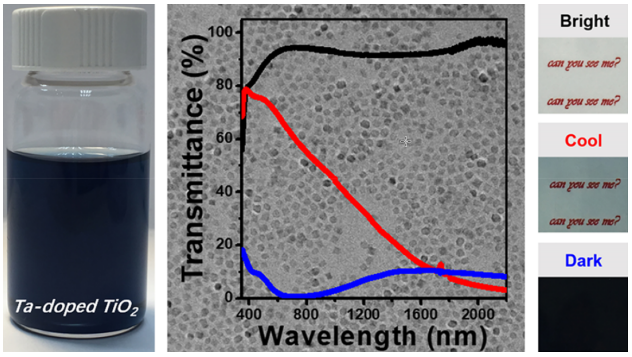

Figure 35: Photograph and TEM image of tantalum doped TiO_2 NCs, which are used as electrochromic material in smart windows.[244] Reprinted with permission from reference.[244] Copyright 2018 American Chemical Society.

5.3 Applications of group 4 metal oxide nanocrystals

5.3.1 Applications of titania nanocrystals

TiO_2 nanocrystals (NCs) are an essential component of dye-sensitized solar cells, also known as the Graetzel cells.[1] The TiO_2 NCs are covered with a ruthenium based dye which is responsible for light absorption. The energy levels of the dye and titania are aligned such that the excited electron is transferred from the dye to titania and subsequently to the electrode. The hole is transferred to the counterelectrode via the electrolyte. Dyes are currently being developed with more abundant metals such as copper.[247] In the realm of sustainable energy, titania is also an attractive anode material for lithium ion batteries since it has a high theoretical specific capacity (335 mA h g^{-1}).[2] Especially the bronze polymorph has attracted interest since it can accomodate more lithium than the other titania phases. The high surface area associated with nanocrystals is beneficial to enhance the charging rate. Given that the bandgap of titania is 3.2 eV, it absorbs blue and UV light. Consequently, titania nanocrystals have been used as a photocatalyst, often to break down organic matter.[3,40] Titania coated glass can be envisaged as self-cleaning windows.[248] Doping of titania NCs with tantalum or niobium introduces free carriers in the conduction band and grants the NCs an infrared plasmon resonance.[4,5] Such doped nanocrystals were integrated in smart windows as electrochromic material: depending on the applied potential, the coated glass is (i) transparent for visible and infrared light, or (ii) absorbing infrared light, or (iii) absorbing both visible and infrared light (Figure 35).

5.3.2 Applications of zirconia nanocrystals

Zirconia nanocrystals are great building blocks for material science. Shaw *et al.* used ZrO_2 nanocrystals to fabricate crack-free coatings.[228,249,250] After deposition, the organic ligands are removed by an oxygen plasma, and the particles simultaneously sinter together (providing mechanical strength to the coating). Note that the ligand original mixture of TOPO,

octylphosphinic acid and octylphosphonic acid anhydride, leads to residual phosphate in the final material. By ligand exchange with oleic acid prior to deposition, this could be minimized.[250] On the other hand, Talapin *et al.* obtained patterns of zirconia (and titania and hafnia) by a method that was coined DOLFIN (direct optical lithography of functional inorganic nanomaterials).[251,252] The surface is first functionalized with photoactive ligands. Irradition by UV light triggers the decomposition of the ligand, and as a result, the nanocrystals are no longer soluble. Patterns are obtained by a three-step process: layer deposition, illumination through a mask, and washing off unexposed nanocrystals. Zirconia nanocrystals are also used in nanocomposites. For example, composites of ZrO_2 NCs and epoxy polymer feature a high refractive index. Such nanocomposites are useful to encapsulate LEDs since the nanocomposite reduces the refractive index mismatch between the semiconductor LED material and air, thereby improving the light-extraction efficiency.[253] The high refractive index was further exploited in volume holography.[197] All-inorganic nanocomposites of ZrO_2 nanocrystals and $YBa_2Cu_3O_{7-\delta}$ superconductors have superior conductive properties over the pure superconductor.[8,222,254] $YBa_2Cu_3O_{7-\delta}$ is a type II superconductor and in high magnetic fields moving vortex currents destroy the superconducting state. The inclusion of nanocrystals pins the vortexes, enhancing the critical current at high magnetic fields. Finally, europium and terbium doped ZrO_2 NCs, stabilized by 2-aminoethyl phosphoric acid ligand, were developed for targeted bioimaging.[15] By coupling the amino group of the ligand with biotin via an amide bond, the nanocrystals obtained a high affinity for avidin. As a result, avidin could be detected via time-resolved Fluorescence Resonance Energy Transfer (FRET).

5.3.3 Applications of hafnia nanocrystals

HfO_2 NCs are being developed as components in next generation memory devices, based on memristors.[10,232] While memristors are traditionally fabricated with thin films of pure oxides, also assemblies of ligand capped nanocrystals can be switched from a high to a low

resistance state. The voltage required to switch from one state to the other, depends on the ligand length and is minimized for shorter ligands.[10] Hafnia nanocrystals are also among the few nanomaterials that made it to real clinical translation.[255] They are used in cancer treatment to locally enhance radiotherapy. The nanocrystals are directly injected in the tumor tissue and convert x-rays into reactive oxygen species that destroy the tumor.[11,12] The high x-ray absorption cross section of hafnia was also exploited in scintillators and medical imaging.[13,256] Nanocomposites of polymer, nanocrystals and dyes were fabricated, where the hafnia absorbs the photons and transfers it to a cascade of dyes, which convert it to visible light. In medical CT (computed tomography), hafnia nanocrystals serve as contrast agents that absorb X-rays more efficiently that soft tissue.[256] Hafnia NCs doped with lanthanides have also been explored as luminescent probes.[14] However, europium doped hafnia NCs, that were capped with 2-[2-(2-methoxyethoxy)ethoxy]acetic acid, are not very stable in water and buffer solutions, causing aggregation during the staining of cells. Finally, hafnia nanocrystals have been used as catalysts for (trans)esterification reactions.[257] The fatty acid substrate was also used as ligand, thereby eliminating the competition of ligands (necessary for colloidal stability) and substrates for the active surface sites.

6 Conclusion and outlook

We provided a comprehensive overview of the nonaqueous chemistry of the group 4 metals, in the context of oxo cluster and oxide nanocrystal formation. Since oxo clusters are the building blocks of MOFs, we thus bridge here two major research communities that otherwise have little interaction: MOFs and nanocrystals. We could link these research fields by starting from the fundamental chemistry: the reactivity of the precursors. Throughout the review, we have focused on the mechanism of precursor conversion and critically evaluated the state–of–the–art, clearly indicating which conclusions are solid and which areas needs further attention. From our literature survey, it is also clear that there are hardly any

studies on the crystallization mechanism (nucleation and growth) of oxide nanocrystals (via nonaqueous strategies). We thus identify this as a major gap, which probably stands in the way of building more complex oxide nanocrystals. Once the mechanisms are known, colloidal inorganic chemistry can rationally implement the concept of *retro-synthesis* and *total inorganic synthesis*, similar to organic chemistry. We envision total inorganic synthesis as a rational step-by-step synthetic strategy for building complex architectures such as core-shell-shell systems with these group 4 oxides. Even for the relatively more simple case of oxo clusters, there is currently little information on the precise formation mechanism other that conceptually vague stages; ligand exchange, esterification and condensation. However, access to the crystallization mechanism would enable researchers to further expand the portfolio of available clusters. From the perspective of a nanoscientist, oxo clusters are exciting because they provide the atomic precision that we strive for. Oxo clusters are sometimes seen as the smallest possible nanocrystals and thus as model systems for nanocrystals. However, it is currently unclear what the similarities and differences between the two systems are, especially regarding chemical stability and surface chemistry. This merits further research. Finally, a pending question is how to bridge the cluster and the nanocrystal realms. While cluster cores are typically 0.5 - 1 nm in size, the smallest nanocrystals are about 2.5 nm in size. It is yet unclear how to access the intermediate size range. We conclude that the chemistry of group 4 oxo clusters and oxide NCs is highly relevant to modern applications, and that there are still plenty of fundamental chemistry questions left unanswered and ready to be explored.

Author biographies

Dietger Van den Eynden completed his Bachelor and Master in chemistry at Ghent University, studying covalent adaptable networks. In 2019 he started his joint PhD under the supervision of Prof. Dr. De Roo at the University of Basel and Prof. Dr. De Buysser at

Ghent University. His research focusses on precise group 4 metal oxo-clusters and nanocrystals, from precursor chemistry to application.

Rohan Pokratath completed his Bachelor in Chemical Engineering from the University of Kerala and Master in Material Science from the Indian Institute of Technology Bombay. He is currently pursuing his Ph.D. under the supervision of Prof. Jonathan De Roo. His research focuses on synthesizing and characterizing group IV metal oxide nanocrystals.

Jonathan De Roo completed his Bachelor and Master in chemistry at Ghent University and obtained his PhD in 2016 on the topic; Surface chemistry of metal oxide nanocrystals. During his PhD, he was also three months at ETH Zurich to study the surface of CsPbBr3 nanocrystals. He conducted postdoctoral research at Columbia University, working on crystallization mechanisms and the design of new ligands. In 2019, he joined the University of Basel as Tenure Track Assistant Professor. His research team focuses on mechanistic aspects in the synthesis of ceramic nanocrystals and atomically precise oxo clusters. Both precursor conversion and crystallization mechanisms are studied.

Acknowledgement

The authors thank the University of Basel for financial support.

References

(1) Oregan, B.; Gratzel, M. A low-Cost, High Effiency Solar-Cell Based on Dye-Sensitized Colloidal TiO2 Films. *Nature* **1991**, *353*, 737–740.

(2) Ren, Y.; Liu, Z.; Pourpoint, F.; Armstrong, A. R.; Grey, C. P.; Bruce, P. G. Nanoparticulate TiO2(B): An Anode for Lithium-Ion Batteries. *Angew. Chem. Int. Ed.* **2012**, *124*, 2206–2209.

(3) Kaniyankandy, S.; Ghosh, H. N. Efficient Luminescence and Photocatalytic Behaviour

in Ultrafine TiO2 Particles Synthesized by Arrested Precipitation. *J. Mater. Chem.* **2009**, *19*, 3523–3528.

(4) Cao, S.; Zhang, S.; Zhang, T.; Lee, J. Y. Fluoride-Assisted Synthesis of Plasmonic Colloidal Ta-Doped TiO2 Nanocrystals for Near-Infrared and Visible-Light Selective Electrochromic Modulation. *Chem. Mater.* **2018**, *14*, 4838–4846.

(5) De Trizio, L.; Buonsanti, R.; Schimpf, A. M.; Llordes, A.; Gamelin, D. R.; Simonutti, R.; Milliron, D. J. Nb-Doped Colloidal TiO2 Nanocrystals with Tunable Infrared Absorption. *Chem. Mater.* **2013**, *25*, 3383–3390.

(6) Zhang, X.; Wang, H.; Xu, B.-Q. Remarkable Nanosize Effect of Zirconia in Au/ZrO2 Catalyst for CO Oxidation. *J. Phys. Chem. B* **2005**, *109*, 9678–9683.

(7) Meunier, F. C.; Kdhir, R.; Potrzebowska, N.; Perret, N.; Besson, M. Unravelling Platinum–Zirconia Interfacial Sites Using CO Adsorption. *Inorg. Chem.* **2019**, *12*, 8021–8029.

(8) De Keukeleere, K.; Cayado, P.; Meledin, A.; Vallès, F.; De Roo, J.; Rijckaert, H.; Pollefeyt, G.; Bruneel, E.; Palau, A.; Coll, M.; ; et al., Superconducting YBa2Cu3O7-δ Nanocomposites Using Preformed ZrO2 Nanocrystals: Growth Mechanisms and Vortex Pinning Properties. *Adv. Electron. Mater.* **2016**, *2*, 1600161.

(9) Kumar, S.; Wang, Z.; Huang, X.; Kumari, N.; Davila, N.; Strachan, J. P.; Vine, D.; Kilcoyne, A. L.; Nishi, Y.; Williams, R. S. Conduction Channel Formation and Dissolution Due to Oxygen Thermophoresis/Diffusion in Hafnium Oxide Memristors. *ACS Nano* **2016**, *10*, 11205–11210.

(10) Wang, J.; Choudhary, S.; De Roo, J.; De Keukeleere, K.; Van Driessche, I.; Crosby, A. J.; Nonnenmann, S. S. How Ligands Affect Resistive Switching in Solution-Processed HfO2 Nanoparticle Assemblies. *ACS Appl. Mater. Interfaces* **2018**, *10*, 4824–4830.

(11) Maggiorella, L.; Barouch, G.; Devaux, C.; Pottier, A.; Deutsch, E.; Bourhis, J.; Borghi, E.; Levy, L. Nanoscale Radiotherapy with Hafnium Oxide Nanoparticles. *Future Oncol.* **2012**, *8*, 1167–1181.

(12) Marill, J.; Anesary, N.; Zhang, P.; Vivet, S.; Borghi, E.; Levy, L.; Pottier, A. Hafnium Oxide Nanoparticles: Toward an In Vitro Predictive Biological Effect? *Radiat. Oncol.* **2014**, *9*, 150.

(13) Liu, C.; Hajagos, T. J.; Kishpaugh, D.; Jin, Y.; Hu, W.; Chen, Q.; Pei, Q. Facile Single-Precursor Synthesis and Surface Modification of Hafnium Oxide Nanoparticles for Nanocomposite γ-Ray Scintillators. *Adv. Funct. Mater.* **2015**, *25*, 4607–4616.

(14) Villa, I.; Villa, C.; Monguzzi, A.; Babin, V.; Tervoort, E.; Nikl, M.; Niederberger, M.; Torrente, Y.; Vedda, A.; Lauria, A. Demonstration of Cellular Imaging by Using Luminescent and Anti-Cytotoxic Europium-Doped Hafnia Nanocrystals. *Nanoscale* **2018**, *10*, 7933–7940.

(15) Liu, Y.; Zhou, S.; Tu, D.; Chen, Z.; Huang, M.; Zhu, H.; Ma, E.; Chen, X. Amine-Functionalized Lanthanide-Doped Zirconia Nanoparticles: Optical Spectroscopy, Time-Resolved Fluorescence Resonance Energy Transfer Biodetection, and Targeted Imaging. *J. Am. Chem. Soc.* **2012**, *134*, 15083–15090.

(16) LeLuyer, C.; Villanueva-Ibañez, M.; Pillonnet, A.; Dujardin, C. HfO2:X (X = Eu3+, Ce3+, Y3+) Sol Gel Powders for Ultradense Scintillating Mater. *J. Phys. Chem. A* **2008**, *112*, 10152–10155.

(17) Chakraborty, A.; Debnath, G. H.; Saha, N. R.; Chattopadhyay, D.; Waldeck, D. H.; Mukherjee, P. Identifying the Correct Host–Guest Combination To Sensitize Trivalent Lanthanide (Guest) Luminescence: Titanium Dioxide Nanoparticles as a Model Host System. *J. Phys. Chem. C* **2016**, *120*, 23870–23882.

(18) Schroeder, U.; Richter, C.; Park, M. H.; Schenk, T.; Pešić, M.; Hoffmann, M.; Fengler, F. P. G.; Pohl, D.; Rellinghaus, B.; Zhou, C.; et al., Lanthanum-Doped Hafnium Oxide: A Robust Ferroelectric Material. *Inorg. Chem.* **2018**, *57*, 2752–2765.

(19) Cavka, J. H.; Jakobsen, S.; Olsbye, U.; Guillou, N.; Lamberti, C.; Bordiga, S.; Lillerud, K. P. A New Zirconium Inorganic Building Brick Forming Metal Organic Frameworks with Exceptional Stability. *J. Am. Chem. Soc.* **2008**, *130*, 13850–13851.

(20) Chen, Z.; Hanna, S. L.; Redfern, L. R.; Alezi, D.; Islamoglu, T.; Farha, O. K. Reticular Chemistry in the Rational Synthesis of Functional Zirconium Cluster-Based MOFs. *Coord. Chem. Rev.* **2019**, *386*, 32 – 49.

(21) Yuan, S.; Qin, J.-S.; Lollar, C. T.; Zhou, H.-C. Stable Metal–Organic Frameworks with Group 4 Metals: Current Status and Trends. *ACS Cent. Sci.* **2018**, *4*, 440–450.

(22) Huang, J.-Y.; Xu, H.; Peretz, E.; Wu, D.-Y.; Ober, C. K.; Hanrath, T. Three-Dimensional Printing of Hierarchical Porous Architectures. *Chem. Mater.* **2019**, *31*, 10017–10022.

(23) Faccioli, F.; Bauer, M.; Pedron, D.; Sorarù, A.; Carraro, M.; Gross, S. Hydrolytic Stability and Hydrogen Peroxide Activation of Zirconium-Based Oxoclusters. *Eur. J. Inorg. Chem.* **2015**, *2015*, 210–225.

(24) Moons, J.; de Azambuja, F.; Mihailovic, J.; Kozma, K.; Smiljanic, K.; Amiri, M.; Cirkovic Velickovic, T.; Nyman, M.; Parac-Vogt, T. N. Discrete Hf18 Metal-oxo Cluster as a Heterogeneous Nanozyme for Site-Specific Proteolysis. *Angew. Chem. Int. Ed.* **2020**, *59*, 9094–9101.

(25) Rozes, L.; Sanchez, C. Titanium Oxo-Clusters: Precursors for a Lego-Like Construction of Nanostructured Hybrid Mater. *Chem. Soc. Rev.* **2011**, *40*, 1006–1030.

(26) Schubert, U. Inorganic-Organic Hybrid Polymers Based on Surface-Modified Metal Oxide Clusters. *Macromol. Symp.* **2008**, *267*, 1–8.

(27) Wang, B.; Lv, X.-L.; Feng, D.; Xie, L.-H.; Zhang, J.; Li, M.; Xie, Y.; Li, J.-R.; Zhou, H.-C. Highly Stable Zr(IV)-Based Metal–Organic Frameworks for the Detection and Removal of Antibiotics and Organic Explosives in Water. *J. Am. Chem. Soc.* **2016**, *138*, 6204–6216.

(28) Vermoortele, F.; Bueken, B.; Le Bars, G.; Van de Voorde, B.; Vandichel, M.; Houthoofd, K.; Vimont, A.; Daturi, M.; Waroquier, M.; Van Speybroeck, V.; et al., Synthesis Modulation as a Tool To Increase the Catalytic Activity of Metal–Organic Frameworks: The Unique Case of UiO-66(Zr). *J. Am. Chem. Soc.* **2013**, *135*, 11465–11468.

(29) Diercks, C. S.; Liu, Y.; Cordova, K. E.; Yaghi, O. M. The Role of Reticular Chemistry in the Design of CO2 Reduction Catalysts. *Nat. Mater.* **2018**, *17*, 301–307.

(30) Kim, B. H.; Shin, K.; Kwon, S. G.; Jang, Y.; Lee, H.-S.; Lee, H.; Jun, S. W.; Lee, J.; Han, S. Y.; Yim, Y.-H.; et al., Sizing by Weighing: Characterizing Sizes of Ultrasmall-Sized Iron Oxide Nanocrystals Using MALDI-TOF Mass Spectrometry. *J. Am. Chem. Soc.* **2013**, *135*, 2407–2410.

(31) Wang, Y.; Zhang, Y.; Wang, F.; Giblin, D. E.; Hoy, J.; Rohrs, H. W.; Loomis, R. A.; Buhro, W. E. The Magic-Size Nanocluster (CdSe)34 as a Low-Temperature Nucleant for Cadmium Selenide Nanocrystals; Room-Temperature Growth of Crystalline Quantum Platelets. *Chem. Mater.* **2014**, *26*, 2233–2243.

(32) Friedfeld, M. R.; Stein, J. L.; Cossairt, B. M. Main-Group-Semiconductor Cluster Molecules as Synthetic Intermediates to Nanostructures. *Inorg. Chem.* **2017**, *56*, 8689–8697.

(33) Gutsev, L. G.; Ramachandran, B. R.; Gutsev, G. L. Pathways of Growth of CdSe Nanocrystals from Nucleant (CdSe)34 Clusters. *J. Phys. Chem. C* **2018**, *122*, 3168–3175.

(34) Pun, A. B.; Mule, A. S.; Held, J. T.; Norris, D. J. Core/Shell Magic-Sized CdSe Nanocrystals. *Nano Lett.* **2021**, *18*, 7651–7658.

(35) Sliem, M. A.; Schmidt, D. A.; Bétard, A.; Kalidindi, S. B.; Gross, S.; Havenith, M.; Devi, A.; Fischer, R. A. Surfactant-Induced Nonhydrolytic Synthesis of Phase-Pure ZrO2 Nanoparticles from Metal–Organic and Oxocluster Precursors. *Chem. Mater.* **2012**, *24*, 4274–4282.

(36) Vioux, A. Nonhydrolytic Sol-Gel Routes to Oxides. *Chem. Mater.* **1997**, *9*, 2292–2299.

(37) Taguchi, M.; Takami, S.; Adschiri, T.; Nakane, T.; Sato, K.; Naka, T. Synthesis of Surface-Modified Monoclinic ZrO2 Nanoparticles using Supercritical Water. *CrystEngComm.* **2012**, *14*, 2132–2138.

(38) Eltzholtz, J. R.; Tyrsted, C.; Jensen, K. M. O.; Bremholm, M.; Christensen, M.; Becker-Christensen, J.; Iversen, B. B. Pulsed Supercritical Synthesis of Anatase TiO2 Nanoparticles in a Water-Isopropanol Mixture Studied by In Situ Powder X-Ray Diffraction. *Nanoscale* **2013**, *5*, 2372–2378.

(39) Sato, K.; Abe, H.; Ohara, S. Selective Growth of Monoclinic and Tetragonal Zirconia Nanocrystals. *J. Am. Chem. Soc.* **2010**, *132*, 2538–2539.

(40) Billet, J.; Dujardin, W.; De Keukeleere, K.; De Buysser, K.; De Roo, J.; Van Driessche, I. Size Tunable Synthesis and Surface Chemistry of Metastable TiO2-Bronze Nanocrystals. *Chem. Mater.* **2018**, *30*, 4298–4306.

(41) Shannon, R. D. Revised Effective Ionic Radii and Systematic Studies of Interatomic Distances in Halides and Chalcogenides. *Acta Crystallogr.* **1976**, *32*, 751–767.

(42) Tang, J.; Fabbri, J.; Robinson, R. D.; Zhu, Y.; Herman, I. P.; Steigerwald, M. L.; Brus, L. E. Solid-Solution Nanoparticles: Use of a Nonhydrolytic Sol-Gel Synthesis To Prepare HfO2 and HfxZr1-xO2 Nanocrystals. *Chem. Mater.* **2004**, *16*, 1336–1342.

(43) Slater, J. C. Atomic Radii in Crystals. *Chem. Phys.* **1964**, *41*, 3199–3204.

(44) Huheey, J., Keiter, E., Keiter, R., Eds. *Inorganic Chemistry : Principles of Structure and Reactivity*, 4th ed.; HarperCollins: New York, 1993; pp 188–189.

(45) Tantardini, C.; Oganov, A. R. Thermochemical Electronegativities of the Elements. *Nat. Commun.* **2021**, *12*, 2087.

(46) Diebold, U. The Surface Science of Titanium Dioxide. *Surf. Sci. Rep.* **2003**, *48*, 53–229.

(47) Patil, R. N.; Subbarao, E. C. Axial Thermal Expansion of ZrO_2 and HfO_2 in the Range Room Temperature to 1400°C. *J. Appl. Crystallogr.* **1969**, *2*, 281–288.

(48) Robertson, J. High Dielectric Constant Oxides. *Eur. Phys. J. Appl. Phys.* **2004**, *28*, 265–291.

(49) Kavan, L.; Grätzel, M.; Gilbert, S. E.; Klemenz, C.; Scheel, H. J. Electrochemical and Photoelectrochemical Investigation of Single-Crystal Anatase. *J. Am. Chem. Soc.* **1996**, *118*, 6716–6723.

(50) Elder, S. H.; DiSalvo, F. J.; Topor, L.; Navrotsky, A. Thermodynamics of Ternary Nitride Formation by Ammonolysis: Application to Lithium Molybdenum Nitride (LiMoN2), Sodium Tungsten Nitride (Na3WN3), and Sodium Tungsten Oxide Nitride (Na3WO3N). *Chem. Mater.* **1993**, *5*, 1545–1553.

(51) Marchand, R.; Brohan, L.; M., T. A New Form of Titanium Dioxide and the Potassium Octatitanate $K_2Ti_8O_{17}$. *Mater. Res. Bull.* **1980**, *15*, 1129–1133.

(52) Latroche, M.; Brohan, L.; Marchand, R.; Tournoux, M. New Hollandite Oxides: TiO_2(H) and $K_{0.06}TiO_2$. *J. Solid State Chem.* **1989**, *81*, 78–82.

(53) Akimoto, J.; Gotoh, Y.; Oosawa, Y.; Nonose, N.; Kumagai, T.; Aoki, K.; Takei, H. Topotactic Oxidation of Ramsdellite-Type $Li_{0.5}TiO_2$, a New Polymorph of Titanium Dioxide: TiO_2(R). *J. Solid State Chem.* **1994**, *113*, 27–36.

(54) Simons, P. Y.; Dachille, F. The structure of TiO_2 II, a high-pressure phase of TiO_2. *Acta Crystallogr.* **1967**, *23*, 334–336.

(55) Sato, H.; Endo, S.; Sugiyama, M.; Kikegawa, T.; Shimomura, O.; Kusaba, K. Baddeleyite-Type High-Pressure Phase of TiO_2. *Science* **1991**, *251*, 786–788.

(56) Dubrovinskaia, N. A.; Dubrovinsky, L. S.; Ahuja, R.; Prokopenko, V. B.; Dmitriev, V.; Weber, H. P.; Osorio-Guillen, J. M.; Johansson, B. Experimental and Theoretical Identification of a New High-Pressure TiO_2 Polymorph. *Phys. Rev. Lett.* **2001**, *87*, 275501.

(57) Mattesini, M.; de Almeida, J. S.; Dubrovinsky, L.; Dubrovinskaia, L.; Johansson, B.; Ahuja, R. High-Pressure and High-Temperature Synthesis of the Cubic TiO_2 Polymorph. *Phys. Rev. B* **2004**, *70*, 212101.

(58) Dubrovinsky, L.; Dubrovinskaia, N.; Swamy, M. J., V; Harrison, N.; Ahuja, R.; Holm, B.; Johansson, B. The Hardest Known Oxide. *Nature* **2001**, *4*, 1104–1116.

(59) Zhang, H.; Banfield, J. F. Understanding Polymorphic Phase Transformation Behavior during Growth of Nanocrystalline Aggregates: Insights from TiO_2. *J. Phys. Chem. B* **2000**, *104*, 3481–3487.

(60) Zhang, H.; Banfield, J. F. Thermodynamic Analysis of Phase Stability of Nanocrystalline Titania. *J. Mater. Chem.* **1998**, *8*, 2073.

(61) Tsampas, M. N.; Sapountzi, F. M.; Vernoux, P. Applications of Yttria Stabilized Zirconia (YSZ) in Catalysis. *Catal. Sci. Technol.* **2015**, *5*, 4884–4900.

(62) Depner, S. W.; Cultrara, N. D.; Farley, K. E.; Qin, Y.; Banerjee, S. Ferroelastic Domain Organization and Precursor Control of Size in Solution-Grown Hafnium Dioxide Nanorods. *Acs Nano* **2014**, *8*, 4678–4688.

(63) Garvie, R. C. The Occurrence of Metastable Tetragonal Zirconia as a Crystallite Size Effect. *J. Phys. Chem.* **1965**, *69*, 1238–1243.

(64) Garvie, R. C. Stabilization of the Tetragonal Structure in Zirconia Microcrystals. *J. Phys. Chem.* **1978**, *82*, 218–224.

(65) Chevalier, J.; Gremillard, L.; Virkar, A. V.; Clarke, D. R. The Tetragonal-Monoclinic Transformation in Zirconia: Lessons Learned and Future Trends. *J. Am. Ceram. Soc.* **2009**, *92*, 1901–1920.

(66) Depner, S. W.; Kort, K. R.; Banerjee, S. Precursor Control of Crystal Structure and Stoichiometry in Twin Metal Oxide Nanocrystals. *CrystEngComm.* **2009**, *11*, 841–846.

(67) Tang, J.; Zhang, F.; Zoogman, P.; Fabbri, J.; Chan, S.-W.; Zhu, Y.; Brus, L.; Steigerwald, M. Martensitic Phase Transformation of Isolated HfO2, ZrO2, and HfxZr1-xO2 (0<x<1) Nanocrystals. *Adv. Funct. Mater.* **2005**, *15*, 1595–1602.

(68) Joo, J.; Yu, T.; Kim, Y. W.; Park, H. M.; Wu, F.; Zhang, J. Z.; Hyeon, T. Multigram Scale Synthesis and Characterization of Monodisperse Tetragonal Zirconia Nanocrystals. *J. Am. Chem. Soc.* **2003**, *125*, 6553–6557.

(69) Hunter, O. J.; Scheidecker, R. W.; Tojo, S. Characterization of Metastable Tetragonal Hafnia. *Ceram.* **1979**, *5*, 137–142.

(70) Ushakov, S. V.; Navrotsky, A.; Yang, Y.; Stemmer, S.; Kukli, K.; Ritala, M.;

Leskelä, M. A.; Fejes, P.; Demkov, A.; Wang, C.; et al., Crystallization in Hafnia- and Zirconia-Based Systems. *Phys. Status Solidi B* **2004**, *241*, 2268–2278.

(71) Zhou, W.; Ushakov, S. V.; Wang, T.; Ekerdt, J. G.; Demkov, A. A.; Navrotsky, A. Hafnia: Energetics of Thin Films and Nanoparticles. *J. Appl. Phys.* **2010**, *107*, 123514.

(72) Waetzig, G. R.; Depner, S. W.; Asayesh-Ardakani, H.; Cultrara, N. D.; Shahbazian-Yassar, R.; Banerjee, S. Stabilizing Metastable Tetragonal HfO2 Using a Non-Hydrolytic Solution-Phase Route: Ligand Exchange as a Means of Controlling Particle Size. *Chem. Sci.* **2016**, *7*, 4930–4939.

(73) Zhao, X.; Vanderbilt, D. First-Principles Study of Structural, Vibrational, and Lattice Dielectric Properties of Hafnium Oxide. *Phys. Rev. B* **2002**, *65*, 233106.

(74) Huan, T. D.; Sharma, V.; Rossetti, G. A.; Ramprasad, R. Pathways Towards Ferroelectricity in Hafnia. *Phys. Rev. B* **2014**, *90*, 064111.

(75) Xu, X.; Huang, F.-T.; Qi, Y.; Singh, S.; Rabe, K. M.; Obeysekera, D.; Yang, J.; Chu, M.-W.; Cheong, S.-W. Kinetically Stabilized Ferroelectricity in Bulk Single-Crystalline HfO2:Y. *Nat. Mater.* **2021**, *20*, 826–832.

(76) Cheema, S. S.; Kwon, D.; Shanker, N.; dos Reis, R.; Hsu, S.-L.; Xiao, J.; Zhang, H.; Wagner, R.; Datar, A.; McCarter, M. R.; et al., Enhanced Ferroelectricity in Ultrathin Films Grown Directly on Silicon. *Nature* **2020**, *580*, 478–482.

(77) Müller, J.; Böscke, T. S.; Schröder, U.; Mueller, S.; Bräuhaus, D.; Böttger, U.; Frey, L.; Mikolajick, T. Ferroelectricity in Simple Binary ZrO2 and HfO2. *Nano Lett.* **2012**, *12*, 4318–4323.

(78) Stähler, A.; Denk, B. Über das Zirkoniumtetrajodid, ZrJ4. *Ber. Dtsch. Chem. Ges.* **1904**, *37*, 1135–1139.

(79) Clearfield, A.; Vaughan, P. A. The Crystal Structure of Zirconyl Chloride Octahydrate and Zirconyl Bromide Octahydrate. *Acta Crystallogr.* **1956**, *9*, 555–558.

(80) Zhang, Y.; de Azambuja, F.; Parac-Vogt, T. N. The Forgotten Chemistry of Group(IV) Metals: A Survey on the Synthesis, Structure, and Properties of Discrete Zr(IV), Hf(IV), and Ti(IV) Oxo Clusters. *Coord. Chem. Rev.* **2021**, *438*, 213886.

(81) Hennig, C.; Weiss, S.; Kraus, W.; Kretzschmar, J.; Scheinost, A. C. Solution Species and Crystal Structure of Zr(IV) Acetate. *Inorg. Chem.* **2017**, *56*, 2473–2480.

(82) Bialowons, H.; Müller, M.; Müller, B. G. Titantetrafluorid – Eine überraschend einfache Kolumnarstruktur. *Z. Anorg. Allg. Chem.* **1995**, *621*, 1227–1231.

(83) Nikiforov, G. B.; Roesky, H. W.; Koley, D. A Survey of Titanium Fluoride Complexes, their Preparation, Reactivity, and Applications. *Coord. Chem. Rev.* **2014**, *258-259*, 16 – 57.

(84) Manzer, L. E.; Deaton, J.; Sharp, P.; Schrock, R. R. *31. Tetrahydrofuran Complexes of Selected Early Transition Metals*; 2007; Vol. 21; pp 135–140.

(85) Hamilton, P. M.; McBeth, R.; Bekebrede, W.; Sisler, H. H. Molecular Addition Compounds of Titanium Tetrachloride with Several Ethers. *J. Am. Chem. Soc.* **1953**, *75*, 2881–2883.

(86) Dyer, D. S.; Ragsdale, R. O. Fluorine-19 Nuclear Magnetic Resonance Study of some Titanium Tetrafluoride-Substituted Pyridine 1-Oxide Adducts. *Inorg. Chem.* **1969**, *8*, 1116–1120.

(87) Jennings, J. S.; Wardlaw, W.; Way, W. J. R. Some Esters of Titanium. *J. Chem. Soc.* **1936**, *0*, 637–640.

(88) Wu, Y.-T.; Ho, Y.-C.; Lin, C.-C.; Gau, H.-M. Stepwise Reactions of TiCl4 and Ti(OiPr)Cl3 with 2-Propanol. Variable-Temperature NMR Studies and Crystal Struc-

tures of [TiCl2(OiPr)(HOiPr)(μ-Cl)]2 and [TiCl2(OiPr)(HOiPr)(μ-OiPr)]2. *Inorg. Chem.* **1996**, *35*, 5948–5952.

(89) Bradley, D. C.; Mehrotra, R. C.; Rothwell, I. P.; Singh, A. *Alkoxo and Aryloxo Derivatives of Metals*; 2001; pp 383–443.

(90) Mehrotra, R. C.; Verma, I. D. Reactions of Ortho-Esters of Titanium .4. Salicylaldehyde Derivatives of Titanium. *J. Less-Common Met.* **1961**, *3*, 321–326.

(91) Matilainen, L.; Klinga, M.; Leskelä, M. Group 4 Metal Alkoxide Complexes as Catalysts for Olefin Polymerization. *J. Chem. Soc., Dalton Trans.* **1996**, *2*, 219–225.

(92) Funk, H.; Rogler, E. On the Reaction of Some Metal Chlorides with Phenol and ss-Naphthol. *Z. Anorg. Allg. Chem.* **1944**, *252*, 323–328.

(93) Pande, K. C.; Mehrotra, R. C. Attempted Preparation of Titanium Tetra-Acetate. *J. Prakt. Chem.* **1957**, *5*, 101–103.

(94) Sartori, P.; Weidenbruch, M. Reactions of Halides of Group IV Elements with Trifluoroacetic Acid. *Angew. Chem. Int. Ed.* **1964**, *3*, 376–377.

(95) Krebs, B. Die Kristallstruktur von Zirkoniumtetrachlorid. *Z. Anorg. Allg. Chem.* **1970**, *378*, 263–272.

(96) Rosenheim, A.; Frank, P. Concerning Zirconium Salt. *Ber. Dtsch. Chem. Ges.* **1907**, *40*, 803–810.

(97) De Keukeleere, K.; Coucke, S.; De Canck, E.; Van Der Voort, P.; Delpech, F.; Coppel, Y.; Hens, Z.; Van Driessche, I.; Owen, J. S.; De Roo, J. Stabilization of Colloidal Ti, Zr, and Hf Oxide Nanocrystals by Protonated Tri-n-octylphosphine Oxide (TOPO) and Its Decomposition Products. *Chem. Mater.* **2017**, *29*, 10233–10242.

(98) Mehrotra, R. C. Synthesis and Properties of Alkoxy and Acyloxysilanes. *Pure Appl. Chem.* **1966**, *13*, 111–132.

(99) Bradley, D. C.; Saad, M. A.; Wardlaw, W. Alcoholates of Thorium Tetrachloride. *J. Chem. Soc.* **1954**, *0*, 2002–2005.

(100) Bradley, D. C.; Abd-El Halim, F. M.; Wardlaw, W. 676. The Chloride Ethoxides of Zirconium. *J. Chem. Soc.* **1950**, *0*, 3450–3454.

(101) Prasad, S.; Devi, K. S.; Biswas, M. Compounds of Zirconium Tetrabromide with Phenols. *Proc. Natl. Acad. Sci. India - Phys. Sci.* **1965**, *35*, 11–13.

(102) Kapoor, R. N.; Mehrotra, R. C. Organic Compounds of Zirconium .6. Reactions of Zirconium Tetrachloride and Isopropoxide with Fatty Acids. *J. Chem. Soc.* **1959**, *0*, 422–426.

(103) Prasad, S.; Devi, K. S.; Sahney, K. Compounds of Zirconium Tetrahalides with Organic Acids. *Proc. Natl. Acad. Sci. India - Phys. Sci.* **1965**, *35*, 14–16.

(104) Kapoor, R. N.; Mehrotra, R. C. Organic Compounds of Zirconium .7. Studies in Zirconium Salicylates. *J. Am. Chem. Soc.* **1960**, *82*, 3495–3498.

(105) Morgan, G. T.; Bowen, A. R. Researches on Residual Affinity and Coordination Part XVIII Interactions of Zirconium Salts and Beta-Diketones. *J. Chem. Soc.* **1924**, *125*, 1252–1261.

(106) Renaut, P.; Tainturier, G.; Gautheron, B. Chlorures de Mono- et Dialkyl-Zirconocene et-Hafnocene. *J. Organomet. Chem.* **1978**, *148*, 35–42.

(107) Spijksma, G. I.; Seisenbaeva, G. A.; Fischer, A.; Bouwmeester, H. J. M.; Blank, D. H. A.; Kessler, V. G. The Molecular Composition of Non-Modified and Acac-Modified Propoxide and Butoxide Precursors of Zirconium and Hafnium Dioxides. *J. Sol-Gel Sci. Technol.* **2009**, *51*, 10–22.

(108) Spijksma, G. I.; Seisenbaeva, G. A.; Bouwmeester, H. J. M.; Blank, D. H. A.; Kessler, V. G. Zirconium and Hafnium Tert-Butoxides and Tert-Butoxo-β-diketonate

Complexes – Isolation, Structural Characterization and Application in the One-Step Synthesis of 3D Metal Oxide Nanostructures. *Polyhedron* **2013**, *53*, 150–156.

(109) Vaartstra, B. A.; Huffman, J. C.; Gradeff, P. S.; Hubert-Pfalzgraf, L. G.; Daran, J. C.; Parraud, S.; Yunlu, K.; Caulton, K. G. Alcohol Adducts of Alkoxides: Intramolecular Hydrogen Bonding as a General Structural Feature. *Inorg. Chem.* **1990**, *29*, 3126–3131.

(110) Fric, H.; Puchberger, M.; Schubert, U. Coordination of Mono- and Diamines to Titanium and Zirconium Alkoxides. *J. Sol-Gel Sci. Technol.* **2006**, *40*, 155–162.

(111) Fric, H.; Puchberger, M.; Schubert, U. Two- and Three-Dimensional Coordination Polymers From the Reaction of Bis- and Tris(2-aminoethyl)amine with Titanium and Zirconium Alkoxides. *Eur. J. Inorg. Chem.* **2007**, *2007*, 376–383.

(112) Doeuff, S.; Dromzee, Y.; Taulelle, F.; Sanchez, C. Synthesis and Solid- and Liquid-State Characterization of a Hexameric Cluster of Titanium(IV): Ti6(μ2-O)2(μ3-O)2(μ2-OC4H9)2(OC4H9)6(OCOCH3)8. *Inorg. Chem.* **1989**, *28*, 4439–4445.

(113) Kickelbick, G.; Feth, M. P.; Bertagnolli, H.; Puchberger, M.; Holzinger, D.; Gross, S. Formation of Organically Surface-Modified Metal Oxo Clusters from Carboxylic Acids and Metal Alkoxides: a Mechanistic Study. *J. Chem. Soc., Dalton Trans.* **2002**, *20*, 3892–3898.

(114) Doeuff, S.; Henry, M.; Sanchez, C.; Livage, J. Hydrolysis of Titanium Alkoxides - Modification of the Molecular Precursor by Acetic Acid. *J. Non. Cryst. Solids* **1987**, *89*, 206–216.

(115) Krishnan, V.; Gross, S.; Müller, S.; Armelao, L.; Tondello, E.; Bertagnolli, H. Structural Investigations on the Hydrolysis and Condensation Behavior of Pure and Chemically Modified Alkoxides. 1. Transition Metal (Hf and Ta) Alkoxides. *J. Phys. Chem. B* **2007**, *111*, 7501–7518.

(116) Sanchez, C.; Livage, J.; Henry, M.; Babonneau, F. Chemical Modification of Alkoxide Precursors. *J. Non. Cryst. Solids* **1988**, *100*, 65 – 76.

(117) Campbell, C.; Bott, S. G.; Larsen, R.; Van Der Sluys, W. G. Preparation of Titanium Fluoroalkoxides by Alcoholysis of Titanium Alkoxides. *Inorg. Chem.* **1994**, *33*, 4950–4958.

(118) Pande, K. C.; Mehrotra, R. C. Titanium Salts of Mono-Carboxylic Acids .2. Reaction of Titanium-Isopropoxide and -Ethoxide with Acetic Anhydride. *Z. Anorg. Allg. Chem.* **1957**, *290*, 95–100.

(119) Pande, K. C.; Mehrotra, R. C. Titanium Salts of Mono Carboxylic-Acids .3. Reaction of Titanium-Ethoxide and Titanium-Isopropoxide with Fatty Acids. *Z. Anorg. Allg. Chem.* **1957**, *291*, 97–102.

(120) Doeuff, S.; Henry, M.; Sanchez, C. Sol-Gel Synthesis and Characterization of Titanium Oxo-Acetate Polymers. *Mater. Res. Bull.* **1990**, *25*, 1519 – 1529.

(121) Schubert, U.; Arpac, E.; Glaubitt, W.; Helmerich, A.; Chau, C. Primary Hydrolysis Products of Methacrylate-Modified Titanium and Zirconium Alkoxides. *Chem. Mater.* **1992**, *4*, 291–295.

(122) Bradley, D. C.; Hancock, D. C.; Wardlaw, W. 524. Titanium Chloride Alkoxides. *J. Chem. Soc.* **1952**, 2773–2778.

(123) Chakraborty, D.; Chandrasekhar, V.; Bhattacharjee, M.; Krätzner, R.; Roesky, H. W.; Noltemeyer, M.; Schmidt, H.-G. Metal Alkoxides as Versatile Precursors for Group 4 Phosphonates: Synthesis and X-ray Structure of a Novel Organosoluble Zirconium Phosphonate. *Inorg. Chem.* **2000**, *39*, 23–26.

(124) Weingarten, H.; Van Wazer, J. R. Exchange of Parts between Molecules at Equi-

librium. VI. Scrambling on Titanium of the Alkoxyl, Dimethylamino, and Halogen Substituents. *J. Am. Chem. Soc.* **1965**, *87*, 724–730.

(125) Arnal, P.; Corriu, R. J. P.; Leclercq, D.; Mutin, P. H.; Vioux, A. A Solution Chemistry Study of Nonhydrolytic Sol-Gel Routes to Titania. *Chem. Mater.* **1997**, *9*, 694–698.

(126) Rasuwajew, G. A.; Bobinowa, L. M.; Etlis, V. S. Gewinnung und Eigenschaften Einiger Titanorganischer Verbindungen. *Tetrahedron* **1959**, *6*, 154–160.

(127) Andrianainarivelo, M.; J. P. Corriu, R.; Leclercq, D.; Hubert Mutin, P.; Vioux, A. Non-Hydrolytic Sol–Gel Process: Zirconium Titanate Gels. *J. Mater. Chem.* **1997**, *7*, 279–284.

(128) Andrianainarivelo, M.; Corriu, R. J. P.; Leclercq, D.; Mutin, P. H.; Vioux, A. Non-hydrolytic Sol-Gel Process: Aluminium and Zirconium Titanate Gels. *J. Sol-Gel Sci. Technol.* **1997**, *8*, 89–93.

(129) Rozes, L.; Steunou, N.; Fornasieri, G.; Sanchez, C. Titanium-Oxo Clusters, Versatile Nanobuilding Blocks for the Design of Advanced Hybrid Mater. *Monatsh. Chem.* **2006**, *137*, 501–528.

(130) Coppens, P.; Chen, Y.; Trzop, E. Crystallography and Properties of Polyoxotitanate Nanoclusters. *Chem. Rev.* **2014**, *114*, 9645–9661.

(131) Guerrero, G.; Mehring, M.; Hubert Mutin, P.; Dahan, F.; Vioux, A. Syntheses and Single-Crystal Structures of Novel Soluble Phosphonato- and Phosphinato-Bridged Titanium Oxo Alkoxides. *J. Chem. Soc., Dalton Trans.* **1999**, *10*, 1537–1538.

(132) Frot, T.; Cochet, S.; Laurent, G.; Sassoye, C.; Popall, M.; Sanchez, C.; Rozes, L. Ti8O8(OOCR)16, a New Family of Titanium–Oxo Clusters: Potential NBUs for Reticular Chemistry. *Eur. J. Inorg. Chem.* **2010**, *2010*, 5650–5659.

(133) Piszczek, P.; Richert, M.; Grodzicki, A.; Głowiak, T.; Wojtczak, A. Synthesis, Crystal Structures and Spectroscopic Characterization of [Ti8O8(OOCR)16] (where R=But, CH2But, C(CH3)2Et). *Polyhedron* **2005**, *24*, 663–670.

(134) Barrow, H.; Brown, D. A.; Alcock, N. W.; Clase, H. J.; Wallbridge, M. G. H. An Octameric Titanium Oxo Metallacycle with Host–Guest Interactions. *J. Chem. Soc., Chem. Commun.* **1995**, *12*, 1231–1232.

(135) Schubert, U. Cluster-Based Inorganic-Organic Hybrid Mater. *Chem. Soc. Rev.* **2011**, *40*, 575–582.

(136) Kickelbick, G.; Schubert, U. Oxozirconium Methacrylate Clusters: Zr6(OH)4O4(OMc)12 and Zr4O2(OMc)12 (OMc = Methacrylate). *Ber. Dtsch. Chem. Ges.* **1997**, *130*, 473–478.

(137) Trimmel, G.; Gross, S.; Kickelbick, G.; Schubert*, U. Swelling Behavior and Thermal Stability of Poly(methylmethacrylate) Crosslinked by the Oxozirconium Cluster Zr4O2(methacrylate)12. *Appl. Organomet. Chem.* **2001**, *15*, 401–406.

(138) Bragaggia, G.; Beghetto, A.; Bassato, F.; Reichenbächer, R.; Dolcet, P.; Carraro, M.; Gross, S. Tuning the Activity of a Hybrid Polymer–Oxocluster Catalyst: A Composition—Selectivity Correlation. *Polymers* **2021**, *13*, 3268.

(139) Gao, Y.; Kogler, F. R.; Peterlik, H.; Schubert, U. Ring-Opening Metathesis Polymerizations with Norbornene Carboxylate-Substituted Metal Oxo Clusters. *J. Mater. Chem.* **2006**, *16*, 3268–3276.

(140) Kickelbick, G.; Wiede, P.; Schubert, U. Variations in Capping the Zr6O4(OH)4 Cluster Core: X-Ray Structure Analyses of [Zr6(OH)4O4(OOC–CH=CH2)10]2(μ-OOC–CH=CH2)4 and Zr6(OH)4O4(OOCR)12(PrOH) (R=Ph, CMe=CH2). *Inorganica Chim. Acta* **1999**, *284*, 1–7.

(141) Kogler, F. R.; Jupa, M.; Puchberger, M.; Schubert, U. Control of the Ratio of Functional and Non-Functional Ligands in Clusters of the Type Zr6O4(OH)(4)(carboxylate)(12) for their Use as Building Blocks for Inorganic-Organic Hybrid Polymers. *J. Mater. Chem.* **2004**, *14*, 3133–3138.

(142) Piszczek, P.; Radtke, A.; Grodzicki, A.; Wojtczak, A.; Chojnacki, J. The New Type of [Zr6(μ_3-O)4(μ_3-OH)4] Cluster Core: Crystal Structure and Spectral Characterization of [Zr6O4(OH)4(OOCR)12] (R=But, C(CH3)2Et). *Polyhedron* **2007**, *26*, 679–685.

(143) Walther, P.; Puchberger, M.; Kogler, F. R.; Schwarz, K.; Schubert, U. Ligand Dynamics on the Surface of Zirconium Oxo Clusters. *Phys. Chem. Chem. Phys.* **2009**, *11*, 3640–3647.

(144) Puchberger, M.; Kogler, F. R.; Jupa, M.; Gross, S.; Fric, H.; Kickelbick, G.; Schubert, U. Can the Clusters Zr6O4(OH)4(OOCR)12 and [Zr6O4(OH)4(OOCR)12]2 Be Converted into Each Other? *Eur. J. Inorg. Chem.* **2006**, *2006*, 3283–3293.

(145) Faccini, F.; Fric, H.; Schubert, U.; Wendel, E.; Tsetsgee, O.; Muller, K.; Bertagnolli, H.; Venzo, A.; Gross, S. [Small Omega]-Mercapto-Functionalized Hafnium- and Zirconium-Oxoclusters as Nanosized Building Blocks for Inorganic-Organic Hybrid Mater.: Synthesis, Characterization and Photothiol-ene Polymerization. *J. Mater. Chem.* **2007**, *17*, 3297–3307.

(146) Heinz, P.; Puchberger, M.; Bendova, M.; Baumann, S. O.; Schubert, U. Clusters for Alkyne-Azide Click Reactions. *Dalton Trans.* **2010**, *39*, 7640–7644.

(147) Kickelbick, G.; Schubert, U. Hydroxy Carboxylate Substituted Oxozirconium Clusters. *J. Chem. Soc., Dalton Trans.* **1999**, *8*, 1301–1306.

(148) Xu, T.; Hou, X.; Wang, Y.; Zhang, J.; Zhang, J.; Liu, B. A Gigantic Polyoxozirconate with Visible Photoactivity. *Dalton Trans.* **2017**, *46*, 10185–10188.

(149) Nateghi, B.; Boldog, I.; Domasevitch, K. V.; Janiak, C. More Versatility than thought: Large Zr26 Oxocarboxylate Cluster by Corner-Sharing of Standard Octahedral Subunits. *CrystEngComm.* **2018**, *20*, 5132–5136.

(150) Bezrukov, A. A.; Törnroos, K. W.; Le Roux, E.; Dietzel, P. D. C. Incorporation of an Intact Dimeric Zr12 Oxo Cluster from a Molecular Precursor in a New Zirconium Metal–Organic Framework. *Chem. Comm.* **2018**, *54*, 2735–2738.

(151) Wu, L.; Liu, J.; Vockenhuber, M.; Ekinci, Y.; Castellanos, S. Hybrid EUV Resists with Mixed Organic Shells: A Simple Preparation Method. *Eur. J. Inorg. Chem.* **2019**, *2019*, 4136–4141.

(152) Fidelli, A. M.; Karadeniz, B.; Howarth, A. J.; Huskić, I.; Germann, L. S.; Halasz, I.; Etter, M.; Moon, S.-Y.; Dinnebier, R. E.; Stilinović, V.; et al., Green and Rapid Mechanosynthesis of High-Porosity NU- and UiO-type Metal–Organic Frameworks. *Chem. Comm.* **2018**, *54*, 6999–7002.

(153) Petit, S.; Morlens, S.; Yu, Z.; Luneau, D.; Pilet, G.; Soubeyroux, J.-L.; Odier, P. Synthesis and Thermal Decomposition of a Novel Zirconium Acetato-Propionate Cluster: [Zr12]. *Solid State Sci.* **2011**, *13*, 665–670.

(154) Piszczek, P.; Radtke, A.; Wojtczak, A.; Muzioł, T.; Chojnacki, J. Synthesis, Structure Characterization and Thermal Properties of [Zr6(μ_3-O)4(μ_3-OH)4(OOCCH2tBu)9(μ_2-OH)3]2. *Polyhedron* **2009**, *28*, 279–285.

(155) Moraru, B.; Kickelbick, G.; Schubert, U. Methacrylate-Substituted Mixed-Metal Clusters Derived from Zigzag Chains of [ZrO8]/[ZrO7] and [TiO6] Polyhedra. *Eur. J. Inorg. Chem.* **2001**, *5*, 1295–1301.

(156) Kreutzer, J.; Czakler, M.; Puchberger, M.; Pittenauer, E.; Schubert, U. On the Question of Site-Selective Ligand Exchange in Carboxylate-Substituted Metal Oxo Clusters. *Eur. J. Inorg. Chem.* **2015**, *17*, 2889–2894.

(157) Chiu, C.-C.; Shieh, F.-K.; Tsai, H.-H. G. Ligand Exchange in the Synthesis of Metal–Organic Frameworks Occurs Through Acid-Catalyzed Associative Substitution. *Inorg. Chem.* **2019**, *58*, 14457–14466.

(158) Gross, S.; Kickelbick, G.; Puchberger, M.; Schubert, U. Mono-, Di-, and Trimetallic Methacrylate-Substituted Metal Oxide Clusters Derived from Hafnium Butoxide. *Monatsh. Chem.* **2003**, *134*, 1053–1063.

(159) Yuan, S.; Qin, J.-S.; Xu, H.-Q.; Su, J.; Rossi, D.; Chen, Y.; Zhang, L.; Lollar, C.; Wang, Q.; Jiang, H.-L.; et al., [Ti8Zr2O12(COO)16] Cluster: An Ideal Inorganic Building Unit for Photoactive Metal–Organic Frameworks. *ACS Cent. Sci.* **2018**, *4*, 105–111.

(160) Jupa, M.; Kickelbick, G.; Schubert, U. Methacrylate-Substituted Titanium-Yttrium Mixed-Metal Oxo Clusters. *Eur. J. Inorg. Chem.* **2004**, *2004*, 1835–1839.

(161) Artner, C.; Kronister, S.; Czakler, M.; Schubert, U. Ion-Size-Dependent Formation of Mixed Titanium/Lanthanide Oxo Clusters. *Eur. J. Inorg. Chem.* **2014**, *2014*, 5596–5602.

(162) Luo, W.; Zou, D.-H.; Yang, S.; Cui, L.-N.; Liu, P.-Y.; Zhu, Q.-Y.; Dai, J. Water-Soluble Lanthanide–Titanium–Oxo Cluster, a Precursor for Biocompatible Nanomaterial. *Inorg. Chem.* **2019**, *21*, 14617–14625.

(163) Chen, R.; Hong, Z.-F.; Zhao, Y.-R.; Zheng, H.; Li, G.-J.; Zhang, Q.-C.; Kong, X.-J.; Long, L.-S.; Zheng, L.-S. Ligand-Dependent Luminescence Properties of Lanthanide–Titanium Oxo Clusters. *Inorg. Chem.* **2019**, *22*, 15008–15012.

(164) Dan-Hardi, M.; Serre, C.; Frot, T.; Rozes, L.; Maurin, G.; Sanchez, C.; Férey, G. A New Photoactive Crystalline Highly Porous Titanium(IV) Dicarboxylate. *J. Am. Chem. Soc.* **2009**, *131*, 10857–10859.

(165) Hendon, C. H.; Tiana, D.; Fontecave, M.; Sanchez, C.; D'arras, L.; Sassoye, C.; Rozes, L.; Mellot-Draznieks, C.; Walsh, A. Engineering the Optical Response of the Titanium-MIL-125 Metal–Organic Framework through Ligand Functionalization. *J. Am. Chem. Soc.* **2013**, *135*, 10942–10945.

(166) Sun, Y.; Lu, D.-F.; Sun, Y.; Gao, M.-Y.; Zheng, N.; Gu, C.; Wang, F.; Zhang, J. Large Titanium-Oxo Clusters as Precursors to Synthesize the Single Crystals of Ti-MOFs. *ACS Mater. Lett.* **2021**, *3*, 64–68.

(167) Nguyen, H. L.; Gándara, F.; Furukawa, H.; Doan, T. L. H.; Cordova, K. E.; Yaghi, O. M. A Titanium–Organic Framework as an Exemplar of Combining the Chemistry of Metal– and Covalent–Organic Frameworks. *J. Am. Chem. Soc.* **2016**, *138*, 4330–4333.

(168) Ly, H. G. T.; Fu, G.; Kondinski, A.; Bueken, B.; De Vos, D.; Parac-Vogt, T. N. Superactivity of MOF-808 toward Peptide Bond Hydrolysis. *J. Am. Chem. Soc.* **2018**, *140*, 6325–6335.

(169) Loosen, A.; de Azambuja, F.; Smolders, S.; Moons, J.; Simms, C.; De Vos, D.; Parac-Vogt, T. N. Interplay between Structural Parameters and Reactivity of Zr6-Based MOFs as Artificial Proteases. *Chem. Sci.* **2020**, *11*, 6662–6669.

(170) Jakobsen, S.; Gianolio, D.; Wragg, D. S.; Nilsen, M. H.; Emerich, H.; Bordiga, S.; Lamberti, C.; Olsbye, U.; Tilset, M.; Lillerud, K. P. Structural Determination of a Highly Stable Metal-Organic Framework with Possible Application to Interim Radioactive Waste Scavenging: Hf-UiO-66. *Phys. Rev. B* **2012-09**, *86*, 125429.

(171) Beyzavi, M. H.; Klet, R. C.; Tussupbayev, S.; Borycz, J.; Vermeulen, N. A.; Cramer, C. J.; Stoddart, J. F.; Hupp, J. T.; Farha, O. K. A Hafnium-Based Metal–Organic Framework as an Efficient and Multifunctional Catalyst for Facile CO2

Fixation and Regioselective and Enantioretentive Epoxide Activation. *J. Am. Chem. Soc.* **2014**, *136*, 15861–15864.

(172) Beyzavi, M. H.; Vermeulen, N. A.; Howarth, A. J.; Tussupbayev, S.; League, A. B.; Schweitzer, N. M.; Gallagher, J. R.; Platero-Prats, A. E.; Hafezi, N.; Sarjeant, A. A.; et al., A Hafnium-Based Metal–Organic Framework as a Nature-Inspired Tandem Reaction Catalyst. *J. Am. Chem. Soc.* **2015**, *137*, 13624–13631.

(173) Salvador, F. E.; Miller, V.; Shimada, K.; Wang, C.-H.; Wright, J.; Das, M.; Chen, Y.-P.; Chen, Y.-S.; Sheehan, C.; Xu, W.; et al., Mechanochemistry of Group 4 Element-Based Metal–Organic Frameworks. *Inorg. Chem.* **2021**, *21*, 16079–16084.

(174) Guillerm, V.; Gross, S.; Serre, C.; Devic, T.; Bauer, M.; Férey, G. A Zirconium Methacrylate Oxocluster as Precursor for the Low-Temperature Synthesis of Porous Zirconium(iv) Dicarboxylates. *Chem. Comm.* **2010**, *46*, 767–769.

(175) Huang, Y.-H.; Lo, W.-S.; Kuo, Y.-W.; Chen, W.-J.; Lin, C.-H.; Shieh, F.-K. Green and Rapid Synthesis of Zirconium Metal–Organic Frameworks via Mechanochemistry: UiO-66 Analog Nanocrystals Obtained in One Hundred Seconds. *Chem. Comm.* **2017**, *53*, 5818–5821.

(176) Trimmel, G.; Fratzl, P.; Schubert, U. Cross-Linking of Poly(methyl methacrylate) by the Methacrylate-Substituted Oxozirconium Cluster Zr6(OH)4O4(Methacrylate)12. *Chem. Mater.* **2000**, *12*, 602–604.

(177) Schubert, U.; Trimmel, G.; Moraru, B.; Tesch, W.; Fratzl, P.; Gross, S.; Kickelbick, G.; Hüsing, N. Inorganic-Organic Hybrid Polymers from Surface-Modified Oxometallate Clusters. *Mater. Res. Soc. Symp. Proc.* **2000**, *628*, CC2.3.

(178) Kogler, F. R.; Schubert, U. Crosslinking Vs. Filler Effect of Carboxylate-Substituted Zirconium Oxo Clusters on the Thermal Stability of Polystyrene. *Polymer* **2007**, *48*, 4990–4995.

(179) Schubert, U.; Völkel, T.; Moszner, N. Mechanical Properties of an Inorganic-Organic Hybrid Polymer Cross-linked by the Cluster Zr4O2(methacrylate)12. *Chem. Mater.* **2001**, *13*, 3811–3812.

(180) Kreutzer, J.; Qin, X.-H.; Gorsche, C.; Peterlik, H.; Liska, R.; Schubert, U. Variation of the Crosslinking Density in Cluster-Reinforced Polymers. *Mater. Today Commun.* **2015**, *5*, 10 – 17.

(181) Gibin, G.; Lorenzetti, A.; Callone, E.; Dirè, S.; Dolcet, P.; Venzo, A.; Causin, V.; Marigo, A.; Modesti, M.; Gross, S. Smart and Covalently Cross-Linked: Hybrid Shape Memory Mater. Reinforced through Covalent Bonds by Zirconium Oxoclusters. *ChemPlusChem.* **2016**, *81*, 338–350.

(182) Gross, S.; Di Noto, V.; Schubert, U. Dielectric Investigation of Inorganic–Organic Hybrid Film Based on Zirconium Oxocluster-Crosslinked PMMA. *J. Non. Cryst. Solids* **2003**, *322*, 154–159.

(183) Graziola, F.; Girardi, F.; Bauer, M.; Di Maggio, R.; Rovezzi, M.; Bertagnolli, H.; Sada, C.; Rossetto, G.; Gross, S. UV-Photopolymerisation of Poly(methyl methacrylate)-Based Inorganic–Organic Hybrid Coatings and Bulk Samples Reinforced with Methacrylate-Modified Zirconium Oxocluster. *Polymer* **2008**, *49*, 4332–4343.

(184) Sangermano, M.; Gross, S.; Priola, A.; Rizza, G.; Sada, C. Thiol-ene Hybrid Organic/Inorganic Nanostructured Coatings Based on Thiol-Functionalized Zirconium Oxoclusters. *Macromol. Chem. Phys.* **2007**, *208*, 2560–2568.

(185) Schubert, U. Polymers Reinforced by Covalently Bonded Inorganic Clusters. *Chem. Mater.* **2001**, *13*, 3487–3494.

(186) Faustini, M.; Nicole, L.; Ruiz-Hitzky, E.; Sanchez, C. History of Organic–Inorganic

Hybrid Mater.: Prehistory, Art, Science, and Advanced Applications. *Adv. Funct. Mater.* **2018**, *28*, 1704158.

(187) Gross, S. Oxocluster-Reinforced Organic–Inorganic Hybrid Mater.: Effect of Transition Metal Oxoclusters on Structural and Functional Properties. *J. Mater. Chem.* **2011**, *21*, 15853–15861.

(188) Armelao, L.; Eisenmenger-Sittner, C.; Groenewolt, M.; Gross, S.; Sada, C.; Schubert, U.; Tondello, E.; Zattin, A. Zirconium and Hafnium Oxoclusters as Molecular Building Blocks for Highly Dispersed ZrO2 or HfO2 Nanoparticles in Silica Thin Films. *J. Mater. Chem.* **2005**, *15*, 1838–1848.

(189) Armelao, L.; Gross, S.; Müller, K.; Pace, G.; Tondello, E.; Tsetsgee, O.; Zattin, A. Structural Evolution upon Thermal Heating of Nanostructured Inorganic-Organic Hybrid Mater. to Binary Oxides MO2-SiO2 (M = Hf, Zr) as Evaluated by Solid-State NMR and FTIR Spectroscopy. *Chem. Mater.* **2006**, *18*, 6019–6030.

(190) Armelao, L.; Bertagnolli, H.; Bleiner, D.; Groenewolt, M.; Gross, S.; Krishnan, V.; Sada, C.; Schubert, U.; Tondello, E.; Zattin, A. Highly Dispersed Mixed Zirconia and Hafnia Nanoparticles in a Silica Matrix: First Example of a ZrO2-HfO2-SiO2 Ternary Oxide System. *Adv. Funct. Mater.* **2007**, *17*, 1671–1681.

(191) Gross, S.; Müller, K. Sol-Gel Derived Silica-Based Organic-Inorganic Hybrid Mater. as "Composite Precursors" for the Synthesis of Highly Homogeneous Nanostructured Mixed Oxides: an Overview. *J. Sol-Gel Sci. Technol.* **2011**, *60*, 283–298.

(192) Vigolo, M.; Borsacchi, S.; Sorarù, A.; Geppi, M.; Smarsly, B. M.; Dolcet, P.; Rizzato, S.; Carraro, M.; Gross, S. Engineering of Oxoclusters-Reinforced Polymeric Mater. with Application as Heterogeneous Oxydesulfurization Catalysts. *Appl. Catal.* **2016**, *182*, 636–644.

(193) Benedetti, C.; Cazzolaro, A.; Carraro, M.; Graf, R.; Landfester, K.; Gross, S.; Muñoz-Espí, R. Dual Role of Zirconium Oxoclusters in Hybrid Nanoparticles: Cross-Linkers and Catalytic Sites. *ACS Appl. Mater. Interfaces* **2016**, *8*, 26275–26284.

(194) Niederberger, M.; Garnweitner, G. Organic Reaction Pathways in the Nonaqueous Synthesis of Metal Oxide Nanoparticles. *Chemistry* **2006**, *12*, 7282–302.

(195) Deshmukh, R.; Niederberger, M. Mechanistic Aspects in the Formation, Growth and Surface Functionalization of Metal Oxide Nanoparticles in Organic Solvents. *Chem. Eur. J.* **2017**, *23*, 8542–8570.

(196) Niederberger, M. Nonaqueous Sol–Gel Routes to Metal Oxide Nanoparticles. *Acc. Chem. Res.* **2007**, *40*, 793–800.

(197) Garnweitner, G.; Goldenberg, L. M.; Sakhno, O. V.; Antonietti, M.; Niederberger, M.; Stumpe, J. Large-Scale Synthesis of Organophilic Zirconia Nanoparticles and their Application in Organic-Inorganic Nanocomposites for Efficient Volume Holography. *Small* **2007**, *3*, 1626–1632.

(198) De Roo, J.; Van den Broeck, F.; De Keukeleere, K.; Martins, J. C.; Van Driessche, I.; Hens, Z. Unravelling the Surface Chemistry of Metal Oxide Nanocrystals, the Role of Acids and Bases. *J. Am. Chem. Soc.* **2014**, *136*, 9650–9657.

(199) De Keukeleere, K.; De Roo, J.; Lommens, P.; Martins, J. C.; Van der Voort, P.; Van Driessche, I. Fast and Tunable Synthesis of ZrO2 Nanocrystals: Mechanistic Insights into Precursor Dependence. *Inorg. Chem.* **2015**, *54*, 3469–3476.

(200) Zhou, S. X.; Garnweitner, G.; Niederberger, M.; Antonietti, M. Dispersion Behavior of Zirconia Nanocrystals and their Surface Functionalization with Vinyl Group-Containing Ligands. *Langmuir* **2007**, *23*, 9178–9187.

(201) Grote, C.; Cheema, T. A.; Garnweitner, G. Comparative Study of Ligand Binding during the Postsynthetic Stabilization of Metal Oxide Nanoparticles. *Langmuir* **2012**, *28*, 14395–14404.

(202) Rechberger, F.; Heiligtag, F. J.; Süess, M. J.; Niederberger, M. Assembly of BaTiO3 Nanocrystals into Macroscopic Aerogel Monoliths with High Surface Area. *Angew. Chem., Int. Ed.* **2014**, *53*, 6823–6826.

(203) Cheema, T. A.; Garnweitner, G. Phase-Controlled Synthesis of ZrO2 Nanoparticles for Highly Transparent Dielectric Thin Films. *CrystEngComm.* **2014**, *16*, 3366–3375.

(204) De Roo, J.; Yazdani, N.; Drijvers, E.; Lauria, A.; Maes, J.; Owen, J. S.; Van Driessche, I.; Niederberger, M.; Wood, V.; Martins, J. C.; et al., Probing Solvent–Ligand Interactions in Colloidal Nanocrystals by the NMR Line Broadening. *Chem. Mater.* **2018**, *30*, 5485–5492.

(205) Niederberger, M.; Bartl, M. H.; Stucky, G. D. Benzyl Alcohol and Titanium Tetrachloride - A Versatile Reaction System for the Nonaqueous and Low-Temperature Preparation of Crystalline and Luminescent Titania Nanoparticles. *Chem. Mater.* **2002**, *14*, 4364–4370.

(206) Suchomski, C.; Weber, D. J.; Dolcet, P.; Hofmann, A.; Voepel, P.; Yue, J.; Einert, M.; Möller, M.; Werner, S.; Gross, S.; et al., Sustainable and Surfactant-Free High-Throughput Synthesis of Highly Dispersible Zirconia Nanocrystals. *J. Mater. Chem. A* **2017**, *5*, 16296–16306.

(207) Ninjbadgar, T.; Garnweitner, G.; Börger, A.; Goldenberg, L. M.; Sakhno, O. V.; Stumpe, J. Synthesis of Luminescent ZrO2:Eu3+ Nanoparticles and Their Holographic Sub-Micrometer Patterning in Polymer Composites. *Adv. Funct. Mater.* **2009**, *19*, 1819–1825.

(208) Pinna, N.; Garnweitner, G.; Antonietti, M.; Niederberger, M. Non-Aqueous Synthesis of High-Purity Metal Oxide Nanopowders using an Ether Elimination Process. *Adv. Mater.* **2004**, *16*, 2196–2200.

(209) Buha, J.; Arčon, D.; Niederberger, M.; Djerdj, I. Solvothermal and Surfactant-Free Synthesis of Crystalline Nb2O5, Ta2O5, HfO2, and Co-Doped HfO2 Nanoparticles. *Phys. Chem. Chem. Phys.* **2010**, *12*, 15537–15543.

(210) De Roo, J.; De Keukeleere, K.; Feys, J.; Lommens, P.; Hens, Z.; Van Driessche, I. Fast, Microwave-Assisted Synthesis of Monodisperse HfO2 Nanoparticles. *J. Nanopart. Res.* **2013**, *15*, 11.

(211) Lauria, A.; Villa, I.; Fasoli, M.; Niederberger, M.; Vedda, A. Multifunctional Role of Rare Earth Doping in Optical Mater.: Nonaqueous Sol–Gel Synthesis of Stabilized Cubic HfO2 Luminescent Nanoparticles. *Acs Nano* **2013**, *7*, 7041–7052.

(212) Niederberger, M.; Garnweitner, G.; Krumeich, F.; Nesper, R.; Cölfen, H.; Antonietti, M. Tailoring the Surface and Solubility Properties of Nanocrystalline Titania by a Nonaqueous In Situ Functionalization Process. *Chem. Mater.* **2004**, *16*, 1202–1208.

(213) Niederberger, M.; Bartl, M. H.; Stucky, G. D. Benzyl Alcohol and Transition Metal Chlorides as a Versatile Reaction System for the Nonaqueous and Low-Temperature Synthesis of Crystalline Nano-Objects with Controlled Dimensionality. *J. Am. Chem. Soc.* **2002**, *124*, 13642–13643.

(214) Hu, M.; Xu, J.; Gao, J.; Yang, S.; Wong, J. S. P.; Li, R. K. Y. Benzyl Alcohol-Based Synthesis of Oxide Nanoparticles: the Perspective of SN1 Reaction Mechanism. *Dalton Trans.* **2013**, *42*, 9777–9784.

(215) Garnweitner, G.; Grote, C. In Situ Investigation of Molecular Kinetics and Particle Formation of Water-Dispersible Titania Nanocrystals. *Phys. Chem. Chem. Phys.* **2009**, *11*, 3767–3774.

(216) Jensen, G. V.; Bremholm, M.; Lock, N.; Deen, G. R.; Jensen, T. R.; Iversen, B. B.; Niederberger, M.; Pedersen, J. S.; Birkedal, H. Anisotropic Crystal Growth Kinetics of Anatase TiO2 Nanoparticles Synthesized in a Nonaqueous Medium. *Chem. Mater.* **2010**, *22*, 6044–6055.

(217) Watzky, M. A.; Finke, R. G. Transition Metal Nanocluster Formation Kinetic and Mechanistic Studies. A New Mechanism When Hydrogen Is the Reductant: Slow, Continuous Nucleation and Fast Autocatalytic Surface Growth. *J. Am. Chem. Soc.* **1997**, *119*, 10382–10400.

(218) Szeifert, J. M.; Feckl, J. M.; Fattakhova-Rohlfing, D.; Liu, Y.; Kalousek, V.; Rathousky, J.; Bein, T. Ultrasmall Titania Nanocrystals and Their Direct Assembly into Mesoporous Structures Showing Fast Lithium Insertion. *J. Am. Chem. Soc.* **2010**, *132*, 12605–12611.

(219) Zhu, J.; Wang, S.; Bian, Z.; Xie, S.; Cai, C.; Wang, J.; Yang, H.; Li, H. Solvothermally Controllable Synthesis of Anatase TiO2 Nanocrystals with Dominant 001 Facets and Enhanced Photocatalytic Activity. *CrystEngComm.* **2010**, *12*, 2219–2224.

(220) Hu, M.-J.; Gao, J.; Yang, S.; Dong, Y.; Ping Wong, J. S.; Xu, J.; Shan, G.; Li, R. K. Y. E1 Reaction-Induced Synthesis of Hydrophilic Oxide Nanoparticles in a Non-Hydrophilic Solvent. *Nanoscale* **2012**, *4*, 6284–6288.

(221) Garnweitner, G.; Tsedev, N.; Dierke, H.; Niederberger, M. Benzylamines as Versatile Agents for the One-Pot Synthesis and Highly Ordered Stacking of Anatase Nanoplatelets. *Eur. J. Inorg. Chem.* **2008**, *2008*, 890–895.

(222) Rijckaert, H.; De Roo, J.; Van Zele, M.; Banerjee, S.; Huhtinen, H.; Paturi, P.; Bennewitz, J.; Billinge, S.; Bäcker, M.; De Buysser, K.; Van Driessche, I. Pair Distribution Function Analysis of ZrO2 Nanocrystals and Insights in the Formation of ZrO2-YBa2Cu3O7 Nanocomposites. *Mater.* **2018**, *11*, 1066.

(223) Gambe, J.; Rémondière, F.; Jouin, J.; Portal, L.; Thomas, P.; Masson, O. Detrimental Effect and Neutralization of in Situ Produced Water on Zirconia Nanoparticles Obtained by a Nonaqueous Sol–Gel Method. *Inorg. Chem.* **2019**, *22*, 15175–15188.

(224) Rauwel, P.; Galeckas, A.; Rauwel, E. One Step Synthesis of Pure Cubic and Monoclinic HfO2 Nanoparticles: Effects of Temperature and Ambient on the Photoluminescent Properties. *ECS Trans.* **2015**, *64*, 19–28.

(225) De Roo, J.; De Keukeleere, K.; Hens, Z.; Van Driessche, I. From Ligands to Binding Motifs and Beyond; the Enhanced Versatility of Nanocrystal Surfaces. *Dalton. Trans.* **2016**, *45*, 13277–83.

(226) Trentler, T. J.; Denler, T. E.; Bertone, J. F.; Agrawal, A.; Colvin, V. L. Synthesis of TiO2 Nanocrystals by Nonhydrolytic Solution-Based Reactions. *J. Am. Chem. Soc.* **1999**, *121*, 1613–1614.

(227) Jun, Y.-w.; Casula, M. F.; Sim, J.-H.; Kim, S. Y.; Cheon, J.; Alivisatos, A. P. Surfactant-Assisted Elimination of a High Energy Facet as a Means of Controlling the Shapes of TiO2 Nanocrystals. *J. Am. Chem. Soc.* **2003**, *125*, 15981–15985.

(228) Shaw, S.; Yuan, B.; Tian, X.; Miller, K. J.; Cote, B. M.; Colaux, J. L.; Migliori, A.; Panthani, M. G.; Cademartiri, L. Building Mater. from Colloidal Nanocrystal Arrays: Preventing Crack Formation during Ligand Removal by Controlling Structure and Solvation. *Adv. Mater.* **2016**, *28*, 8892–8899.

(229) Pokratath, R.; Van den Eynden, D.; Rudd Cooper, S.; Katja Mathiesen, J.; Waser, V.; Devereux, M.; J. L. Billinge, S.; Meuwly, M.; Jensen, K.; De Roo, J. Mechanistic insight into the precursor chemistry of ZrO2 and HfO2 nanocrystals; towards size-tunable syntheses. *JACS Au*

(230) Tirosh, E.; Markovich, G. Control of Defects and Magnetic Properties in Colloidal HfO2 Nanorods. *Adv. Mater.* **2007**, *19*, 2608–2612.

(231) Sugimoto, T. Underlying Mechanisms in Size Control of Uniform Nanoparticles. *J. Colloid Interface Sci.* **2007**, *309*, 106–118.

(232) De Roo, J.; Zhou, Z.; Wang, J.; Deblock, L.; Crosby, A. J.; Owen, J. S.; Nonnenmann, S. S. Synthesis of Phosphonic Acid Ligands for Nanocrystal Surface Functionalization and Solution Processed Memristors. *Chem. Mater.* **2018**, *30*, 8034–8039.

(233) Dhaene, E.; Billet, J.; Bennett, E.; Van Driessche, I.; De Roo, J. The Trouble with ODE: Polymerization during Nanocrystal Synthesis. *Nano Lett.* **2019**, *19*, 7411–7417.

(234) Koo, B.; Park, J.; Kim, Y.; Choi, S.-H.; Sung, Y.-E.; Hyeon, T. Simultaneous Phase- and Size-Controlled Synthesis of TiO2 Nanorods via Non-Hydrolytic Sol-Gel Reaction of Syringe Pump Delivered Precursors. *J. Phys. Chem. B* **2006**, *110*, 24318–24323.

(235) Pinna, N.; Niederberger, M. Surfactant-Free Nonaqueous Synthesis of Metal Oxide Nanostructures. *Angew. Chem. Int. Ed.* **2008**, *47*, 5292–5304.

(236) Liu, C.; Hajagos, T. J.; Chen, D.; Chen, Y.; Kishpaugh, D.; Pei, Q. Efficient One-Pot Synthesis of Colloidal Zirconium Oxide Nanoparticles for High-Refractive-Index Nanocomposites. *ACS Appl. Mater. Interfaces* **2016**, *8*, 4795–4802.

(237) Buonsanti, R.; Grillo, V.; Carlino, E.; Giannini, C.; Kipp, T.; Cingolani, R.; Cozzoli, P. D. Nonhydrolytic Synthesis of High-Quality Anisotropically Shaped Brookite TiO2 Nanocrystals. *J. Am. Chem. Soc.* **2008**, *130*, 11223–11233.

(238) Gordon, T. R.; Cargnello, M.; Paik, T.; Mangolini, F.; Weber, R. T.; Fornasiero, P.; Murray, C. B. Nonaqueous Synthesis of TiO2 Nanocrystals Using TiF4 to Engineer Morphology, Oxygen Vacancy Concentration, and Photocatalytic Activity. *J. Am. Chem. Soc.* **2012**, *134*, 6751–6761.

(239) Zhang, Z.; Wu, Q.; Johnson, G.; Ye, Y.; Li, X.; Li, N.; Cui, M.; Lee, J. D.; Liu, C.;

Zhao, S.; et al., Generalized Synthetic Strategy for Transition-Metal-Doped Brookite-Phase TiO2 Nanorods. *J. Am. Chem. Soc.* **2019**, *42*, 16548–16552.

(240) Joo, J.; Kwon, S. G.; Yu, T.; Cho, M.; Lee, J.; Yoon, J.; Hyeon, T. Large-Scale Synthesis of TiO2 Nanorods via Nonhydrolytic Sol-Gel Ester Elimination Reaction and Their Application to Photocatalytic Inactivation of E. coli. *J. Phys. Chem. B* **2005**, *109*, 15297–15302.

(241) Zhang, Z.; Zhong, X.; Liu, S.; Li, D.; Han, M. Aminolysis Route to Monodisperse Titania Nanorods with Tunable Aspect Ratio. *Angew. Chem. Int. Ed.* **2005**, *44*, 3466–3470.

(242) Huo, Z.; Tsung, C.-K.; Huang, W.; Fardy, M.; Yan, R.; Zhang, X.; Li, Y.; Yang, P. Self-Organized Ultrathin Oxide Nanocrystals. *Nano Lett.* **2009**, *9*, 1260–1264.

(243) Cozzoli, P. D.; Kornowski, A.; Weller, H. Low-Temperature Synthesis of Soluble and Processable Organic-Capped Anatase TiO2 Nanorods. *J. Am. Chem. Soc.* **2003**, *125*, 14539–14548.

(244) Cao, S.; Zhang, S.; Zhang, T.; Fisher, A.; Lee, J. Y. Metal-Doped TiO2 Colloidal Nanocrystals with Broadly Tunable Plasmon Resonance Absorption. *J. Mater. Chem. C* **2018**, *6*, 4007–4014.

(245) Boyle, T. J.; Steele, L. A. M.; Burton, P. D.; Hoppe, S. M.; Lockhart, C.; Rodriguez, M. A. Synthesis and Structural Characterization of a Family of Modified Hafnium tert-Butoxide for Use as Precursors to Hafnia Nanoparticles. *Inorg. Chem.* **2012**, *51*, 12075–12092.

(246) Tandon, B.; Gibbs, S. L.; Zydlewski, B. Z.; Milliron, D. J. Quantitative Analysis of Plasmonic Metal Oxide Nanocrystal Ensembles Reveals the Influence of Dopant Selection on Intrinsic Optoelectronic Properties. *Chem. Mater.* **2021**, *33*, 6955–6964.

(247) Housecroft, C. E.; Constable, E. C. The Emergence of Copper(I)-Based Dye Sensitized Solar Cells. *Chem. Soc. Rev.* **2015**, *44*, 8386–8398.

(248) Watté, J.; Lommens, P.; Pollefeyt, G.; Meire, M.; De Buysser, K.; Van Driessche, I. Highly Crystalline Nanoparticle Suspensions for Low-Temperature Processing of TiO2 Thin Films. *ACS Appl. Mater. Interfaces* **2016**, *8*, 13027–13036.

(249) Shaw, S.; Colaux, J. L.; Hay, J. L.; Peiris, F. C.; Cademartiri, L. Building Mater. from Colloidal Nanocrystal Arrays: Evolution of Structure, Composition, and Mechanical Properties upon the Removal of Ligands by O2 Plasma. *Adv. Mater.* **2016**, *28*, 8900–8905.

(250) Shaw, S.; Silva, T. F.; Bobbitt, J. M.; Naab, F.; Rodrigues, C. L.; Yuan, B.; Chang, J. J.; Tian, X.; Smith, E. A.; Cademartiri, L. Building Mater. from Colloidal Nanocrystal Assemblies: Molecular Control of Solid/Solid Interfaces in Nanostructured Tetragonal ZrO2. *Chem. Mater.* **2017**, *29*, 7888–7900.

(251) Wang, Y.; Fedin, I.; Zhang, H.; Talapin, D. V. Direct Optical Lithography of Functional Inorganic NanoMater. *Science* **2017**, *357*, 385–388.

(252) Pan, J.-A.; Rong, Z.; Wang, Y.; Cho, H.; Coropceanu, I.; Wu, H.; Talapin, D. V. Direct Optical Lithography of Colloidal Metal Oxide NanoMater. for Diffractive Optical Elements with 2π Phase Control. *J. Am. Chem. Soc.* **2021**, *5*, 2372–2383.

(253) Tao, P.; Li, Y.; Siegel, R. W.; Schadler, L. S. Transparent Dispensible High-Refractive Index ZrO2/Epoxy Nanocomposites for LED Encapsulation. *J. Appl. Polym. Sci.* **2013**, *130*, 3785–3793.

(254) Rijckaert, H.; Pollefeyt, G.; Sieger, M.; Hanisch, J.; Bennewitz, J.; De Keukeleere, K.; De Roo, J.; Huhne, R.; Backer, M.; Paturi, P.; ; et al., Optimizing Nanocomposites through Nanocrystal Surface Chemistry: Superconducting YBa2Cu3O7 Thin Films

via Low-Fluorine Metal Organic Deposition and Preformed Metal Oxide Nanocrystals. *Chem. Mater.* **2017**, *29*, 6104–6113.

(255) Min, Y.; Caster, J. M.; Eblan, M. J.; Wang, A. Z. Clinical Translation of Nanomedicine. *Chem. Rev.* **2015**, *115*, 11147–90.

(256) McGinnity, T. L.; Dominguez, O.; Curtis, T. E.; Nallathamby, P. D.; Hoffman, A. J.; Roeder, R. K. Hafnia (HfO2) Nanoparticles as an X-Ray Contrast Agent and Mid-Infrared Biosensor. *Nanoscale* **2016**, *8*, 13627–13637.

(257) De Roo, J.; Van Driessche, I.; Martins, J. C.; Hens, Z. Colloidal Metal Oxide Nanocrystal Catalysis by Sustained Chemically Driven Ligand Displacement. *Nano Lett.* **2016**, *15*, 517–521.

Graphical TOC Entry